DESIGN AND CHARACTERIZATION OF A CRYOGENIC CONTROL VALVE PLUG WITH EQUAL PERCENT CHARACTERISTICS

By

Austin Everett Grake

A THESIS

Submitted to
Michigan State University
in partial fulfillment of the requirements
for the degree of

Chemical Engineering–Master of Science

2025

ABSTRACT

Automated valves are used in the process industry for precise control of process parameters (*e.g.* flow, pressure, temperature). For the proper process design of a system, it is crucial to ensure that these valves possess the appropriate flow coefficient to effectively regulate the fluid flow within these systems. Although automated control valves are widely available, very few domestic (USA) manufacturers offer automated control valves for cryogenic applications, especially helium systems where there is a need for control valves with precise flow control and low flow regulation (*i.e.*, flow coefficient < 1.0). The present research aims to establish a comprehensive design methodology for developing an equal percent valve plug for use in a cryogenic control valve. The methodology adopts a holistic approach that integrates analytical, computational, and experimental techniques. An analytical model is developed to estimate the geometrical profile of an equal percent control valve plug for use in a commercially available cryogenic control valve. This model serves as the fundamental framework for estimating the valve flow characteristics. Predicted valve flow characteristics from the analytical model are be compared against results obtained from a computational fluid dynamics model (CFD). The implemented CFD model further enhances the understanding of the valve flow characteristics under various operating conditions through characterization of the internal flow across the valve plug profile. Results from both these theoretical models are validated against experimental measurements. Experimental results are obtained using a valve flow characterization test bench, which is designed and built to measure the flow and corresponding pressure drop across developed valve plug profile(s) under different operating conditions. The relationship between the valve lift and the flow coefficient characteristics for the developed profile(s) are captured from the measurements and compared against the theoretical predictions. The developed design methodology can assist cryogenic system designers and operators to generate control valve plug profiles based on a commercial control valve, as needed for efficient process control.

To my family, thank you for your unwavering support.

ACKNOWLEDGEMENTS

First and foremost, I would like to express my deepest gratitude to my parents, Amy Grake and David Grake, for their support and belief in my goals, even during times when I doubted myself. Your encouragement has been my foundation throughout my academic career. I would also like to thank my sister, Addison Grake, for her support and the fun times we shared on campus.

I am grateful to Carolynn Calin for her constant love, support, and encouragement, especially during this final year: her understanding and reassurance helped me stay grounded and focused. I would also like to extend my thanks to Amalia Calin and Liviu Calin for their kindness, support, and the many home-cooked meals.

I would also like to express my gratitude to my friends Matthew Wu, Seyon Elankumaran, and Logan Jacobson for their support, friendship, and the relaxing gaming sessions.

I would like to extend special thanks to the following individuals, each of whom has played a pivotal role in my academic journey at the Facility for Rare Isotope Beams and Michigan State University:

Dr. Nusair Hasan, your guidance and insights throughout this research have been invaluable. Your willingness to help, share your expertise, and offer constructive feedback has helped me navigate some of the most challenging aspects of my work. I am truly grateful for your support.

Dr. Jonathon Howard, I cannot thank you enough for the knowledge you shared and your willingness to help with various technical aspects of my research. Your insights have enriched my understanding and contributed significantly to the quality of my work.

Scott Anthony, your help and support have been truly appreciated. From troubleshooting issues to brainstorming new ideas, your practical advice and problem-solving skills have had a lasting impact on my project.

Finally, I would like to express my appreciation to Dr. Barton, my academic advisor in the Chemical Engineering Department.

Thank you to these individuals for sharing their knowledge and offering invaluable help throughout my research. Your insights and assistance have been vital to my success.

This material is based upon work supported by the U.S. Department of Energy, Office of Science, Office of High Energy Physics, under Award Number DE-SC0018362.

TABLE OF CONTENTS

Chapter 1: INTRODUCTION

1.1 Background

Automated control valves are essential components used to regulate the flow and pressure of fluids within process systems. These valves operate by varying the size of the flow passage (plug diameter) as directed by a controller (air pressure actuator), which, in turn, adjusts the position of the valve stem (stroke).

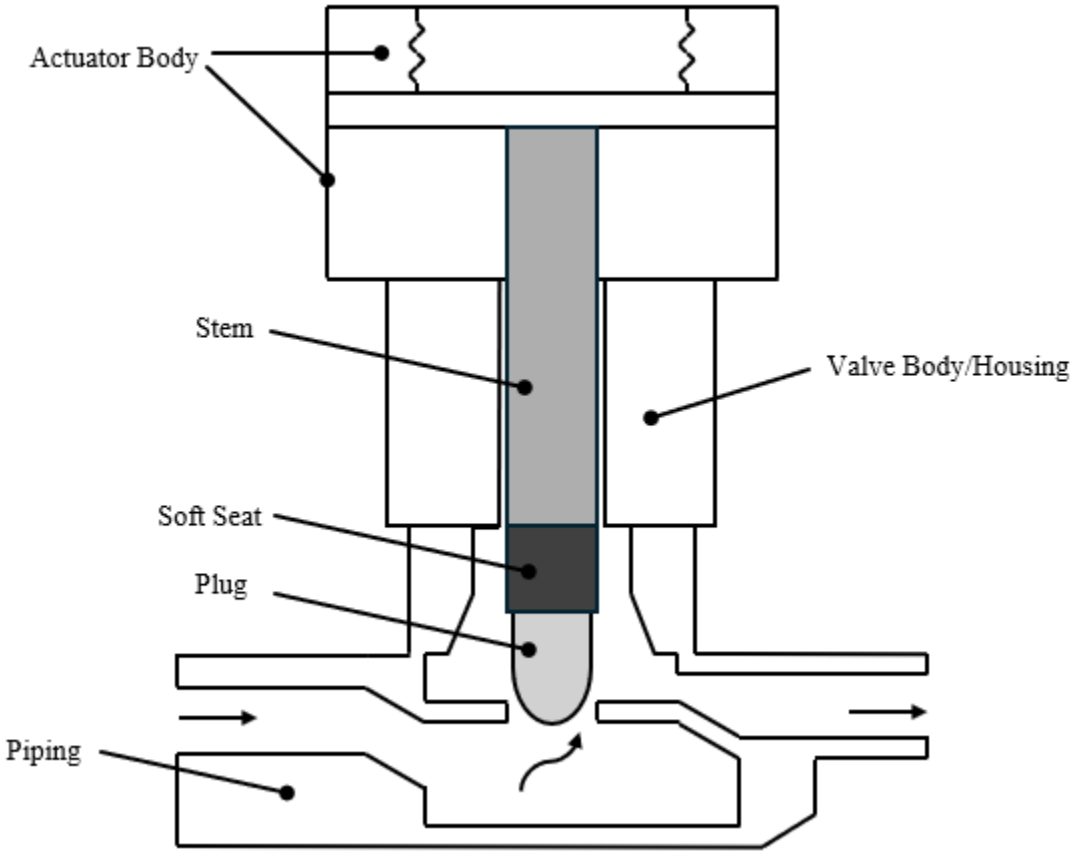

Figure 1.1: Simplified Pneumatic Actuated Control Valve Cross-section

Figure 1.1 details the cross-section of a typical control valve. The individual components noted are generally ubiquitous in a pneumatic control valve design. The actuator converts a control signal (usually from a process controller) into mechanical motion, and can be pneumatic, electric, or hydraulic depending on the specific application and the required response time. Generally, an LVDT (Linear Variable Differential Transformer) is equipped within an actuator for precise stroke measurement. As the actuator applies pressure, the stem and plug move vertically, controlling the

cross-sectional flow area and thereby regulating fluid flow. However, in place of an LVDT a pneumatic positioner was used. The design of the stem is critical for minimizing friction and wear during operation, contributing to the valve's longevity and performance. The plug is the primary component that obstructs or allows fluid flow; it typically has a conical or cylindrical shape in globe valves and is designed to minimize flow resistance and prevent cavitation [1]. Process sealing capabilities are enhanced by the valve's soft seat (also referred to as a disk), which is often made of materials such as rubber or PTFE (Teflon) [2].

The soft seat is positioned at the interface between the plug and the valve stem body, providing a reliable sealing surface to prevent leakage when the valve is closed. Additionally, the piping serves as the necessary inlet and outlet connections for the fluid, ensuring proper alignment and size to optimize flow characteristics while minimizing pressure drop.

The valve housing, or body, encases all internal components, providing structural integrity to the valve assembly. It is designed to withstand both internal pressure and external forces during operation, with materials chosen based on fluid properties, operating temperature, and pressure requirements.

Control valves in cryogenic applications, particularly those managing fluids like helium at its Nominal Boiling Point (NBP of 4.2 K) and nitrogen (NBP of 77 K), require special design considerations. Such considerations specifically for cryogenic control valves servicing helium incorporate thermal intercepts and longer valve stems. Thermal intercepts are strategically placed to reduce the heat load conduction from the warmer environment (300K) to the cryogenic fluid. Longer valve stems are also necessary to establish an increased distance between the warm valve body and the cryogenic operating environment [3].

The extended length helps mitigate the effects of heat transfer, allowing for better thermal performance and reduced thermal loading on the valve components. These design features are critical for minimizing thermal losses (i.e. heat in-leak) and ensuring efficient and reliable operation of the control valve. Each of the features typically present for helium control valves can be seen in *Figure 1.2.*

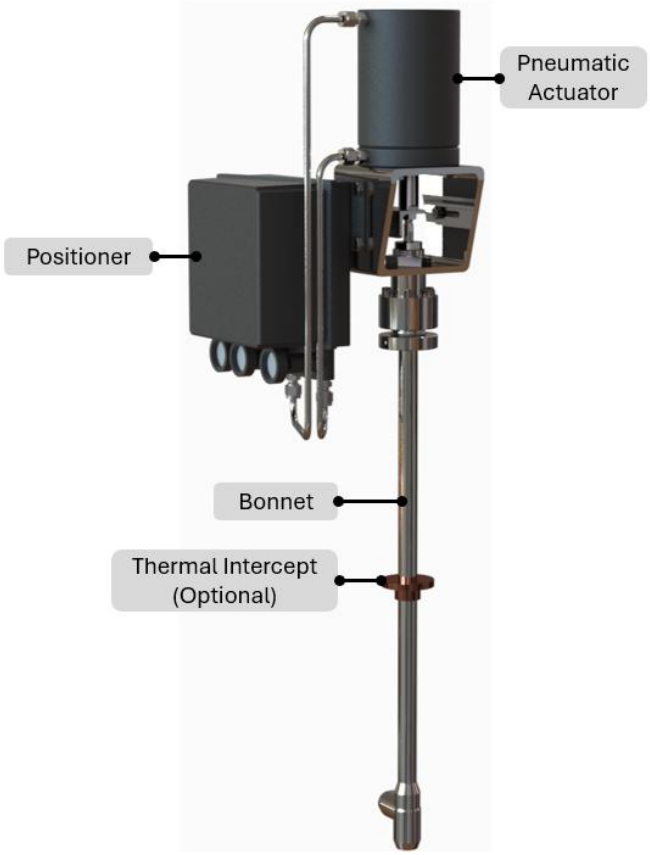

Figure 1.2: Installed Cryogenic Control Valve Model

Additionally, materials selected for the construction of the cryogenic control valve must withstand the low temperature conditions without compromising performance. The materials used for stem spacing must be compatible with cryogenic temperatures to prevent brittleness or deformation. These materials must also have low thermal conductivity, as to minimize heat leak through the valve stem into the cryogenic fluid. Additionally, the green material, known as G-10, is a composite material formed by layering sheets of fiberglass fabric and injecting them with epoxy resin. G-10 maintains the alignment and stability of the valve stem while accommodating the thermal contractions that occur at low temperatures. Properly designed valve stems using G-10 ensure that the valve operates smoothly without binding, which could lead to mechanical failure, while minimizing heat in-leak into the cryogenic process. The valve plug and process piping directly interact with the operating fluid, and therefore stainless steel 304 (SST 304) is often selected as a construction material due to its corrosion resistance and mechanical strength at low

temperatures, making it suitable for cryogenic applications. As seen in *Figure 1.3*, the valve plug directly threads into the stainless steel stem body. Between the stem and plug there must be a reliable seal that can withstand cryogenic conditions. Polychlorotrifluoroethylene (PCTFE), known in industry as Kel-F, is a soft seat seal specifically designed for use in cryogenic control valves. This sealing material is manufactured to withstand extremely low temperatures while maintaining its durability and sealing capabilities. The use of Kel-F soft seals limits leakage between the valve seat and plug when the valve is closed, which is critical for maintaining the integrity of cryogenic systems. Moreover, the contact between the Kel-F and stainless-steel valve plug mitigates wear by eliminating metal to metal contact between piping and plug. The durability and performance of Kel-F seals contribute significantly to the overall reliability and performance of cryogenic control valves, reducing the likelihood of failure and ensuring proper sealing.

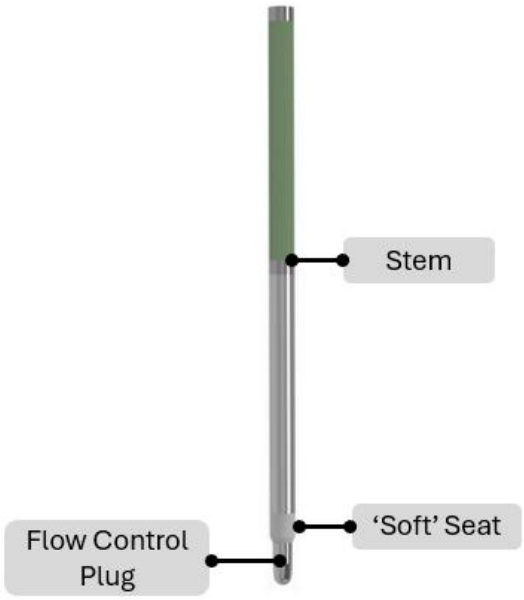

Figure 1.3: Cryogenic Control Valve Stem Materials

A general parameter for characterizing valve performance is the flow coefficient (C_v), a parameter which incorporates the mass flow rate (GPM), pressure (PSI), differential pressure (PSI), and the specific gravity of the fluid (SG) being studied. . It is specifically defined as the amount of water at 60°F (in gallons) that can flow through the valve per minute when there is a pressure drop of 1 psi across the valve [2]. The units provided are commonly used for the flow

coefficient input parameters, as described in multiple reference handbooks [2] [4] .

The flow coefficient equation provides insights into how these variables interact when characterizing the valve's performance. Measuring temperature (T), pressure (P), mass flow rate (m), and differential pressure (ΔP) enables the calculation of the valve C_v, which can be analyzed based on the relationship with valve lift or stroke (*i.e.* determining C_v based on valve position). This relationship allows for characterization of the valve's flow characteristics across its operational range, facilitating valve selection and control strategies for specific process applications.

As seen in *Figure 1.4,* the valve characterization curve (C_v vs Stroke) , shown in red, represents the relationship between the control valve's flow coefficient (C_v) and its stroke length (%) under specific process conditions(1.1 Bar Inlet Pressure, 0.1 Bar Pressure Drop) for a given single-phase fluid. This curve can be used to calculate the mass flow rate through the valve along the entire stroke range. For example, in the case of helium, the mass flow is determined at two different temperatures, 80 K and 300 K, using the same process conditions and valve characterization curve. These different temperatures result in varying mass flow rates due to the changes in fluid properties, such as density and viscosity, at the respective temperatures.

Similarly, for nitrogen at 80 K, the mass flow is calculated from the valve's characterization curve, assuming the inlet conditions remain constant. This approach highlights how the characterization curve can be used to estimate mass flow for various fluids under different conditions, enabling more accurate flow control in cryogenic systems.

This methodology is like the Fanning friction factor versus Reynolds number plot, which is commonly used in fluid dynamics to estimate mass flow through ducts. Given a pressure drop and known flow characteristics, such as the Reynolds number and friction factor, the mass flow rate can be calculated. Likewise, by analyzing the C_v vs. Stroke curve, one can determine the mass flow rate through the valve given process conditions, this means that the valve characterization curve is fully independent of a fluid and its properties.

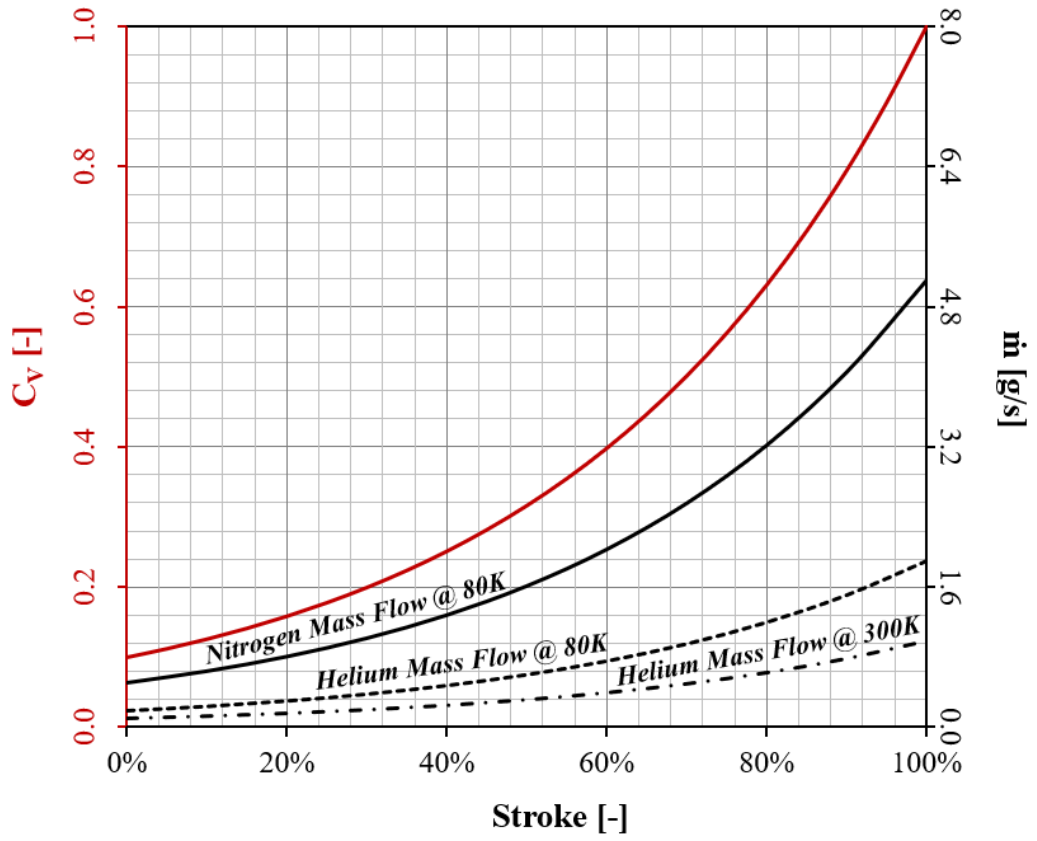

Figure 1.4: Flow coefficient vs. stroke and mass flow rate vs. stroke for an equal pct. flow plug with helium (80K and 300K) and nitrogen (80K) and a constant pressure differential (0.1 bar) with an Inlet pressure of 1.1 bar

Flow characteristics through control valves are determined by the cross-sectional flow area established by the interaction between the valve plug and valve seat geometries. Valve plugs are typically categorized into three plug profiles: quick open, linear, and equal percentage, with sample profiles of each provided in *Figure 1.5*.

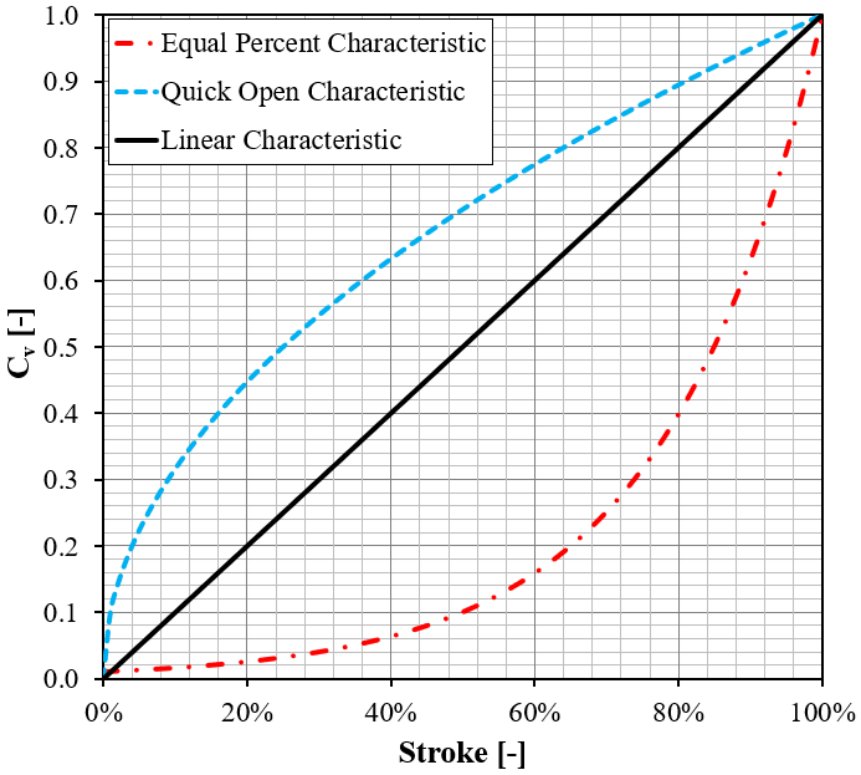

Figure 1.5: Valve Plug Characteristic Curves

Quick open valves provide a significant increase in flow rate with marginal stem lift. These valves are ideal for applications requiring rapid flow changes. However, quick open plugs are less precise at lower stroke percentages, which can lead to difficulties in achieving precise flow control due to overshooting or undershooting the desired flow rate. Linear valves offer a directly proportional relationship between the valve stem position and the flow rate, allowing for consistent control throughout the valve's range. This characteristic makes them suitable for processes that demand steady flow rates. Equal percentage valves, on the other hand, deliver a flow rate that increases exponentially with valve stem travel. This profile is particularly advantageous for processes with wide-ranging operational conditions, as it allows for better control at both low and moderate flow rates while maintaining a high maximum flow rate [4].

By modifying the plug profile, as seen in *Figure 1.6*, the flow area changes and therefore the inherent flow characteristics can be modified with respect to valve lift. An analytical model can be developed to create these plug profiles with the desired maximum flow coefficient and rangeability based upon fundamental equations.

The plug profiles were generated by the analytical model used an intended stroke length,

seat diameter of the control valve, nozzle coefficient, and desired maximum flow coefficient. The analytical models provided a more precise and consistent method of calculating plug profiles for equal percent valve plugs. Additionally, using the equal percent analytical model, the combination of a higher maximum flow coefficient profile and a lower flow coefficient profile can be combined where the flow coefficient is matches at the same stroke percentage allowing for a 'hybrid plug'.

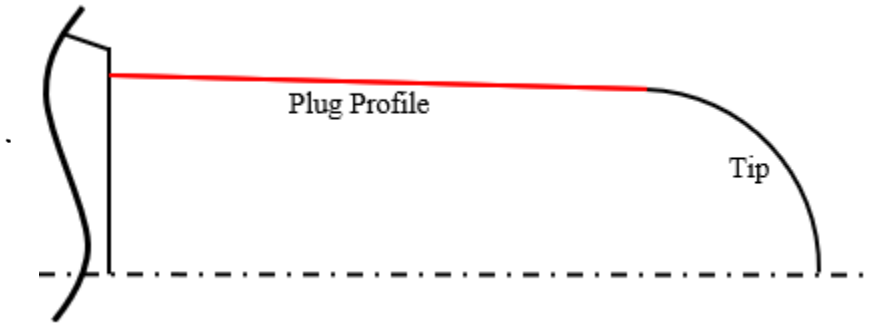

Figure 1.6: Valve Plug Cross-Section

1.2 Valve Flow Characteristics

Control valve performance is typically quantified by how fluid resistance changes with valve position. To characterize these changes, engineers rely on key dimensionless parameters such as the flow resistance coefficient and valve flow coefficient (C_v), both of which are defined in various standards and design references.

Flow Resistance Coefficient

The flow resistance coefficient (ζ) is a dimensionless parameter that quantifies pressure drop across a restriction due to hydraulic resistance. It is defined by Eqn. (1.1) [5]:

$$\Delta p = \zeta \frac{\rho v^2}{2} \tag{1.1}$$

Here, Δp is the pressure drop across a component, ρ is the inlet fluid density and v is the fluid velocity. The flow resistance coefficient is a function of the geometric effects of the valve or pipe fitting, including shape, surface roughness, fluid viscosity and flow regime (laminar or turbulent). A wide range of empirically derived values for various fluid network components can be found in [5].

Valve Flow Coefficient (C_v)

For practical applications, a valve flow coefficient (C_v) is used to characterize the flow resistance across a valve under different process conditions. Historically, for hydraulic (water) flow, C_v is defined as the number of gallons of water at 60°F that will pass through a valve per minute with a 1 psi pressure drop [4]. This flow coefficient allows engineers to assess and compare valve capabilities across different designs and sizing schemes. The explicit form of the incompressible flow coefficient is seen below in Eqn. (1.2).

$$C_v = \frac{Q\ [GPM]}{\sqrt{\Delta P[PSI]}} \tag{1.2}$$

For application with other fluids (gaseous or liquid, viscous or inviscid) and flow conditions (laminar or turbulent), appropriate corrections are made to account for compressibility and geometry effects, which are addressed by the ANSI/ISA-S75 standards. Hence, for the same valve flow coefficient, and pressure differential the mass flow rate across the valve can be different based on the fluid and process conditions. The ANSI/ISA-S75 standard provide means to estimate the flow rate under different process conditions and flow regimes as well as guidelines for design, and characterization of valve plugs.

Standardization of C_v per ANSI/ISA-S75

To ensure consistency and repeatability in C_v measurements and valve sizing across different vendors and designs, the ANSI/ISA-S75.01 standard [6] provides an implicit methodology for calculating C_v for both incompressible and compressible flow. This standard specifies corrections to handle choke flow, critical pressure drops, flow regime, etc.

All C_v values experimentally calculated in this thesis are calculated using procedures specified in ANSI/ISA-S75.01, ensuring comparability and adherence to industry-standard valve sizing methods.

The initial flow coefficient for an incompressible and compressible single-phase fluid, based on ISA Flow Equations for Sizing Control Valves (ANSI/ISA-S75.01) are seen below in Eqns. (1.3) and (1.4).

$$C_v = \left(\frac{Q}{N_1}\right)\sqrt{\frac{\rho_1}{\Delta P \rho_o}} \tag{1.3}$$

$$C_v = (W)\left(N_6 * \left(1 - \frac{\Delta P}{P * 3 * F_\gamma * x_T}\right) * \sqrt{\Delta P \rho_1}\right)^{-1} \quad (1.4)$$

The correction factors relating and associated factors needed to calculate the compressible flow coefficient are as follows (including additional factors listed in alternative forms to Eqn. (1.4) found in ANSI/ISA-S75.01):

- x_T – Pressure differential ratio factor of a control valve without attached fittings at choked flow
- $x -$ Ratio of pressure differential to inlet absolute pressure $\left(\frac{\Delta P}{P_1}\right)$
- $Y -$ Expansion factor
- $Z -$ Compressibility factor
- $F_\gamma -$ Specific heat ratio factor
- $F_L -$ Liquid pressure recovery factor of a control valve without attached fittings
- $F_F -$ Liquid critical pressure ratio factor
- $F_R -$ Reynolds number factor
- $F_P -$ Piping geometry factor

$$\mathrm{x} < F_\gamma x_T \quad (1.5)$$

If the compressible flow is choked (where x is greater than or equal to$F_\gamma x_T$), as seen based on Eqn. (1.5). The initial flow coefficient for a compressible choked flow is then used as seen in Eqn. (1.6).

$$C_v = (W)\left(0.667 * N_6 * \sqrt{F_\gamma * x_T * P_1 * \rho_1}\right)^{-1} \quad (1.6)$$

Therefore, the calculated flow coefficient calculation routine was dependent on these initial equations and then an iterative routine. The iterative method can be found In Appendix A and in the ANSI/ ISA-S75.01 standards for full iterative calculations of flow coefficient at each trial.

Valve Flow Characterization Testing per ANSI/ISA S75.02

To experimentally determine a valve's C_v across its stroke range, ANSI/ISA S75.02 outlines standardized testing procedures for control valve characterization. This includes typical components seen in *Figure 1.7*, such as: fluid source, throttling valve, temperature sensor, flow measurement device, pressure taps (differential pressure sensor), test specimen (valve), and a downstream throttling valve

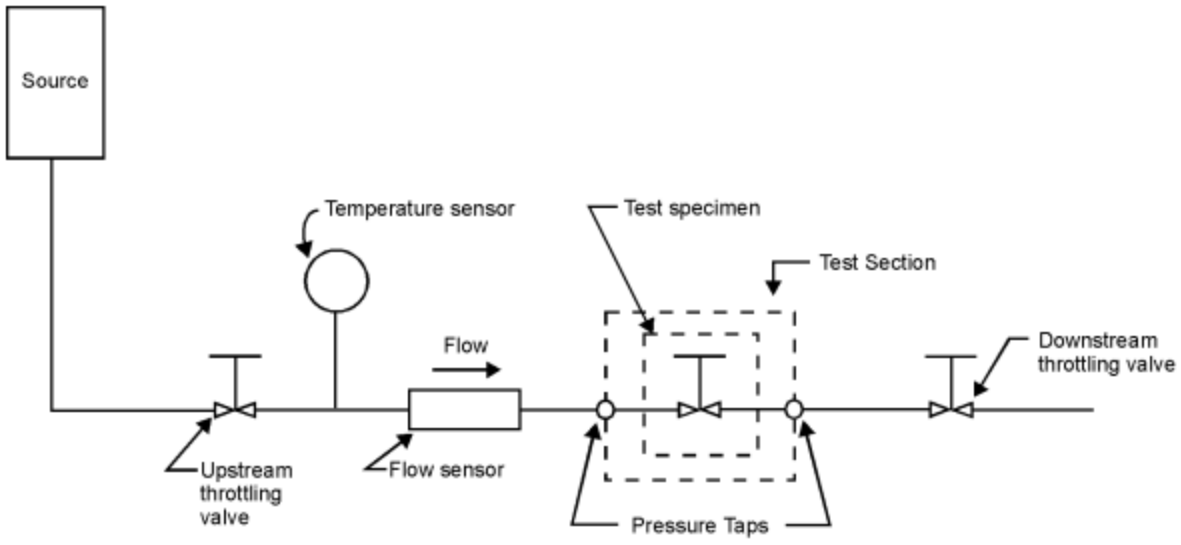

Figure 1.7: Standard Flow Test System , adapted from [7]

Characterization of both incompressible and compressible flow through control valves requires standard testing conditions. For incompressible flow, water at ambient conditions is generally used. For compressible flow, gas properties (density, pressure, temperature) must be well controlled and monitored to ensure reproducible measurements and to detect any transition to choked flow.[7]

In this thesis, a custom valve characterization bench was designed and constructed to evaluate plug profiles under various operating conditions using gaseous nitrogen. This bench complies with ANSI/ISA S75.02 recommendations to ensure data quality and reproducibility.

1.3 Motivation

The Facility for Rare Isotope Beams (FRIB) utilizes large-scale helium cryogenic systems to support refrigeration loads for components that require low operational temperatures, such as superconducting magnets and superconducting radiofrequency (SRF) cavities. Within these systems, precise control of the cryogenic fluids (such as helium and nitrogen) is essential. The implementation of control valve plugs designed specifically for cryogenic applications enhances the operational efficiency, stability, and reliability of these systems.

The superconducting components are submerged in saturated liquid helium baths, which require active control of the liquid level. A PID control program controls for the liquid levels, dependent on valve size, plug characteristic, and heat load needed to be removed from the cryostat. *Figure 1.8* depicts a simplified schematic of a cryostat using a control valve at the inlet to manage

subcooled helium entering a cryostat. The diagram includes the subcooled helium inlet, the cryostat vessel, vapor return piping, and a variable heat-in leak (Q). Actively maintaining a constant liquid level is essential for stable operation, as excessive boil-off or inadequate cooling can compromise superconducting performance. The inlet valve (and therefore it's valve plug) plays a crucial role in regulating the helium supply rate.

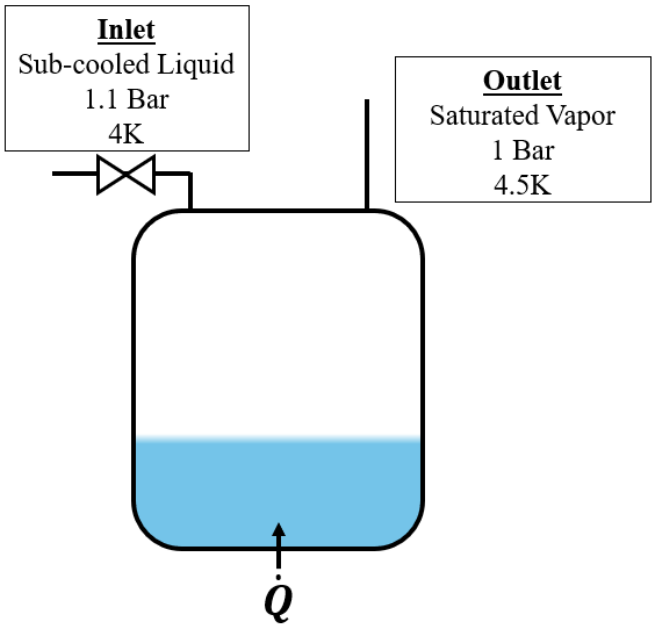

Figure 1.8: Simplified Helium Cryostat

As seen in *Figure 1.9*, this precise control is vital, as the lower flow coefficient (C_v) valves can maintain a steadier position instead of rapidly actuating on and off. This stability is particularly beneficial in cryogenic applications, where maintaining consistent flow is crucial to managing the temperature and pressure within the system. In such systems, fully closing a valve is undesirable, as it can lead to heat buildup at the inlet due to the surrounding warmer environment. This heat can cause localized warming of the cryogenic fluid, potentially creating a 'hot shot' when the valve is reopened. Such a scenario introduces vapor or warmer liquid into the cryostat, resulting in thermal shock to sensitive components and disrupting system performance. The hybrid plug's advantage lies in its ability to support cooldown like a $C_v > 1.0$, while also maintaining active control in steady-state operation, thus preventing the heat buildup and ensuring stable cryogenic conditions and therefore a stable liquid level.

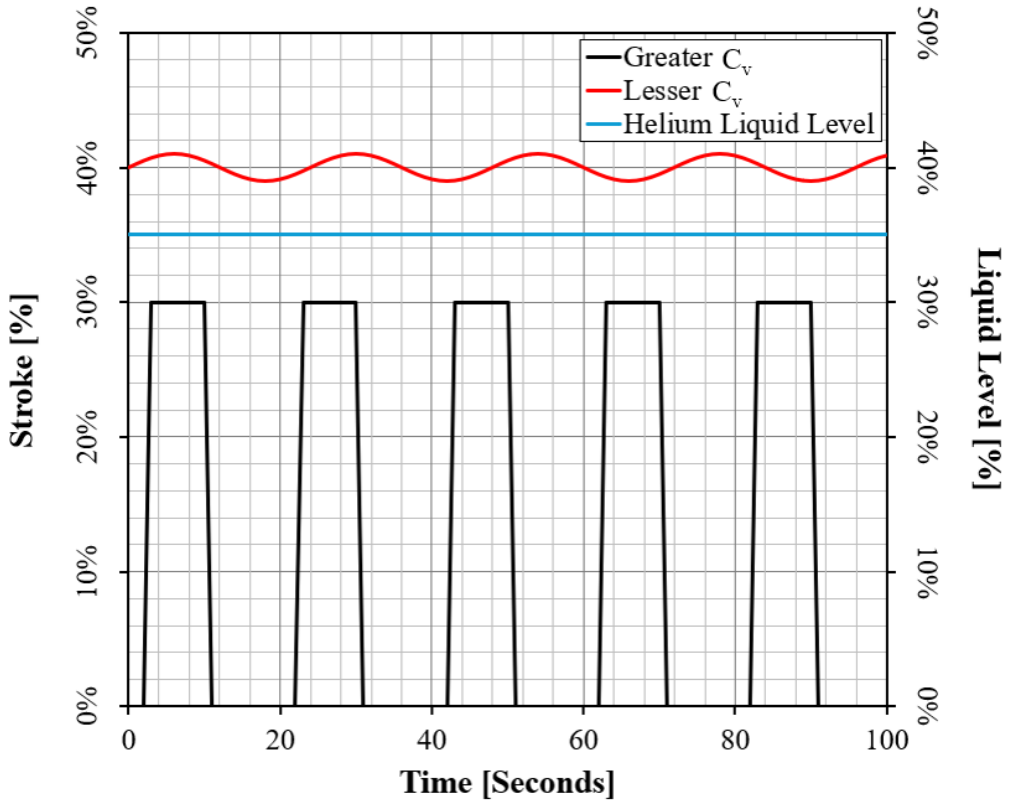

Figure 1.9: Flow Coefficient Effects on Valve Opening Percentage per Time while Maintaining Constant Liquid Level

Figure 1.10 illustrates the relationship between reduced pressure and reduced specific volume for gases near the two-phase dome (red). For single-phase gas flow in this study, the operating conditions of nitrogen were selected such that both the reduced pressure and reduced specific volume remain above the ideal gas region (i.e., above the blue curve), indicating superheated vapor well outside the two-phase region.

Under these conditions, the gas behaves closely to an ideal gas, and thus, ideal gas assumptions are valid for calculating flow coefficients (C_v). This simplifies the analytical modeling without compromising accuracy, as real gas effects are minimal in the superheated region away from the critical point or saturation curve. Therefore, the C_v values reported in this thesis, derived under single-phase conditions, can be interpreted using ideal gas relations.

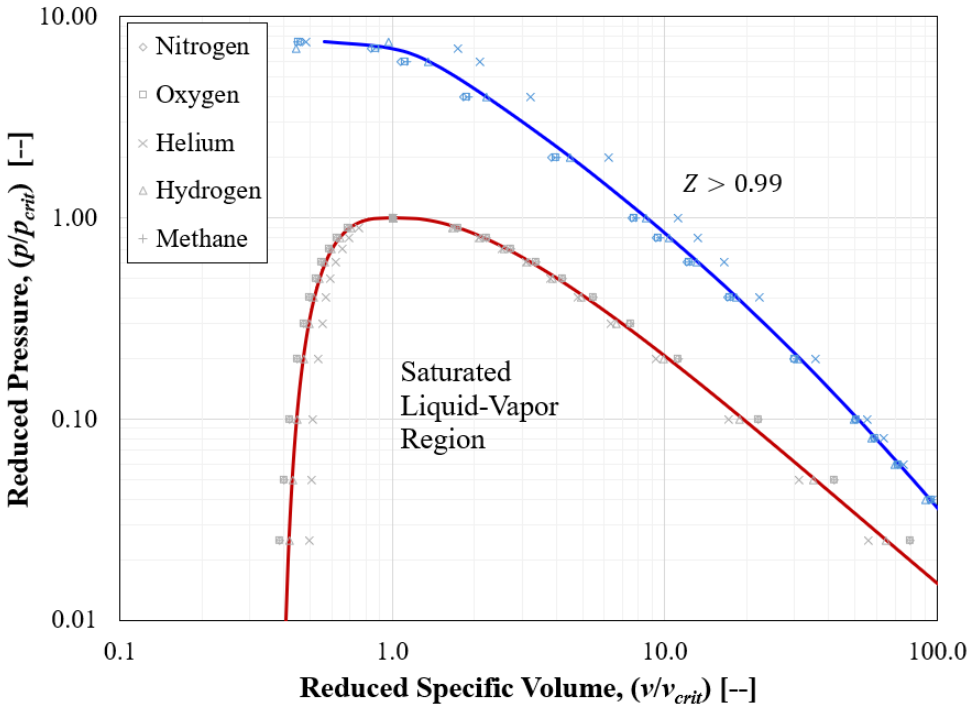

Figure 1.10: Reduced Pressure vs. Reduced Specific Volume for Gases Near Two-Phase Dome

Additionally, a calibrated control valve with a specific flow plug can eliminate the need for an additional flowmeter. This reduces the requirement for extra process piping and conserves space within the process design envelope. Furthermore, the reduction in auxiliary equipment minimizes thermal mass and heat-in leak, which is particularly critical in cryogenic systems where even minor heat gains can lead to increased boil-off and degraded system performance.

The ability to accurately control and measure single-phase flow with a calibrated control valve, whether liquid or vapor, is essential for the safe and efficient operation of cryogenic systems. Single-phase flow control ensures stable thermodynamic conditions and enables accurate regulation of mass flow to downstream components. In cryogenic applications, where heat transfer and phase stability are tightly coupled, precise flow measurement is also necessary for system diagnostics, performance optimization, and safety. By integrating flow measurements into the control valve plug itself, designers can achieve real-time feedback and control with minimal thermal and mechanical intrusion (heat in-leak), supporting more compact, responsive, and efficient system designs.

1.4 Scope and Objectives

This thesis aims to design and fabricate equal percent and hybridized plugs for a control valve,

specifically tailored for cryogenic applications. The objectives of this research include the following:

- Develop an analytical model that utilizes fundamental equations to design control valve plug featuring both equal percent and hybridized plug profiles. This model will serve as a framework for understanding the flow characteristics and performance metrics associated with different plug designs. Although, testing and validation must be considered.
- Establish a comprehensive computational fluid dynamics (CFD) model that simulates the performance of the control valve plugs. This model will be validated against the analytical approach outlined in the ANSI/ISA-S75.01: Flow Equations for Sizing Control Valves standards [6], as well as empirical data obtained from an experimental test bench. The integration of CFD modeling is intended to provide a reliable tool for future studies, significantly reducing the need for extensive experimental testing and experimental valve plug fabrication while improving design accuracy.
- Design and build an experimental test bench that allows for rigorous testing of the fabricated valve plugs. This setup will facilitate the assessment of flow coefficient and performance under various operational conditions using gaseous nitrogen, ensuring that the experimental results align with both the analytical and the CFD validated.
- Develop a method for utilizing a characterized valve plug (valve stroke vs C_v) as an alternative to a traditional flowmeter, where the valve inlet pressure, temperature, differential pressure, and plug characterization (valve stroke vs C_v) can be used to calculate a mass flow rate without the need for a traditional flowmeter. This process will also be validated against experimentally measured mass flow values.
- Provide a thorough evaluation of the control valve plug designs, focusing on their efficacy in cryogenic applications. This evaluation will include an analysis of flow rates (valve stroke vs C_v), pressure drops, and overall operational efficiency, contributing valuable insight into the optimization of cryogenic control valve plug design.

Chapter 2: LITERATURE REVIEW

Automated control valves play a pivotal role in process control systems across a wide range of industries, ensuring the precise regulation of fluid flow, pressure, and temperature. These valves are critical in maintaining the operational efficiency and safety of systems in sectors such as oil and gas, chemical processing, power generation, and specialized applications like cryogenics.

Control valves in cryogenic applications, such as those involving liquefied gases like helium and nitrogen, face unique challenges due to the extremely low temperatures (at or below the NBP of each respective fluid) and phase transitions that affect fluid properties. Issues such as material integrity, thermal stress, heat in-leak, and precise flow control become a challenge for maintaining system stability and performance. Consequently, the need for valves with enhanced durability, sealing capabilities, and precise control capabilities have garnered interest in research and innovation in cryogenic valve technologies.

This chapter reviews the literature surrounding the industrial applications of control valves, with a particular focus within cryogenic systems. It discusses the challenges encountered in cryogenic applications and the innovative solutions developed to address these issues, including advancements in control valve plug design and CFD-based methodologies for plug characterization. Furthermore, the chapter highlights the role of experimental validation in confirming theoretical models and improving valve performance in real-world conditions.

In review of previous control valve advancements, this chapter aims to emphasize the necessity for ongoing research and development in this field. As industries necessitate greater efficiency and reliability in control systems, particularly in cryogenics. Ultimately, this chapter demonstrates that continuous innovation in control valve technology is essential for meeting the evolving demands of modern industrial processes, ensuring both efficiency and safety across a broad spectrum of applications.

2.1 Industrial Applications of Control Valves and Cryogenic Applications

The application of control valves in process industries provides safe and efficient operations addressing the complex demands of modern processes. In the context of cryogenic applications, Barron (1985) outlines the complexities associated with using cryogens, including the designs necessary to maintain integrity under extreme low temperature conditions. First, outlining the two modifications of cryogenic control valve designs which are necessary to efficiently maintain a cryogenic environment, which include extended-stem valves and vacuum-jacketed valves.

Extended-stem valves are akin to conventional valves but feature a lengthened stem. This design feature serves to keep the valve actuator or handle at ambient temperatures, while ensuring minimal thermal heat in-leak to the cryogenic process. Additionally, this extended stem configuration allows sealing to occur at ambient rather than cryogenic temperatures, which significantly enhances valve reliability by addressing common sealing issues encountered at extremely low temperatures [3].

Vacuum-jacketed valves are an evolution of the extended-stem valve, with the addition of a vacuum jacket that surrounds both the extended stem and the valve body, further minimizing heat transfer. Within the vacuum jacket, it is often designed with multilayer insulation to reduce heat leakage and improve thermal efficiency surrounding the valve body. This construction allows for convenient maintenance, as the valve stem, plug, and seal can be removed for inspection without disturbing the vacuum integrity of the system. The incorporation of these design features plays a critical role in reducing heat in-leak, which in highly energy intensive cryogenic processes leads to appreciable operational cost savings.

Two-phase flow phenomena frequently occurs when a fluid exists in both liquid and gas phases simultaneously, and it commonly arises in systems where the fluid is subjected to significant temperature and pressure variations, such as cryogenic applications [3]. In cryogenic systems, the working fluid often operates at low temperatures near its boiling point, where it can coexist as both liquid and vapor. This phenomenon typically happens in processes like heat exchangers, piping systems, and dewars[3].Two-phase flow encountered in cryogenic fluid systems, complicate the prediction of pressure drops due to the variability in flow patterns, which can include stratified, wavy, slug, and annular flows. These flow regimes can vary along the length of the piping because of changes in fluid quality due to heat transfer or pressure variations. As such, understanding these flow characteristics is essential for the effective design and optimization of cryogenic control valves [3].

Bruckner et al. (1996) highlight significant advancements in low-temperature valve technologies, focusing on the design improvements that enhance reliability and performance. They discuss the importance of developing valves that can withstand the unique demands of cryogenic applications, emphasizing the need for innovative materials and construction methods. These advancements address challenges such as maintaining material integrity at extremely low temperatures, minimizing heat in-leak, and ensuring precise flow control despite applications

involving phase changes of cryogenic fluids like helium and nitrogen [8].Materials such as austenitic stainless steels and specialized alloys are used for cryogenic valves, ensuring they can endure thermal cycling without significant degradation. The use of such materials not only improves the lifespan of the valve components but also enhances sealing capabilities, which are critical in preventing leaks that could compromise system stability and conservation of the process fluid [9].

Bruckner et al. also explore design improvements related to valve actuation mechanisms. In cryogenic systems, the reliability of actuator is challenged by extreme temperatures, which can impact the performance of pneumatic or electric actuators. The authors highlight the development of actuators with improved thermal insulation and robust mechanical linkages that ensure reliable performance even in severe conditions [8].

The insights provided by Bruckner et al. (1996) are complemented by the work of Sotoodeh (2022), who discusses cryogenic valve design features specifically within the context of liquefied natural gas (LNG) plants. Sotoodeh emphasizes the importance of sealing and flow characteristics under varying pressures and temperatures, which aligns with the challenges highlighted by Bruckner et al. The use of specialized materials and construction techniques, such as multi-layer insulation and advanced sealing mechanisms, are critical in maintaining system integrity in LNG applications, like the requirements present in other cryogenic systems. These design strategies are instrumental in preventing heat in-leak and ensuring the reliability of cryogenic control valves, thus demonstrating how advancements in valve technologies are applied across different sectors of industry [10].

Barron (1985) and Bruckner provide foundational insights into the complexities associated with cryogenic systems, including the specific requirements for maintaining valve integrity under extreme conditions. Barron's work underlines the necessity for specialized valve types, such as extended-stem and vacuum-jacketed valves, which are designed to mitigate the effects of heat in-leak and thermal stresses. The principles discussed by Bruckner et al. align closely with those described by Barron, particularly regarding the need for innovative materials and construction methods to ensure reliable performance. These valve designs considerations are critical in minimizing heat transfer and accommodating the unique fluid dynamics associated with cryogenic conditions, such as two-phase flow and rapid phase transitions [9].

Collectively, the studies by Bruckner et al. (1996), Sotoodeh (2022), and Barron (1985)

provide details on the evolution of cryogenic valve technologies and their application across various industries. These advancements underscore the importance of continuous innovation in materials, design, and construction techniques to meet the stringent requirements of cryogenic systems. The lessons learned from these studies provide valuable insights into developing robust cryogenic control valves capable of ensuring efficiency, reliability, and safety in demanding industrial environments.

2.2 Control Valve Plug Design

In pursuit of an effective and reproducible plug design for a variety of process applications, analytical equations are necessary to design control valve plugs with respect to a typical performance metric, known as the flow coefficient. Various design methodologies based on analytical equations require the use of the flow coefficient as a basis for comparative measurement. These analytical equations are not solely applicable to cryogenic applications discussed in the previous section. The flow coefficient (for incompressible fluids) can be calculated from the mass flow, inlet density, and pressure drop across the valve, as expressed in Eqn. (2.1) [11]. However, for compressible fluid, such as gaseous nitrogen, the flow coefficient equation is not as straightforward. As provided in the ISA Control valve standards, a method for an initial equation to size for a C_v is denoted, as described in Eqn. (2.2) [6]. However, both the compressible and incompressible equations for C_v can be further refined through iterative methods as outlined in the ISA standards [6].

$$C_v = Q\left(\frac{\rho}{\sqrt{\Delta P}}\right) \tag{2.1}$$

$$C_v = \frac{W}{N_6 Y \sqrt{x P_1 \rho_1}} \tag{2.2}$$

A shortcoming of using the ISA: Flow Equations for Sizing Control Valves and general equations to determine flow coefficient is determining the valve plug profile necessary for a given target C_v. Establishing the required valve C_v, the ISA Standard equations can be used to back out necessary parameters such as flow rate and pressure drop. But the challenge remains of designing the proper valve plug profile (contour as denoted in Weidmann and Rowan [12]) to match the target C_v.

The design of the plug profile is necessary to ensure that proper flow with respect to valve opening. Three ubiquitous equations outlined in ‘Coulson and Richardson’s Chemical

Engineering'[11] and other sources in various forms provide preliminary valve characteristics: equal percent (Eqn. (2.3) [11]), linear (Eqn. (2.4) [11]), and quick opening (Eqn. (2.5))[4] [11]. Additionally, rangeability (denoted as R) for an equal percent characteristic valve is ratio of maximum flow coefficient to minimum flow coefficient [4]. The non-dimensional plug travel, or non-dimensional stroke, is defined as ξ. This parameter ranges from 0 to 1, where 0 is fully open, providing a maximum flow coefficient, and 1 is fully closed, with the plug being fully seated.

$$C_V = C_{V,max} \cdot R^{(\xi-1)} \tag{2.3}$$

$$C_V = C_{V,max} \cdot \xi \tag{2.4}$$

$$C_V = C_{V,max} \cdot \sqrt{\xi} \tag{2.5}$$

$$R = \left(\frac{C_{v,max}}{C_{v,o}}\right) \tag{2.6}$$

Wiedmann and Rowan (1956) highlight several key design strategies for optimizing control valve plugs, including the use of contoured plug profiles to achieve desired flow characteristics such as equal percentage, linear, or quick opening. The authors also discuss the importance of rangeability, as defined in Eqn. (2.6) [4]. High rangeability is desirable in applications where the valve must perform effectively across a broad spectrum of flow rates. Wiedmann and Rowan (1956) emphasize that the choice of plug profile can significantly impact rangeability, and therefore careful consideration must be given to the specific requirements of the application when designing the plug. Weidman and Rowan strongly suggest maintaining the rangeability of the valve between 20 and 50 [12].

Furthermore, Wiedmann and Rowan (1956) delve into the role of flow dynamics in plug design. Understanding the interaction between the fluid and the valve components is essential for minimizing energy losses due to entropy generation (*i.e.* turbulence, flow separation, *etc.*). The authors suggest that contoured plug designs can help streamline the flow path, thereby reducing pressure drop across the valve and minimizing the losses. By optimizing the plug geometry, it is possible to achieve smoother flow transitions and reduce the likelihood of flow instabilities that can negatively affect valve performance.

The plug contour (or plug profile) presented by Wiedmann and Rowan is chosen by developing a plug around the surface area of a truncated cone, as detailed in Appendix B [12].

Essentially, the described method establishes a flow area and then uses this flow area in conjunction with the plug diameter to determine the contour of the plug for a truncated cone. At the time, this was a sufficient way to reliably back out a conical plug design for an equal percentage plug. Since this publication, there has been a lack of additional comprehensive analytical design procedures available in open literature.

Additionally, Patel's study [13] is further discussed in **Section 2.5**, it is worth noting here that there was a method of designing an equal percent flow plug, however the shortcomings of this study was that it required CFD modeling to back out the desired equal percent characteristics. Using the program ANSYS Fluent and then curve fitting that data at each point of flow coefficient versus valve lift position calculated a polynomial to create a plug radial profile (radial contour). This method was not proven experimentally and is using numerical analysis to find the plug shape unlike Weidmann and Rowan's analytical design.

Other analytical methods based upon flow area were discussed in sources [14] & [15]. Although, these models are able to generate a characteristic curve for a given valve plug (Flow coefficient versus opening percentage) this was previously well documented in both Weidmann and Rowan [12] as well in various other sources [11] [6]. However, there is a lack of a generalized design methodology in designing a proper flow plug for a given characteristic. This is significant, in the sense of validating what has been done in ISA sizing and previous handbooks [5]. However, the lack of analytical models to develop new valve profiles (or contours) without the restraint of a single conical shape seen in Weidmann and Rowan are lacking.

2.3 CFD Modeling of Control Valves and Control Valve Plugs

CFD has become fundamental in the design and analysis of control valves, enabling detailed numerical analyses of flow characteristics prior to experimental validation. The work of [16] provide a comprehensive methodology into designing the geometry of a globe control valve. Within the context of the control valve plug, a 2-D axisymmetric analysis methodology is used. Note: The ISA flow coefficient equation used is for incompressible non-cavitating flow. Three plugs are modeled, with the first having linear characteristics and the other two equal percent characteristics. An example of the numerical model setup is provided in *Figure 2.1*. They denote that the 2-D geometry computes faster than the respective 3-D model, which is useful when modifying stroke positions and plug geometries quickly while maintaining reasonable computational times.

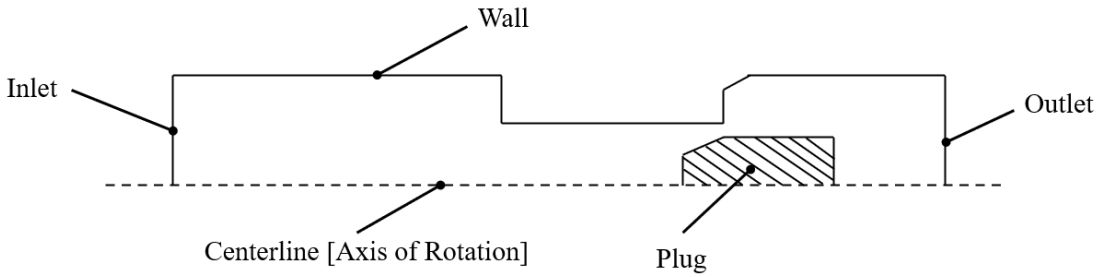

Figure 2.1: Generic 2-D Axisymmetric Valve Plug Geometry for CFD

Davis and Stewart modeled both linear and equal percent valve plug profiles. The analysis was performed in 10% stroke increments [16]. In this context, the gap between the valve plug diameter and the throat (opening) diameter was kept large enough to enable sufficient meshing for stable and accurate results. Additionally, it is noted that the *k*-epsilon turbulence model was implemented in the analysis; however, the specific justification for this selection was not provided. According to the authors, changing the turbulence model (while maintaining the default parameters) had little to no effect on the numerical results [16]. The boundary conditions required by their ANSYS simulations included a symmetry condition at the centerline, a no-slip condition at the wall, a specified inlet velocity (which converts to mass flow), and a uniform pressure at the outlet.

Numerical results from the analysis were compared to experimentally obtained performance characterizations. The general trends seen for the linear plug from 10%-70% showed the anticipated linear trend for flow coefficient versus percent opening, however at higher stroke percentages the model overpredicts flow coefficient. Moreover, for the equal percent plugs, the agreement between numerical and experimental results showed good agreement until 90% open, where a maximum error of ~12% was seen.

The results gleaned from the numerical and experimental comparison indicated that qualitatively it matches the valve characteristics. However, as the valve opens to higher stroke percentages the error increases considerably. Therefore, it is a good indicator of qualitative trends, such as classifying a valve plug as linear or equal percent, however, experimental results are still necessary for complete performance characterization [16] [17].

Sreekala and Thirumalini investigated globe valves with cage apertures using ANSYS FLUENT, with a methodology for improved flow performance analysis. This method utilized a 3-D model and refined mesh, as well as the k-Epsilon turbulence model. The goal of the model was to back out the valve flow coefficient given an input of mass flow and a specified outlet pressure to find the pressure drop through the aperture [15], similar to [16]. However, a different geometry was considered for this study. A similar trend using numerical analysis was observed, with the experimental and numerical results aligning more closely at lower percent opening and diverging at higher precent openings.

Patel et. al describes plug characteristics with respect to flow coefficient and percent opening and detail the design of a valve plug including numerical results for cryogenic flow [13]. First, a design for an equal plug with basic geometry was analyzed to establish and validate the numerical model within ANSYS. As before, the k-epsilon model was selected while again denoting that there is little to no effect when compared to the results using other turbulence models. Furthermore, to solve for the pressure drop to enable calculation of the flow coefficient, a mass flow (inlet velocity) is selected as well as an outlet pressure. The fluid chosen was liquid helium at 4.5K, allowing for analysis of the control valve for cryogenic applications.

As mentioned by other authors, the significance of a proper mesh is stressed especially for their 3-D geometry where an excessive number of nodes will cause a significant increase in computational cost and time. The criteria checked in this case was the aspect and Jacobian ratios approaching a value of one, and the skewness approaching a value of one-half.

A shortcoming from this study is that there was no experimental validation of the numerical results. While their numerical model aligned well with a maximum RMS error of 1.5, there is no clear indication that the valve characteristics displayed in the model would necessarily be achieved in experimental applications. As seen in previous studies, the top end of the stroke usually starts to deviate from the experimental results and therefore may not accurately characterize the valve performance in this region.

CFD modeling is a useful computational tool, however, unless validated experimentally, caution should be taken when using the results. While results from analytical and numerical models may produce the desired performance characteristics, experimental valve characteristics detail the real-world effects and may diverge from the solutions obtained from modeling.

2.4 Experimental Studies with Control Valve Plugs

Experimental validation remains critical to confirm the accuracy of theoretical models and ensure effective control valve performance in real-world applications. This was advocated for when Weidmann and Rowan commented on this observation after an analytical model underpredicted the flow coefficient when compared to experimental testing. Similarly, the research highlighted in **Section 2.3** have an experimental validation component or advocate for experimental testing.

Davis and Stewart (2002) in Part II of their research on control valve performance emphasized the importance of experimental verification in predicting globe control valve performance. This study highlights the correlation between simulation results and actual performance metrics, providing a framework for validating CFD models through experimental data [17]. The researchers conducted a series of controlled experiments to measure parameters to calculate flow coefficient, such as pressure drop, and response time, comparing these results to the predictions made by CFD simulations. This linkage between theory and practice is essential for ensuring the desired performance characteristics of control valve designs in practical applications.

The experimental test-setup was created by connecting the valve, known as 'Test Section', to a flow meter, and two pressure gauges to account for pressure drop across the valve. Experimental uncertainty is also emphasized accounting for instrument error and its effect on further calculations. This study also underscores the role of experimental testing in identifying discrepancies between modeled and observed behaviors. Such discrepancies can arise due to simplifications in the CFD models, such as assumptions about fluid properties or boundary conditions that do not fully capture the complexities encountered during real-world operation. It is seen that the CFD model had a maximum error of 21% compared to the experimental measurements.

Furthermore, Geng et al. (2024) performed an experimental study to analyze flow characteristics and rangeability of plug control valves, contributing valuable empirical data to the understanding of valve behavior [15]. The findings from this study provide insight into how well theoretical models align with actual performance, reinforcing the need for empirical testing in the design process. The study utilized a range of operating conditions to assess the valve's behavior under different flow rates and pressure drops, allowing for a comprehensive comparison between predicted and observed performance metrics. As seen in [17], a similar test-bench is created where the 'Test Section' is accompanied by an upstream throttle valve, flow measuring device, pressure

taps, temperature measurement, and a downstream throttle valve. Geng reiterates the idea that although the plugs are designed for equal percent characteristics, the actual installed characteristics deviate to various degrees due to manufacturing errors. Also, it is emphasized that lower flow maximum flow coefficient plugs are prone to manufacturing errors which cause greater distortion in the flow area. Smaller flow coefficient plugs, with current fabrication equipment at FRIB, needed a tolerance of +-0.0002 in. of the plug profile's diameter due to the resolution required to capture the diameter gradient between geometric profile points in the analytical model.

The experimental results from Geng et al. also highlighted the importance of rangeability in plug valve design, showing that the ability to maintain effective control over a wide range of flow coefficient change is essential for optimizing valve performance. By testing different plug configurations, the study was able to determine which designs provided the most stable and reliable control, contributing to the development of guidelines for plug design in cryogenic control valves. The measured experimental data is invaluable for validating computational models, such as those developed using CFD, and ensuring that the valve designs are robust enough to handle the complexities of real-world fluid dynamics.

The combination of experimental studies by Geng et al. (2024) and Davis and Stewart (2002) demonstrate the critical role of empirical validation in the design of control valves. Experimental testing not only helps validate the accuracy of theoretical models but also provides insights into the practical challenges that may not be fully captured in simulations. By integrating experimental findings with computational models, engineers can develop control valve designs that are both theoretically sound and practically effective, ensuring reliable performance across a wide range of industrial applications, including those involving cryogenic fluids.

2.5 Control Valve Plug as a Flowmeter

The use of valve plugs as flowmeters was an innovative approach to measuring flow rates in control systems without the need for additional equipment. This method utilized the inherent relationship between valve position, flow characteristics, and differential pressure to calculate the flow rate, effectively combining control and measurement functionalities without the need for a more expensive counterpart such as a Coriolis flowmeter. The ideality of no flowmeter installed would minimize heat-in leak for cryogenic systems as well.

The dual-purpose use of a control valve as both a flowmeter and a flow controller introduce an alternative to conventional flow measurement and control setups. Traditionally, flow control

systems consist of separate components: a flowmeter, a control valve, pressure sensors, and a controller to adjust the valve position based on the setpoint and feedback. However, as outlined by Atmanand and Konnur (1999), Choi (2012), and Z. Ma et. al (2019), the inherent pressure drop across a control valve can be leveraged for flow measurement, thereby eliminating the need for a standalone flowmeter device [18].

Control valves regulate flow by introducing a restriction of flow area due to plug geometry, causing a differential pressure across the valve. By developing a relationship between the differential pressure and the mass flow rate, the valve itself can serve as a flowmeter. The fundamental relationship for this is derived from the control valve's flow coefficient, which relates flow rate to parameters such as differential pressure, inlet pressure, fluid properties. Therefore, based upon proper stem calibration the valve position (in % or mm) and the flow coefficient (C_v). Classification of the valve position vs flow coefficient can be found.

This method requires calibration of the valve to determine its flow coefficient characteristics at various positions (stroke), real-time measurement of differential pressure, static pressure, and temperature, and a processor or data acquisition system to compute the flow rate iteratively based on the valve's position and the calibrated flow coefficient data.

Atmanand and Konnur (1999) proposed a novel method of utilizing a control valve for both measurement and regulation of flow. By relating the differential pressure to mass flow rate, the need for additional equipment (flowmeter) could be eliminated. Although this method can be used for any fluid, the experimental fluid used was air. The flow coefficient was determined by experimental data for the differential pressure, inlet pressure, temperature, and valve position. To properly use the valve as a flowmeter, calibration is needed. To calibrate the control valve for a specific plug, the mass flow is computed, and then the difference between the actual and set flow rate was minimized. The specific plug used was a 'conventional plug-type control valve of 50mm size'. The valve stroke was measured using an LVDT, also known as the linear variable differential transformer, as discussed in **Chapter 1**, The flowmeter used to validate the actual versus set flow was a servo positive-displacement flowmeter. Considering additional equipment such as pressure and temperature sensors, the overall accuracy of the system was ±1.5%. Once calibrated, the flow coefficient versus position can be used solely with a control valve and that specific valve plug to compute mass flow rate [18].

Similarly, Choi (2012) and Mu et al. (2019) advanced the concept of eliminating standalone

flowmeters based upon the same concept, with a more detailed and focused approach on butterfly valves and flow coefficient estimation. The principles of the flow coefficient are the same, therefore the same measured data was recorded being the inlet pressure, differential pressure, temperature, mass flow rate, and valve position. The curve-fit for the flow coefficient versus stroke percentage was fit based on an $R^2 > .99$ [19].

While Choi (2012), validates Atmanand and Konnur's (1999) work utilizing a different valve type, Mu et al. (2019) expands on this specifically for use in HVAC systems. The study developed a flow model based on the Bernoulli equation, with the discharge coefficient (C_d) as a critical parameter. Computational Fluid Dynamics (CFD) simulations and experimental validation revealed that C_d stabilized at 0.67–0.70 for Reynolds numbers (Re) exceeding 5000. The system demonstrated minimal measurement errors (less than 5%) when validated experimentally and a significant reduction in permanent pressure losses at larger valve openings. By integrating measurement and control into a single valve, this approach offers a practical, energy-efficient solution for HVAC systems [20].

The proposed methods offer advantages by eliminating the need for a dedicated flowmeter, thereby reducing equipment costs, and minimizing losses caused by the additional pressure drop introduced by certain conventional flowmeters. Furthermore, the approach can be implemented with modern control systems for real-time computation and control. The accuracy of flow measurement is heavily influenced by the precision of pressure and temperature measurements, as well as the valve's calibration data. Additionally, determining the flow rate requires calculations, which necessitate additional workload. While laboratory results are promising, broader implementation in industrial settings requires further testing to validate the approach in field conditions with the help of CFD modeling.

The ability to integrate flow measurement and control into a single device is particularly advantageous for cryogenic systems, where minimizing additional components and heat-in leak is crucial. By adapting the principles outlined by the above research, cryogenic control valves can achieve enhanced efficiency and reduced complexity, making this approach a valuable addition to process engineering.

2.6 Conclusion

Control valves are essential components in industrial systems that require precise control of fluid flow and pressure. As industrial processes evolve, the need for advanced valve technologies,

particularly in cryogenic applications, becomes increasingly important. Cryogenic systems present unique challenges, such as thermal contractions of materials, phase transitions of the process fluid, minimization of heat transfer to the process, and material fatigue, which require specialized valve designs to ensure reliable performance.

Advancements in valve plug design, including the use of innovative materials and equal percent plug configurations, have improved the precision and durability of control valves. CFD modeling has become a valuable tool for optimizing valve designs, allowing engineers to simulate fluid dynamics and predict potential issues before physical testing. However, experimental validation remains critical to confirm the accuracy of theoretical models and ensure that control valves perform effectively in real-world applications.

Ongoing research in control valve technology, including the integration of neural network technologies [21] and advanced materials, will continue to drive innovations that enhance performance, efficiency, and safety in industrial applications. As the demand for more efficient cryogenic systems grows, the development of specialized control valves will play a key role in meeting the challenges posed by these extreme conditions.

Chapter 3: DEVELOPMENT OF VALVE FLOW CHARACTERIZATION TEST BENCH

3.1 Overview of Test Setup

The development of a test bench was necessary to characterize the performance of cryogenic control valve plugs accurately. This test bench enables the systematic evaluation of mass flow rate, pressure drops, inlet pressures and temperature under controlled operating conditions, which is crucial for validating the design of each valve plug and their associated flow characteristics. *Figure 3.1* shows the P&I diagram for the control valve test bench, which includes the various components required to measure parameters of interest.

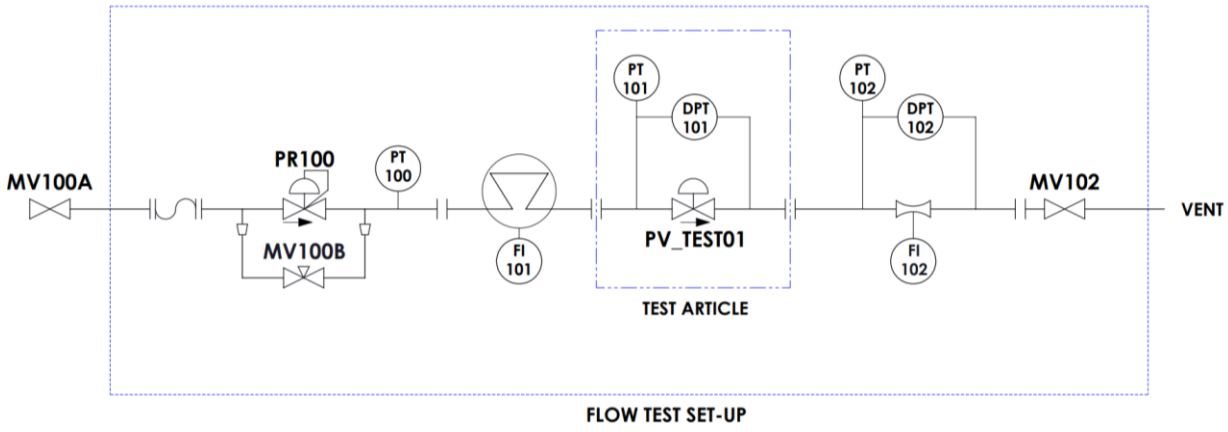

Figure 3.1: Test Bench - Process and Identification Diagram

As structured in *Figure 3.1*, the overall control volume is denoted as 'FLOW TEST SET-UP,' which encompasses the entirety of the test loop, while the cryogenic control valve and its associated instrumentation are denoted as 'PV_TEST01.' This test setup is designed to regulate the pressure upstream of the valve, enabling precise flow control and performance characterization of the test article (flow plug). The setup incorporates measurements of pressure both upstream and downstream of the cryogenic control valve being characterized. The coriolis flow meter provides accurate mass flow rate readings and upstream temperature. In addition to the coriolis flow meter, a venturi is also encorporated to validate the flow measurement. Differential pressures are recorded across both the venturi tube and the test article (control valve) to quantify the mass flow and flow coefficient, respectively. The operating fluid used was ambient gaseous nitrogen supplied by MV100A.

The various tests involved the installation and evaluation of seven distinct flow plugs, each tailored to specific use cases. As seen in *Figure 3.2*, The 3-D Model and actualized test-setup(*Figure 3.3*) are shown with slight variation in pipe orientation due to limitations with spacing and piping.

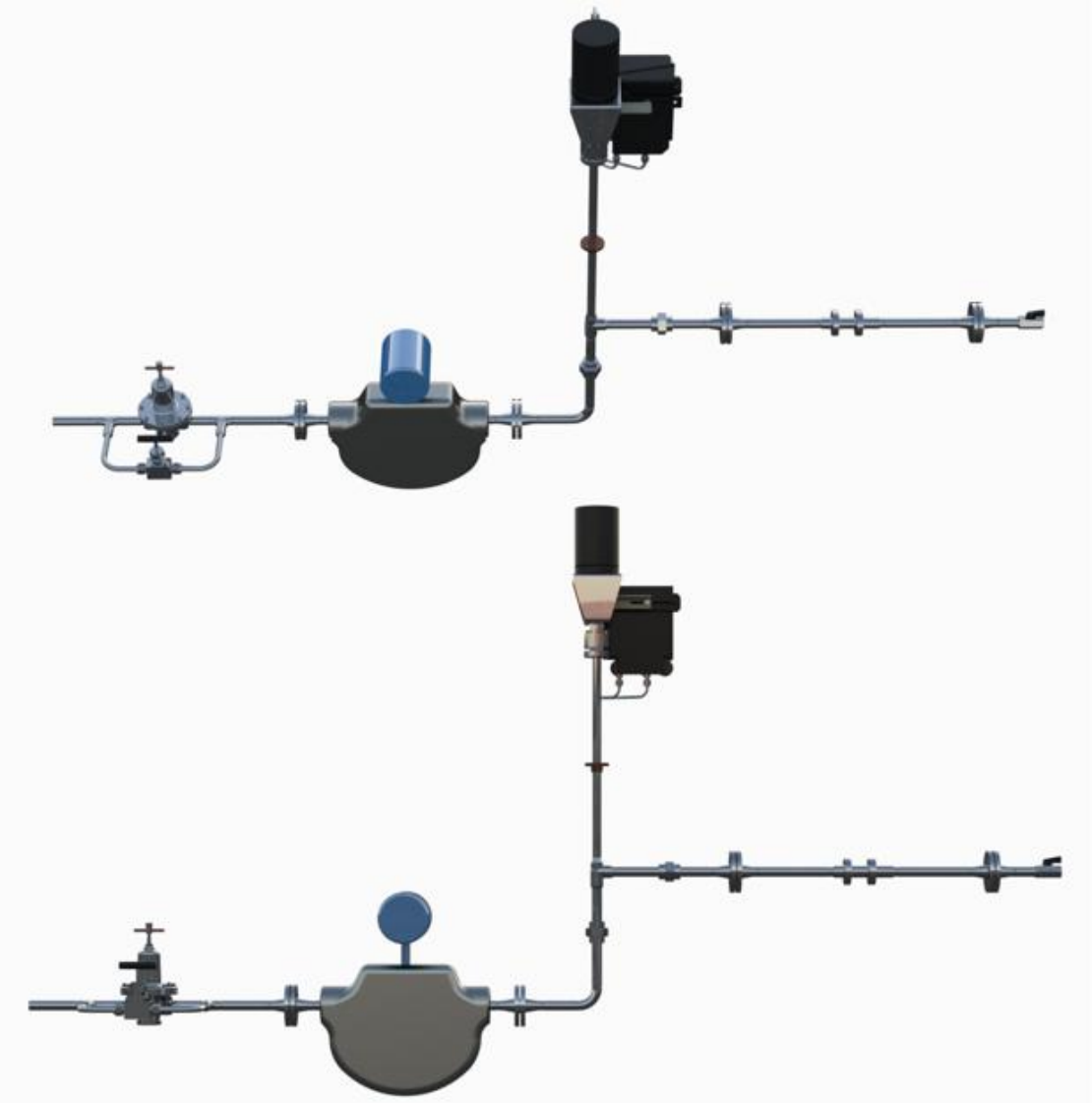

Figure 3.2: Test Bench Model Angled (Top) and Front-Facing (Bottom)

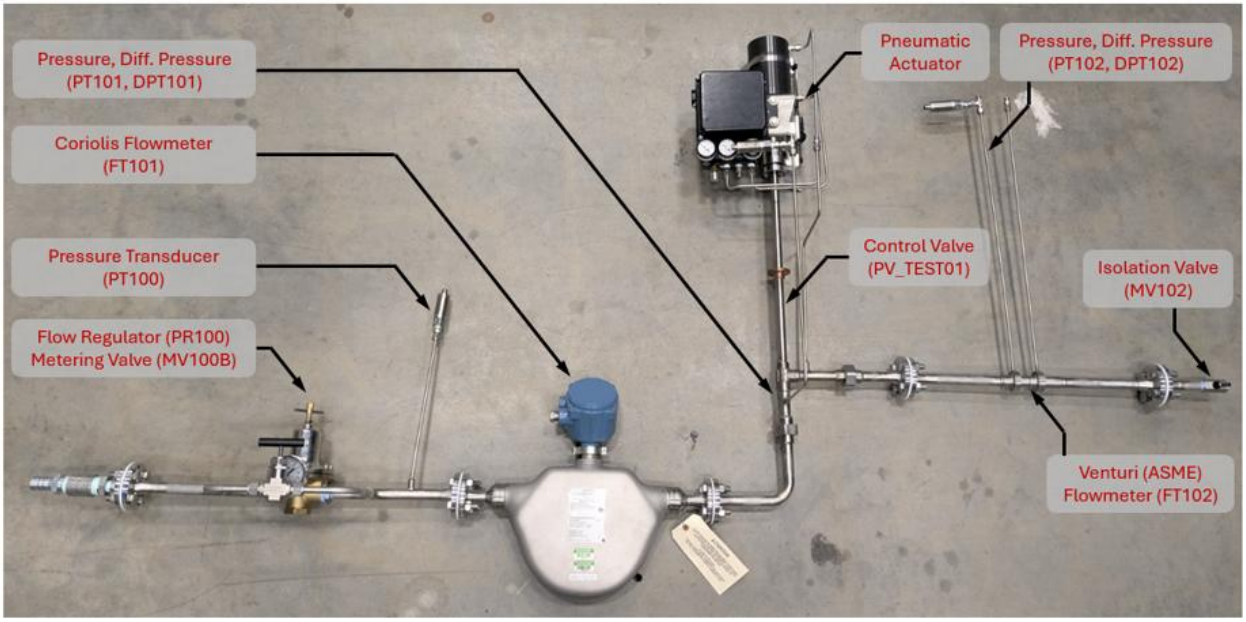

Figure 3.3: Test Bench Set-up

Detailed results for these plugs, including their respective analytical performance characteristics, are summarized in *Table 3.1*. Discussion of the analytical model and experimental validation are dicussesd in detail within the later chapters. The comprehensive instrumentation and modular design of this setup provide a robust platform for evaluating control valve performance over a wide range of operating conditions.

Table 3.1: Valve Plug Models Tested

Part ID [-]	$C_{v,m}$ [-]	R [-]	ℓ_{stroke} [in.]	ℓ_{plug} [in.]	D_{Base} [in.]	Character [-]
OEM	1.0	9.1	0.75	0.875	0.4105	Eq %
A1	0.3	3.0	0.75	0.948	0.411	Eq %
A2	0.3	3.7	0.75	0.948	0.412	Eq %
A3	0.3	7.4	0.75	0.946	0.414	Eq %
A4	0.3	3.7	0.75	1.000	0.412	Eq %
B1	0.8	7.9	0.75	0.920	0.411	Hybrid
B2	0.8	9.9	0.75	0.919	0.412	Hybrid
B3	0.8	19.7	0.75	0.915	0.414	Hybrid

Table 3.1 summarizes the specifications of the seven novel plug designs and OEM, highlighting their desired maximum flow coefficients ($C_{v,m}$), profile lengths (based on valve stroke and plug diameter derived from the analytical model in Chapter 4), and corresponding rangeability. The rangeability values are determined using the characteristic equations outlined in Chapter 2.

The overall length of each plug was tailored to meet specific design requirements, particularly the shape of the plug tip. For instance, designs A2 and A4 share identical analytical characteristics but differ in overall length; A2 features a blunt tip, while A4 incorporates a sharp tip. Each plug was tested across the full range of valve stroke in 5% increments, ensuring consistent operating conditions and utilizing the same equipment for all tests.

3.2 Instrumentation and Component Selection

The test bench P&I displays both the test article and overall control volume, including the individual components populated within each of these regions. The denotations for pressure, temperature, mass flow and differential pressure sensors are referred to as *PT, T, FI, and DPT*, respectively. Specifications of each of the components used within the test bench are provided in *Table 3.2*, and include the test bench identification number as shown in the P&I.

Table 3.2: Process Instrumentation Chart

Instrument Type	***Instrument Tag (Ref Figure P&I)***	***Fluid Service***	***Vendor***	***Part Number***	***Range (min to max)***	***Accuracy***
Test Article (Cryogenic Control Valve)	PV_TEST01	Helium	[-]	[-]	[-]	[-]
Digital Caliper	PV_TEST01	[-]	Mitutoyo [22]	572-211-30	0-150 mm	0.01mm
Pressure Regulating Valve	PR100	Nitrogen	McMaster-Carr [23]	49305K23	5 to 55 psig spring	[-]
Pressure Gauge	PI100	Nitrogen	McMaster-Carr [24]	4088K6	0 to 100 psig dial	[-]
Metering Valve	MV100	Nitrogen	Swagelok [25]	SS-18RS8	0 - 5.5 Flow Coeff.	[-]
Ball Valve	MV102	Nitrogen	McMaster Carr [26]	45395K214	1 - 5.5 Flow Coeff.	[-]
Pressure Transducer	PT100	Nitrogen	GE/UNIK [27]	PTX 5062-tc-a1-ca-h0-pe	0 to 7 bar	.04% of Span
Pressure Transducer	PT101	Nitrogen	GE/UNIK [27]	PTX 5062-tc-a1-ca-h0-pe	0 to 7 bar	.04% of Span
Pressure Transducer	PT102	Nitrogen	GE/UNIK [27]	PTX 5062-tc-a1-ca-h0-pe	0 to 7 bar	.04% of Span
Temperature Sensor	T101	Nitrogen	Emerson [28]	CMFS025M	33.15 K - 623.15 K	0.5% of Reading
Differential Pressure Transducer	PDT101	Nitrogen	Rosemount [29]	3051CD1A1AS5Q4	0 to 62.1 mBar	.10% of Span
Differential Pressure Transducer	PDT102	Nitrogen	Rosemount [29]	3051CD2A02A1AS5	0 to 620 mBar	.10% of Span
Coriolis Flow Meter	FI101	Nitrogen	Emerson [28]	CMFS025M	0 – 25 g/s	0.25% of Reading
Venturi	FI102	Nitrogen	Flow-Dyne	VP050270SB	[-]	Calculated

Cryogenic Control Valve

The cryogenic control valve is the focal point of the test bench. This valve was studied with

a particular emphasis on the performance and design of the installed flow plug. Different plug geometries were tested to evaluate their flow characteristics and suitability for achieving equal percent flow control at varied process specifications.

The plug's design directly impacts the valve's ability to regulate flow rates with precision. By interchanging and testing different plug configurations, the study aimed to develop plug designs that enhanced flow control and ensured consistent performance under cryogenic conditions. The data gathered during this testing phase will contribute to the broader goal of advancing cryogenic control valve technology.

The cryogenic control valve installed in the flow test bench is shown in *Figure 3.4*, displaying the positioner body, overall stem length, thermal intercept, and pressure taps designed to measure absolute and differential pressure across the test article. The actuator body panel was opened to adjust the stroke changes to capture the same resolution of movement at each 5% step change, therefore both the bottom spring and mechanical lever were adjusted to achieve this at the low and high end of the stroke, respectively.

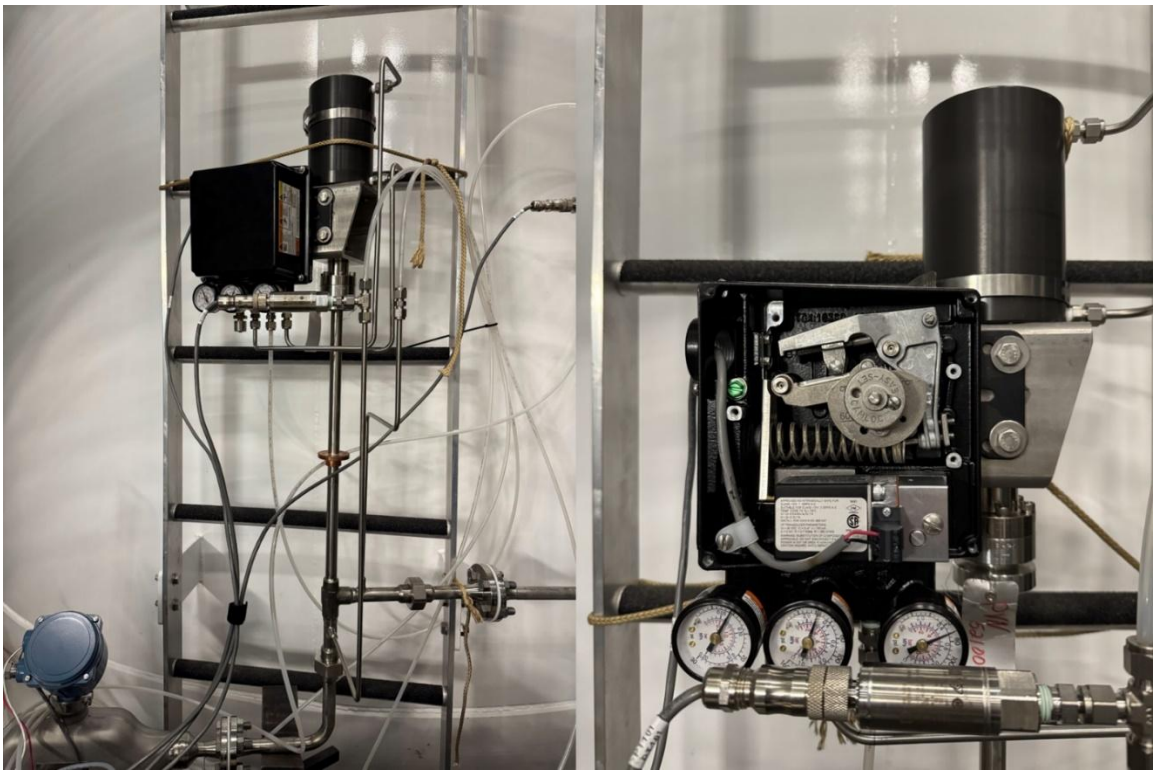

Figure 3.4: Cryogenic Control Valve within Test Bench (Left) and Positioner Internals (Right)

Flowmeters

The Coriolis flow meter (Emerson), depicted in blue on *Figure 3.5*, is a precision instrument that directly measures mass flow based on the Coriolis effect. This phenomenon occurs when fluid flowing through vibrating tubes induces measurable phase shifts due to the fluid's inertia. In this setup, the Coriolis flow meter provides high-accuracy measurements of mass flow in units of g/s, ensuring precise data collection for experimental analysis. Unlike volumetric flow meters, it directly measures mass flow independent of fluid properties, eliminating the need for density or temperature corrections. Additionally, this specific model incorporates an integrated temperature sensor (T101), which records the fluid's temperature at the inlet. These features make it indispensable for ensuring reliable and repeatable measurements. The accuracy, as displayed in *Table 3.2* is .1% of the mass unit per time unit reading.

Figure 3.5: Emerson ELITE Coriolis Flow Meter [29]

Figure 3.6: Coriolis Inner Body [29]

As seen in *Figure 3.5*, the Coriolis flow meter is displayed as a front facing graphic like *Figure 3.3*. However, the main difference seen is the detachment of the sensor head in the actualized test-set up. Additionally, in *Figure 3.6* the inside view from the bottom up is shown, with the vibrating tubes and additional supports being shown without the outer body casing. The minimum measurable mass flow rate through the Coriolis flow meter is approximately 0.45 grams

per second. Therefore, measurement of flow rates below this value required the instillation of a venturi tube flow meter, which was installed downstream of the control valve.

The venturi tube flow meter complements the Coriolis flow meter by providing a secondary method for measuring mass flow, thus enabling cross-validation of flow data. The venturi meter operates on the Bernoulli principle, utilizing the relationship between pressure and velocity in fluid flow to determine mass flow rate. As fluid flows through the constricted section of a venturi tube, its velocity increases, causing a measurable pressure drop. This pressure differential, combined with temperature and inlet pressure data, enables calculation of the mass flow rate using the Bernoulli equation and the continuity principle [30].

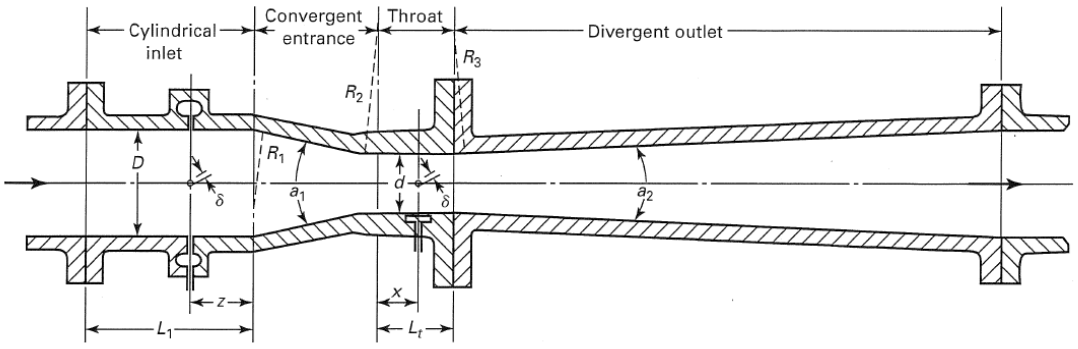

Figure 3.7: Venturi Cross-Section [31]

The cross-sectional area of a typical venturi tube is provided in *Figure 3.7*, denoting the upstream (inlet) and throat diameters as D and d, respectively. The values of the installed venturi tube diameters are provided in *Table 3.2*, listed as D_1 and D_2.

In this test bench, the Coriolis flow meter (FI101) serves as a validation tool for the venturi tube (FI102). The differential pressure (PDT102) across the venturi is measured, while the inlet pressure (PT102) and temperature (T101) provide additional parameters for an accurate density calculation. Using these measurements, the mass flow can be calculated by Eqn. (3.1)[31]:

$$\dot{m} = \frac{\xi \epsilon \pi d^2}{4\sqrt{1-\beta^4}} \sqrt{2\Delta P \rho} \tag{3.1}$$

By comparing the mass flow rate derived from the venturi with the direct measurement provided by the Coriolis Flow Meter, any discrepancies can be identified and accounted for, ensuring accuracy and cross-verification between the two measurements. This redundancy is

particularly valuable in experimental setups, as it helps to validate the reliability of the flow data under varying operating conditions.

In *Figure 3.8*, the mass flow rate through the venturi was determined using Eqn. (3.1). While the Coriolis flowmeter is highly accurate, with a precision of ±0.25% of the measured flow, it displayed reliable readings only for flow rates exceeding 2 g/s. At flow rates below 0.4 g/s, the Coriolis flowmeter was unable to register any readings. Additionally, for flow rates below 2 g/s, the relative error exceeded 5%, suggesting that the accuracy specified in *Table 3.2* is applicable only for flow rates above this threshold. The trendline of the Flowmeter Reading, represented by $y=0.967x$, indicates that the Coriolis flowmeter consistently underpredicted the mass flow compared to the venturi calculation, with significant underprediction and increased relative error with respect to the venturi at flow rates below 2 g/s. Consequently, for the error analysis of the flow coefficient, the venturi-calculated mass flow was utilized for consistent analysis.

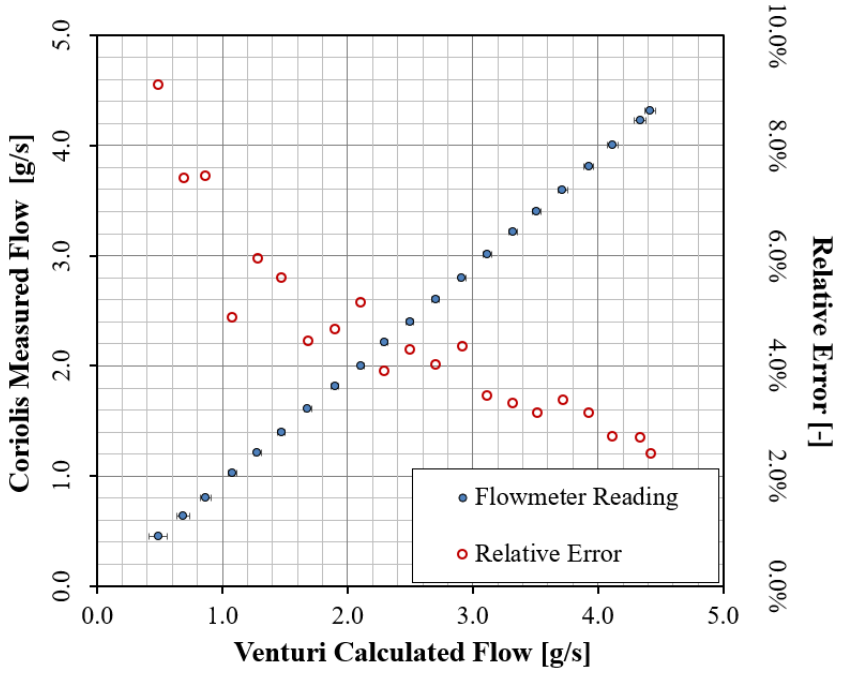

Figure 3.8: Flowmeter Calibration

Pressure Measurements

The test bench incorporates pressure taps, which connect to Rosemount differential pressure transmitters and GE/UNIK 5000 pressure transducers for accurate pressure monitoring and data.

The Rosemount differential pressure transmitters measure the pressure drop (DPT101 & DPT102) across the control valve (FI101) and venturi tube (FI102), respectively. By connecting the pressure taps upstream and downstream of each component, the transmitter provides accurate data required for calculating mass flow rate through the venturi and flow coefficient of the control valve. The high precision and wide operating range of the transmitter makes it suitable for cryogenic applications where small pressure changes can significantly impact results. DPT101 and DPT102 have specified ranges of measurement with a specified accuracy of .1% of the reading span for both instruments. The DPT101 has a span of 0 to 250 inH_2O and DPT102 spans 0 to 25 inH_2O [29].

Figure 3.9: Rosemount Differential Pressure Sensor [29]

The GE/UNIK 5000 pressure transducers measure the absolute pressures of PT100, PT101, and PT102. These correspond to the initial inlet pressure shortly after PR100, the inlet pressure to the control valve, and the inlet pressure to the venturi, respectively. All GE/UNIK 5000 pressure transducers used in the test bench had a span from 0 to 7 bar [27].These measurements, along with temperature (T101), are used to calculate fluid density.

Figure 3.10: UNIK 5000 Series Pressure Transducers [27]

Additional Process Equipment

The additional process equipment was pertinent to the overall testing procedures, however, did not contribute to the data collection process. These will be discussed below:

A pressure regulator (PR100), shown in *Figure 3.11*, is vital for maintaining consistent inlet pressures to downstream components. It compensates for fluctuations in upstream pressure from MVXXX (manual valve supplying gaseous nitrogen), ensuring a stable output pressure for sensitive instrument measurements. The operating range of the installed pressure regulator was 5 to 55 psi and -40 to 165 Fahrenheit allowing for safe testing of inert gases. The "cleaned and bagged" designation indicates that the valve is specially prepared for environments requiring high cleanliness, such as those involving cryogenic fluids or ultra-pure gases. Cleaning removes oils, particulates, and contaminants, while bagging protects the component from environmental exposure until installation.

Figure 3.11: Pressure Regulator [23]

Additionally, the glycerin filled pressure gauge shown in *Figure 3.12*, can be used, if necessary, as an analog pressure measurement device. This is installed at the pressure regulator (PR100) to validate the on-screen reading of the pressure transducer (PT100) downstream of PR100.

Figure 3.12: Stainless Steel Pressure Gauge [24]

The metering valve, shown in *Figure 3.13*, is designed to expand the operational range of the regulator by increasing its flow span. When the flow exceeds the regulator's maximum capacity, the metering valve opens as a bypass, allowing additional mass flow to pass through the control valve without affecting the regulator's function. This enables the regulator to continue regulating pressure while handling higher flow rates. Constructed from stainless steel, the valve is highly resistant to corrosion and capable of withstanding high pressures, ensuring durability and reliability under harsh conditions. The integral bonnet design minimizes potential leak paths, enhancing safety and reducing maintenance requirements [2]. This valve is particularly important for experiments requiring accurate modulation of flow rates to maintain consistent and reproducible conditions.

Figure 3.13: Metering Valve [25]

The ball valve, shown in *Figure 3.14*, functions as a critical safety and isolation mechanism for the gas supply. It's simple yet effective design allows for quick and secure manual operation, making it easy to shut off gas flow when necessary. The 316 stainless steel construction provides excellent durability, high-pressure tolerance, and resistance to corrosion, making it suitable for cryogens and other demanding applications [3]. The compact design ensures easy integration into the test bench without occupying excessive space, while the lever handle allows operators to isolate specific sections of the system for maintenance or emergency shutdowns without disrupting the entire setup.

Figure 3.14: On/Off Ball Valve [26]

The caliper model, as show in *Figure 3.15*, is needed for recording of the precise length of the valve stroke l. A caliper (dark grey) and modeled 3D-printed parts (red) were needed for valve fitment and were attached to the valve body via hose clamps for secure placement. Generally, an

LVDT (Linear Variable Differential Transformer) would be used for more compact instrumentation. The actuator installed in the test bench had no LVDT compatibility, therefore a digital caliper was used for accurate stroke measurement.

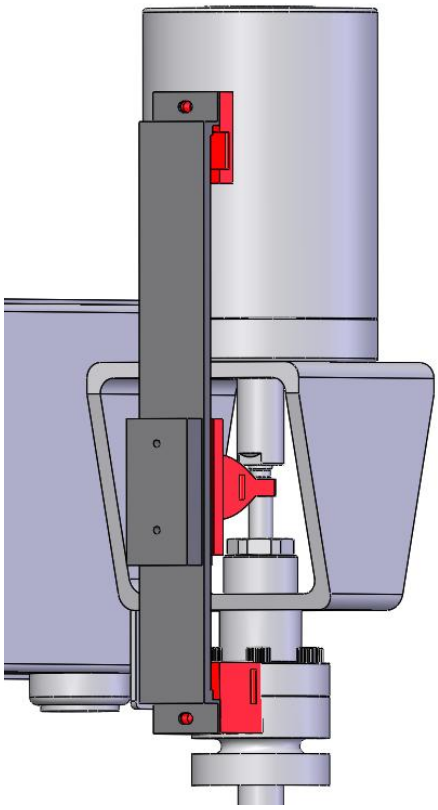

Figure 3.15: 3D-Printed Caliper Mount

3.3 Test Plan

The test plan, *Figure 3.16*, was developed to systematically log data for key parameters, including *FI, PT, DPT, and T*. This ensured comprehensive monitoring of the system's performance. To enhance efficiency and accuracy, a script was implemented to automate the venturi calculations and flow coefficient calculations. This provided immediate feedback during testing, enabling the team to validate the real-time feedback from this automated system was crucial for two main purposes:

1. The real-time data ensured that the mass flow rates derived from the venturi meter and Coriolis Flow Meter were consistent. Any discrepancies between the two methods could be quickly identified and investigated, allowing for adjustments to the setup or recalibration of instruments as needed.

2. The flow coefficient (C_v) calculated from experimental data was continuously compared with the predicted values from the analytical model. This comparison highlighted deviations in the control valve's performance, helping to assess the accuracy of the analytical model and refine the experimental methodology.

To account for potential errors, measurement offsets between the reading and known atmospheric conditions were carefully noted during periods of no gas flow. These offsets, caused by factors such as sensor drift or environmental conditions, were used to recalibrate the system and recalculate parameters, ensuring that subsequent measurements were as accurate as possible. This offset correction was especially important for maintaining the reliability of low-flow or zero-flow data, which are often more susceptible to noise. This is due to the DPT and PT sensors having the same error over the entire span, meaning they are more sensitive at low values.

The combination of automated data logging, real-time calculations, and offset correction provided a robust framework for validating the test results and ensuring that the experimental findings were consistent. This approach not only enhanced the quality of the experimental data but also streamlined the testing process, enabling quicker identification of system anomalies and more efficient troubleshooting.

Test Day	Test Time

Fluid	Nitrogen	#
MW	28.013	[g/mol]
Z	1.000	[-]
kS	1.401	[-]

Pressure Offsets					
P100	P101	P102	PDT101	PDT102	
[bar]	[bar]	[bar]	[mBar]	[mBar]	

Measured Data												
Trial #	Stroke [-]	Stroke [mm]	P100 [BAr]	P101 [BAr]	T101 [K]	DPT101 [mBAr]	P102 [BAr]	T102 [K]	DPT102 [mBAr]	FT101 [g/s]		
1	5%											
2	10%											
3	15%											
4	20%											
5	25%											
6	30%											
7	35%											
8	40%											
9	45%											
10	50%											
11	55%											
12	60%											
13	65%											
14	70%											
15	75%											
16	80%											
17	85%											
18	90%											
19	95%											
20	100%											
21	95%											
22	90%											
23	85%											
24	80%											
25	75%											
26	70%											
27	65%											
28	60%											
29	55%											
30	50%											
31	45%											
32	40%											
33	35%											
34	30%											
35	25%											
36	20%											
37	15%											
38	10%											
39	5%											

Corrected Data												
Trial #	Stroke [-]	Stroke [mm]	P100 [BAr]	P101 [BAr]	T101 [K]	DPT101 [mBAr]	P102 [BAr]	T102 [K]	DPT102 [mBAr]	FT101 m [g/s]	FT102 m [g/s]	PV_TEST10 Cv [-]	CV Select V or C [-]
1	5%												
2	10%												
3	15%												
4	20%												
5	25%												
6	30%												
7	35%												
8	40%												
9	45%												
10	50%												
11	55%												
12	60%												
13	65%												
14	70%												
15	75%												
16	80%												
17	85%												
18	90%												
19	95%												
20	100%												
21	95%												
22	90%												
23	85%												
24	80%												
25	75%												
26	70%												
27	65%												
28	60%												
29	55%												
30	50%												
31	45%												
32	40%												
33	35%												
34	30%												
35	25%												
36	20%												
37	15%												
38	10%												
39	5%												

Figure 3.16: Sample Test Data Sheet

3.4 Uncertainty Analysis of Flow Coefficient

The uncertainty analysis for direct measurements and calculated values were performed as follows:

The percentage offset for direct measurements is given by vendors for the FI01, DPT, PT, and T101. From the provided offset percentages, based on vendor information, the uncertainty for each measured variable at every stroke percentage considered can be found using the methodology described in [32]. The following Eqns. (3.2) and (3.3)[32] for the uncertainty analysis will be based upon 'Experimental Methods for Engineers' [32], however, substitutions for specific test bench values and measurements will be shown instead of generalized/generic inputs as would be seen in the reference text above.

$$\sigma = (\%\ Offset) * Reading \tag{3.2}$$

$$\sigma = (\%\ Offset) * Span \tag{3.3}$$

Standardized equations of uncertainty can be found in [32], however each equation listed below is in terms of this test-bench set up. The uncertainty for each measurement is based on vendor specifications, and the uncertainty is analyzed for each measurement obtained during the testing process.

For the analysis, uncertainty in density at the inlet of the venturi, uncertainty of the calculated mass flow, and uncertainty of flow coefficient with respect to either Coriolis or venturi mass flow are all considered. First, to calculate the uncertainties pertaining to the venturi flow equation, the ideal gas equation of state was used to calculate the density to the inlet of the venturi using the specific ideal gas constant (J/kg·K), T101, and PT102. Starting with the ideal gas equation, and subsequently transforming it into its specific form, the density can be found, as described in Eqns. (3.4) through (3.6). Also, the ideal gas assumption may not be accurate dependent on the fluid and it's properties such as pressure and temperature. Ideal gas assumption was used as the analysis for gaseous nitrogen at ambient temperatures.

$$PV = NRT \tag{3.4}$$

$$Pv = RT \tag{3.5}$$

$$\rho = \frac{P}{RT} \tag{3.6}$$

Once calculated, the partial derivatives with respect to both measurements PT102 and T101 are derived as seen in Eqns. (3.7) and (3.8).

$$\frac{\partial \rho}{\partial P} = \frac{1}{RT} \tag{3.7}$$

$$\frac{\partial \rho}{\partial T} = \frac{P}{RT^2} \tag{3.8}$$

The span for both the pressure measurement and temperature measurement is provided in *Table 3.2*. This span will change depending on the units used for calculation. Additionally, T101 will need to use units in relation to the units used prior.

$$\sigma_{P102} = (.04\%) * (0 - 7Bar) \tag{3.9}$$

$$\sigma_{T101} = (.1\%) * T101 \tag{3.10}$$

The uncertainty of P102 and T101 are calculated based upon Eqns. (3.9) and (3.10), calculated using the measurement reading multiplied by the vendor % offset specified. To calculate the RMS error in density, the uncertainty results for pressure and temperature are combined with the partial derivates derived in Eqns. (3.7) and (3.8), resulting in equation (3.11).

$$\sigma_\rho = \sqrt{\left(\frac{\partial \rho}{\partial P}\sigma_{P102}\right)^2 + \left(\frac{\partial \rho}{\partial T}\sigma_{T101}\right)^2} \tag{3.11}$$

A calculated mass flow rate can be obtained via Eqn. (3.12) ,(using specific measured variables now in place of general) and then using the general equations as provided for an uncertainty analysis, the RMS uncertainty can be calculated for the mass flow. This derivation is provided below.

$$\dot{m} = \frac{\xi \epsilon \pi d^2}{4\sqrt{1-\beta^4}} \sqrt{2 * DPT102 * \rho} \tag{3.12}$$

The discharge coefficient(ξ) was chosen as 0.995 based upon ISO 5167. The expansibility factor (ε) and throat-to-pipe diameter ratio(β) can also be calculated from ISO 5167 [31]. The partial derivatives of interest associated with the mass flow rate equation are provided in Eqns. (3.13) and (3.14).

$$\frac{\partial \dot{m}}{\partial \rho} = \left(\frac{\xi \epsilon \pi d^2}{8\sqrt{1-\beta^4}}\right) \sqrt{(2 * DPT102)\rho^{-1}} \tag{3.13}$$

$$\frac{\partial \dot{m}}{\partial DPT102} = \left(\frac{\xi \epsilon \pi d^2}{8\sqrt{1-\beta^4}}\right)\sqrt{(2 * \rho)DPT102^{-1}} \tag{3.14}$$

Applying proper unit conversions dependent on pressure and density units as well as required mass flow units, the venturi derived mass flow partial derivatives can be used in the uncertainty equation, forming Eqn. (3.15). The use of consistent and proper units allows for accurate calculation.

$$\sigma_{\dot{m},venturi} = \sqrt{\left(\frac{\partial \dot{m}}{\partial DPT102}\sigma_{DPT102}\right)^2 + \left(\frac{\partial \dot{m}}{\partial \rho}\sigma_{\rho}\right)^2} \tag{3.15}$$

The flow coefficient equation from the ISA Valve Sizing Standards[6] , Eqn. (3.16), is used to determine a valve's flow capacity under specific operating conditions. In this equation, the flow coefficient can be calculated as shown above for an initial assessment, with ISA Standards specifically detailing a logic tree using iteration. The term ṁ denotes the mass flow rate, while N_6 is a dimensionless factor dependent on units used. The expansion factor Y, which accounts for compressibility effects in the fluid, is calculated as the innermost set of parentheses. γ is the specific heat ratio and x_T is the pressure differential ratio. Other variables include P corresponding to PT101, the differential pressure ΔP corresponding to DPT101, and ρ, the fluid density calculated via inputs of PT101 and T101. The equation ensures accurate flow control by considering fluid compressibility, pressure conditions, and valve-specific characteristics.

$$C_v = (\dot{m})\left(N_6 * \left(1 - \frac{\Delta P}{P * 3 * \gamma * x_T}\right)\sqrt{\Delta P \rho_1}\right)^{-1} \tag{3.16}$$

From here, the flow coefficient can be calculated via the Coriolis mass flow or venturi mass flow. The use of MATLAB (or a similar program) is critical, as based upon the ISA: Flow Equations for Sizing Control Valves [6], an iterative routine must be used which is dependent on several factors. The compressible (non-choked) flow coefficient equation is shown as the initial calculation. The partial derivatives or gradients of each independent measurement were calculated as numerical gradients due to the iterative nature of the flow coefficient calculation process. A 10% artificial step change was introduced around the nominal measurement for this purpose. For instance, when varying the mass flow rate by ±10%, the modified values (1.1 × ṁ, 1 × ṁ, 0.9 × ṁ) were used while keeping all other measurements constant. This step change allowed the corresponding C_v values to be determined. Although the resulting C_v values do not differ by exactly 10%, the designation of 1.1 and 0.9 reflects the proportional step change applied to the mass flow

rate or other measured variables. A generic process for derivative approximation can be seen using the finite difference method [33]. Partial derivatives of the C_v equation for each parameter of interest are derived below, as described in Eqns. (3.17) through (3.20). Likewise, the uncertainty of the required input parameters are given in Eqns. (3.21) through (3.24). The uncertainty analysis can be seen in **Appendix B**.

$$\frac{\partial C_v}{\partial \dot{m}} = \frac{C_{v_{1.1}} - C_{v_{0.9}}}{\dot{m}_{1.1} - \dot{m}_{0.9}} \tag{3.17}$$

$$\frac{\partial C_v}{\partial P} = \frac{C_{v_{1.1}} - C_{v_{0.9}}}{P_{1.1} - P_{0.9}} \tag{3.18}$$

$$\frac{\partial C_v}{\partial \Delta P} = \frac{C_{v_{1.1}} - C_{v_{0.9}}}{\Delta P_{1.1} - \Delta P_{0.9}} \tag{3.19}$$

$$\frac{\partial C_v}{\partial T} = \frac{C_{v_{1.1}} - C_{v_{0.9}}}{T_{1.1} - T_{0.9}} \tag{3.20}$$

$$\sigma_{\dot{m},coriolis} = (.1\%) * FI101 \tag{3.21}$$

$$\sigma_{PT101} = (.4\%) * (0 - 7Bar) \tag{3.22}$$

$$\sigma_{DPT101} = (.1\%) * DPT101 \tag{3.23}$$

$$\sigma_{T101} = (.5\%) * T101 \tag{3.24}$$

If using the venturi for flow measurement, $\sigma_{\dot{m},venturi}$ is provided above in Eqn. (3.15), and can be substituted for the Coriolis uncertainty parameter. Therefore, the generic $\dot{m}$ symbol can be either the Coriolis measurement or venturi calculation. Combining these equations, the C_v uncertainty analysis is derived as Eqn. (3.25).

$$\sigma_{C_v} = \sqrt{\left(\frac{\partial C_v}{\partial \dot{m}}\sigma_{\dot{m}}\right)^2 + \left(\frac{\partial C_v}{\partial P}\sigma_{PT101}\right)^2 + \left(\frac{\partial C_v}{\partial \Delta P}\sigma_{DPT101}\right)^2 + \left(\frac{\partial C_v}{\partial T}\sigma_{T101}\right)^2} \tag{3.25}$$

Along with the process measurements, there is an uncertainty in the stroke length as well of 0.01mm. However, this has no effect on the flow coefficient calculation and therefore is considered separately. The uncertainty associated with the stroke length measurement can be directly found using the caliper vendor information.

Chapter 4: DESIGN OF CONTROL VALVE FLOW PLUG

4.1 Analytical Design of Equal Percent Flow Plug

A valve plug analytical model was developed to generate an equal percentage valve plug profile based upon desired maximum flow coefficient, rangeability, etc. Although flow coefficient and valve sizing standards are available [6], developing a valve plug profile design was only conceived for a single conical shape in Weidmann and Rowan [12]. Based upon fundamental relations and characteristic properties of a valve plug, a radial or diametrically based plug profile can be generated with respect to the centerline. As seen in *Figure 4.1*, the axisymmetric profile generated between D_{Base} and D_{Int} denoted as the plug profile in red. The bullet tip, as seen in black, as the arc starting at D_{Int} and the length of the plug (from Base to end of Tip) were investigated using ANSYS Fluent, a computational Fluid dynamics (CFD) software. The base diameter (D_{Base}) denotes the maximum diameter of the plug at the base of the plug profile, the interface diameter (D_{int}) denotes the intersection between plug profile and start of the plug tip. Additionally, effects of variation in D_{Base} and D_{Int} were studied using CFD. Since the length of the profile was constrained to 0.75", other parameters, such as overall length, were varied by adjusting the tip profile. Likewise, the interface diameter and base diameter were modified based upon design constraints and maximum flow coefficient requirements. CFD was required to investigate the effects of these geometrical changes, which were not inherently captured within the analytical model.

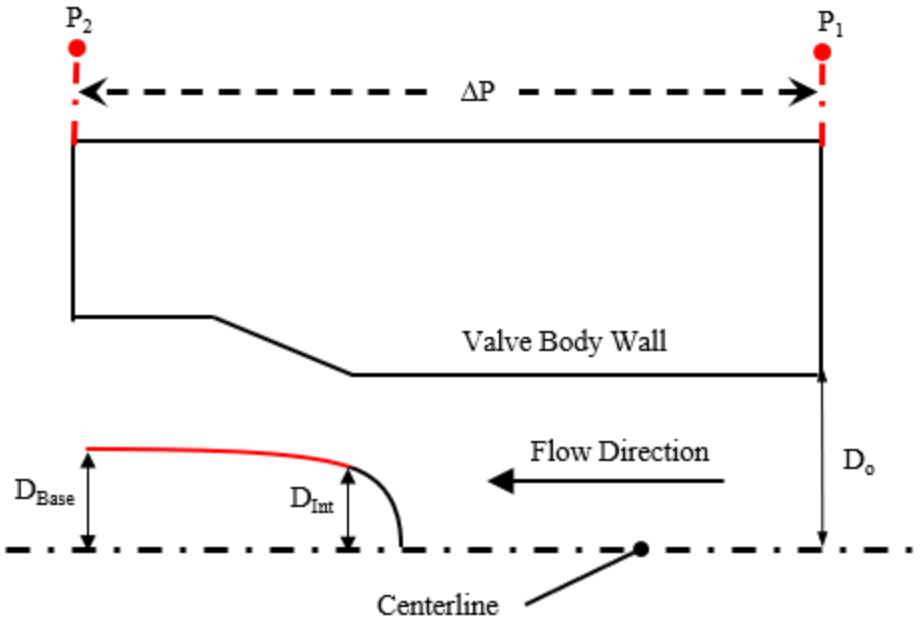

Figure 4.1: Analytical Bullet Profile

A generic valve plug (as implemented into CFD) is provided in *Figure 4.1*, where D_{int} as described previously, aligns with opening of the upstream diameter of the valve body wall (D_o). D_t represents the throat diameter, comparable to the hydraulic diameter of flow through an orifice. Here the orifice gap is exaggerated for readability. As the plug approaches D_{Base}, the flow coefficient decreases until the plug becomes fully seated on the Kel-F seat, as described previously.

The pressure drop across the valve is an important design parameter when properly sizing a valve. The schematic shown in *Figure 4.1* details a generic valve plug profile displayed with the pressure locations at inlet and outlet. The ΔP represents the pressure differential between the upstream inlet pressure (P_1) and the downstream outlet pressure (P_2). Additionally, the flow direction symbolizes that Q, the volumetric flow rate, flows from P_1 to P_2 (*i.e.* P_1 is greater than P_2). The analytical equations presented below will follow the definitions established in the schematic.

The analytical design of the equal percent flow plug begins with the flow coefficient, alternatively defined as the volumetric flow rate of the fluid that can pass through an opening with a defined pressure drop. It is specifically defined as the amount of water at 60°F (in gallons) that can flow through the valve per minute when there is a pressure drop of 1 psi across the valve [4].

This is the principal design feature for the process control valve, specifically the geometry of the valve plug and valve body wall.

Model Justification

The initial design of the control valve plugs employs the incompressible flow assumption to simplify the analytical development of flow area versus stroke relationships. This approach treats the working single-phase fluid (typically liquid or low-speed gas) as having constant density, which is reasonable during preliminary design phases where the primary objective is to shape the plug profile to achieve a desired flow characteristic (e.g., equal percent).

The assumption is justified for early-stage plug development because it isolates geometric effects on flow area without introducing complex fluid property variations. This allows for easier comparison between plug geometries and supports faster iterations using analytical tools instead of needing an iterative routine.

It is important to note that the incompressible flow assumption is used exclusively in the design stage. It does not apply to final characterization or experimental performance validation. Instead, the full behavior of the valve plug under experimental conditions is evaluated using a comprehensive iterative routine (as seen in Appendices A and B).

Experimental and CFD-based characterizations apply the ANSI/ISA S75.01 standard, which accounts for compressibility effects, pressure recovery factors, and fluid thermodynamic properties. This ensures that the final experimental flow coefficient values are applicable to real-world conditions.

Analytical Modeling of Valve Plug Geometry

The general incompressible equation for the flow coefficient has the form [11]:

$$C_V = \frac{Q[gpm]}{\sqrt{\Delta P[psi]}} \tag{4.1}$$

The incompressible flow coefficient equation detailed in the ISA standards, with N_1 representing a constant which translates Eqn. (4.1) into SI units, is provided in Eqn. (4.2) [6].

$$C_v = \frac{Q}{N_1}\sqrt{\frac{\rho_1/\rho_o}{\Delta P}} \tag{4.2}$$

The compressible flow coefficient equations from ISA (adapted for clarity) for gaseous fluid flow is shown in Eqn. (4.3), where additional parameters present are described in the ISA manual [6]:

$$C_v = (W)\left(N_6 * \left(1 - \frac{\Delta P}{P * 3 * \gamma * x_T}\right)\sqrt{\Delta P \rho_1}\right)^{-1} \tag{4.3}$$

Finally, the equational definitions of rangeability [11] and equal percentage characteristics [4] are provided in Eqns. (4.4) and (4.5), as presented before:

$$C_V = C_{V,m} \cdot R^{(\xi-1)} \tag{4.4}$$

$$R = \left(\frac{C_{v,m}}{C_{v,o}}\right) \tag{4.5}$$

Figure 4.2 displays the maximum ($C_{v,m}$) and minimum ($C_{v,o}$) flow coefficients of a generic equal percent profile, with the flow profile provided as a function of the non-dimensional valve position. At a non-dimensional value of 1 (ξ=1), the position corresponds to 100% valve stroke or fully open. Likewise, the non-dimensional valve of 0 (ξ=0) corresponds to the minimum flow coefficient at 0% valve stroke or fully closed. The analytical model does not capture a full seat, but the minimum position in actual applications corresponds to the position where the Kel-F seat fully seals the upstream valve body segment, thereby equating to a flow coefficient of 0. However, in the analytical model the minimum flow coefficient corresponds to (the throat opening without accounting for the presence of the Kel-F seal. If there was full closure predicted using the analytical model, that would indicate the D_{Base} is the same as D_o, signifying the presence of metal-on-metal contact between valve wall and plug (leading to possible wear or damage of the metal surfaces).

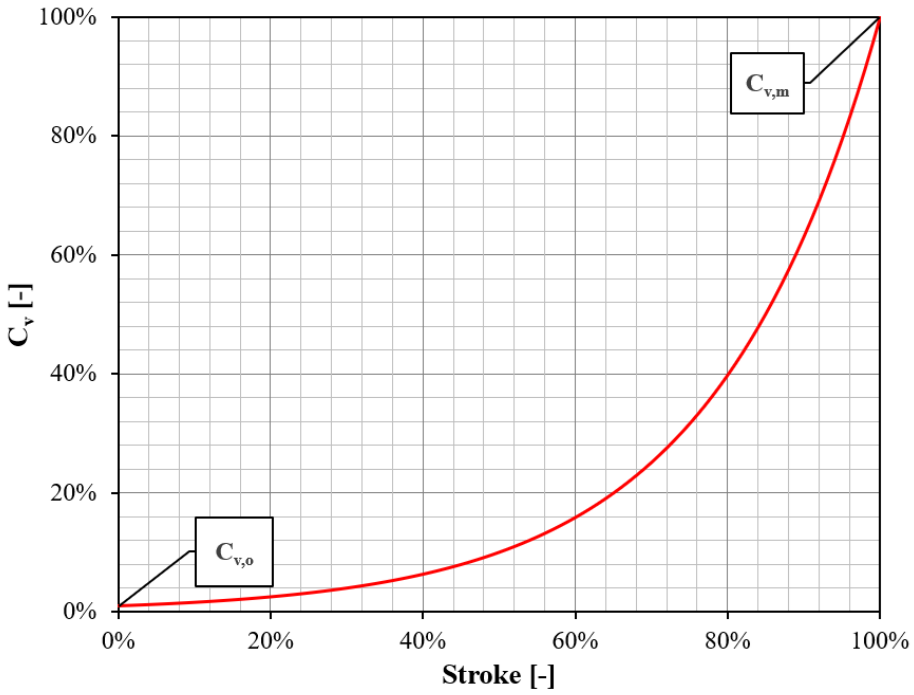

Figure 4.2: Flow Coefficient Max/Min of Equal Percent Characteristic

From the Bernoulli equation, the flow through an orifice for an incompressible fluid can be described using Eqn. (4.6) [30]. The K value, provided in Eqn. (4.7), represents the nozzle coefficient. The nozzle coefficient is comprised of the discharge coefficient, C_d, defined as the ratio of theoretical to actual incompressible flow, and β, the ratio of throat to upstream diameter ($\frac{D_t}{D_o}$). The parameter A_t refers to the throat area, which can be equated to D_t through Eqn. (4.8).The throat diameter, as mentioned previously, is comparable to the hydraulic diameter.

The pressure drop across the valve cross section (ΔP, as described in *Figure 4.1*) represents the pressure drop induced by fluid flowing through the constriction between valve plug and valve body.

$$Q = (KA_t)\sqrt{\frac{2 \cdot \Delta P}{\rho}} \tag{4.6}$$

$$K = \frac{C_d}{\sqrt{1-\beta^4}} \tag{4.7}$$

$$A_t = \frac{\pi}{4} D_t^2 \tag{4.8}$$

Eqn. (4.6) was rewritten for SI unit conversion, including both the left hand side, Eqn. (4.9), and the right hand side, Eqn. (4.10). Combining the units conversions into constants, Eqns. (4.11) and (4.12) are developed, with the constants $N_0 = 37.992$ and $N_{01} = 29.839$ (which are required for proper unit conversion into SI units).

$$Q[gpm]\left(\frac{1ft^3}{7.480519gal}\right)\left(\frac{(0.3048)^3 m^3}{1ft^3}\right)\left(\frac{1min}{60s}\right) \tag{4.9}$$

$$K \cdot A_t[in^2]\left(\frac{0.0254m}{1in}\right)^2 \left\{2 \cdot \Delta p[psi]\left(\frac{101325Pa}{14.69595psi}\right)\left(\frac{1}{\rho\left[\frac{kg}{m^3}\right]}\right)\right\}^{\frac{1}{2}} \tag{4.10}$$

$$C_V = \frac{Q[gpm]}{\sqrt{\Delta p[psi]}} = N_0 \cdot (K \cdot A_t[in^2]) \tag{4.11}$$

$$C_V = \frac{Q[gpm]}{\sqrt{\Delta p[psi]}} = N_{01} \cdot (K \cdot {D_t}^2[in^2]) \tag{4.12}$$

Now, using Eqn. (4.12), the flow coefficient can be expressed along the plug profile in terms of D_t, *i.e.* the diameter associated with the flow area between the upstream diameter and the plug diameter ($D_{Int} \leq D \leq D_{Base}$). The expression of the plug profile diameter can be simplified using the relationships derived in Eqns. (4.13) through (4.17).

$$D_t = \sqrt{{D_o}^2 - D^2} \tag{4.13}$$

$$D_{t,o} = \sqrt{{D_o}^2 - {D_{Int}}^2} \tag{4.14}$$

$$D_{t,m} = \sqrt{{D_o}^2 - {D_{Base}}^2} \tag{4.15}$$

$$\Delta = D/D_o \tag{4.16}$$

$$D_t{}^2 = D_o{}^2(1 - \Delta^2) \tag{4.17}$$

Once the non-dimensional ratio of the plug diameter to upstream diameter is found, an equal perentage plug profile is developed in terms of the non-dimensional gap between plug and upstream valve body wall. To relate the diameter change to equal percent characteristics, the equal percent charactersitic equation can be modified to include rangeability. Here C_v represents the flow coefficent anywhere along the non-dimensional opening ($0 \leq \xi \leq 1$) from $C_{v,o} \leq C_v \leq C_{v,m}$. Rearranging, C_v can be described in terms of rangeability and non-dimensional stroke.

$$ln\left(\frac{C_V}{C_{V,0}}\right) = (\ln R)\xi \tag{4.18}$$

$$C_V = C_{V,0} \cdot R^{\xi} \tag{4.19}$$

$$C_V = C_{V,m} \cdot R^{(\xi-1)} \tag{4.20}$$

By substituting the D_t parameter from Eqn (4.17) into Eqn. (4.12), which is equal to C_v, Eqn. (4.21) can be derived, as seen below.

$$C_V = N_{01} \cdot K \cdot D_o{}^2(1 - \Delta^2) \tag{4.21}$$

$$C_{V,0} \cdot R^{\xi} = N_{01} \cdot K \cdot D_o{}^2(1 - \Delta^2) \tag{4.22}$$

$$C_{V,m} \cdot R^{(\xi-1)} = N_{01} \cdot K \cdot D_o{}^2(1 - \Delta^2) \tag{4.23}$$

The ζ term is defined as one minus the square of non-dimensional diameter change, where D_o would be considered 1, as seen in Eqn. (4.17). This simplifies the above Eqns. (4.21), (4.22), and (4.23) into their respective counterparts Eqns. (4.25), (4.26),and (4.27).

$$\zeta = (1 - \Delta^2) \tag{4.24}$$

$$\zeta = \frac{C_V}{N_{01} \cdot K \cdot {D_o}^2} \tag{4.25}$$

$$\zeta_0 = \frac{C_{V,0}}{N_{01} \cdot K \cdot {D_o}^2} \tag{4.26}$$

$$\zeta_m = \frac{C_{V,m}}{N_{01} \cdot K \cdot {D_o}^2} \tag{4.27}$$

Then, the rangeability can be expressed as a ratio of Eqn. (4.27) to (4.26).

$$R = \frac{C_{V,m}}{C_{V,0}} = \frac{\zeta_m}{\zeta_0} \tag{4.28}$$

So, the plug profile can non-dimensionally be expressed as:

$$\Delta = \sqrt{1 - \zeta_0 \cdot R^{\xi}} = \sqrt{1 - \zeta_m \cdot R^{(\xi - 1)}} \tag{4.29}$$

$$\zeta = 1 - \Delta^2 = \zeta_0 \cdot R^{\xi} = \zeta_m \cdot R^{(\xi - 1)} \tag{4.30}$$

Figure 4.3 provides the variance in the non-dimensional diameter change (ΔD) as a function of the non-dimensional opening (ξ), where the black dotted line refers to the upstream wall diameter (D_o). The three profiles are designed with equivalent desired maximum C_v, however, by varying the rangeability the base diameter changes, leading to a steeper curve along the plug profile for the higher rangeability design.

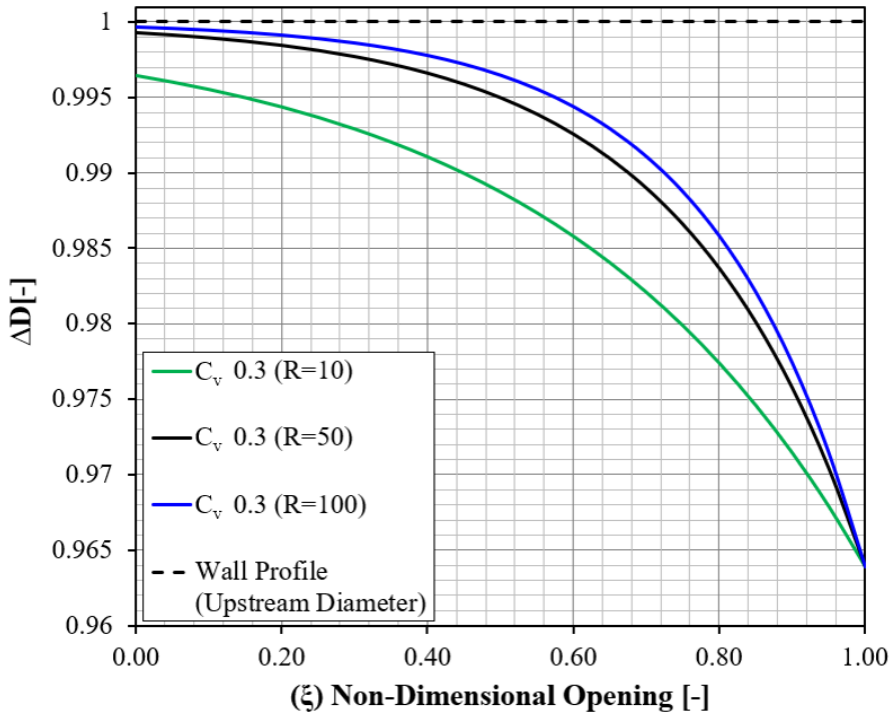

Figure 4.3: Non-Dimensional Equal Percent Plug Profile with Varied Rangeability

The design of the equal percent profile proceeds as follows:

1. Identify maximum flow coefficient ($C_{v,m}$) desired at full open ($C_{v,(\xi=1)}$)
2. Design the profile ($0< \xi <1$), selecting $C_{v,m}$, using geometrical inputs of D_{Base}, $C_{v,m}$, D_o, ℓ_{plug} and K. Although length does not affect the non-dimensional profile, for fabrication purposes a dimensional length (in.) is selected.
3. Establish the profile ($0 < \xi < 1$), using the above values by variation of R (rangeability) to match the desired process parameters.

The results from the analytical model for the plug profile is provided in *Figure 4.3*, and the flow coefficient versus opening for each design is shown in

Figure 4.4. As previously stated, the analytical model does not account for the soft seat (Kel-F) seal, which is not accounted for in the plug profile design. Therefore, at full close (0%), the design flow coefficient is not zero. The flow coefficient versus opening display the operational effects of the rangeability, enforcing a maximum flow coefficient and varying the rangeability to manipulate the minimum flow coefficient (at 0% opening). The increase in rangeability, constrained by a maximum flow coefficient, reduces the minimum flow coefficient needed to satisfy Eqn. (4.5) [11].

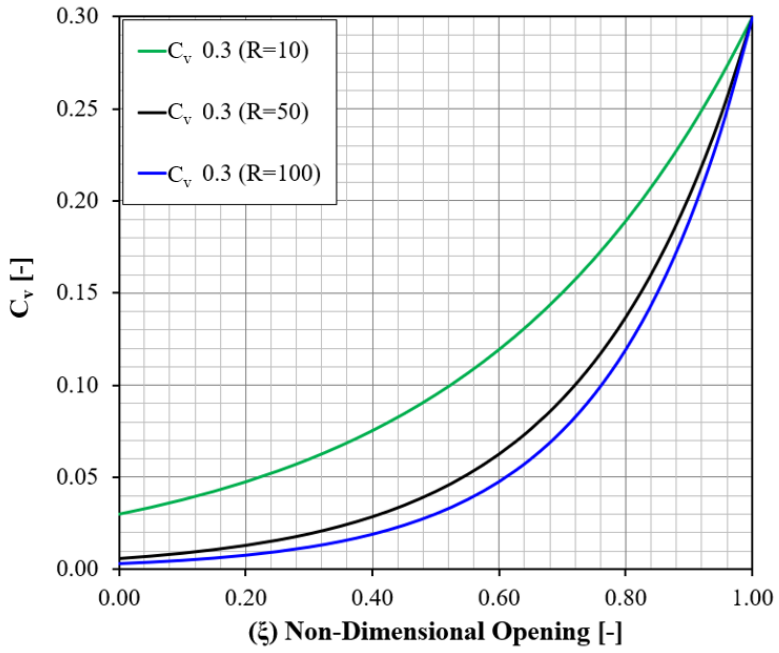

Figure 4.4: Equal Percent Analytical Characterization

Analytical profiles were generated to assess the viability of the analytical model methodology. The generated plug profiles included modeling of the OEM valve plug and creating several unique valve plug geometries. The developed plug profiles listed in *Table 4.1* include the OEM 'remake' and the plugs A1-A4, denoted as 'A-series', which consist of a maximum design C_v of 0.3 while varying the rangeability, and therefore base diameter, within reason. The OEM values listed in the table are therefore of the analytical model generation, not the physical OEM plug, as will be discussed later in further detail. Each of the developed valve plug profiles were produced using equivalent valve body geometries, *i.e.* each plug will be installed in the same valve body. The values of maximum flow coefficient and rangeability are the desired values for each plug based upon the above analytical model.

Table 4.1: Equal Percent Analytical Parameters

Part ID	$C_{v,m}$	R	ℓ_{stroke}	ℓ_{plug}	D_{Base}	Character
[-]	[-]	[-]	[in.]	[in.]	[in.]	[-]
OEM	1.0	9.1	0.75	0.875	0.4105	Eq %
A1	0.3	3.0	0.75	0.948	0.4110	Eq %
A2	0.3	3.7	0.75	0.948	0.4120	Eq %
A3	0.3	7.4	0.75	0.946	0.4140	Eq %
A4	0.3	3.7	0.75	1.000	0.4120	Eq %

The generated characterization curves of the 'A-series' are shown in *Figure 4.5*, where the non-dimensional opening, representing the stroke (lift) of the valve plug, is plotted against the flow coefficient (C_v). These characterization curves detail the relationship between plug displacement and flow capacity, providing insight into the performance characteristics of the equal percent analytical valve plug models.

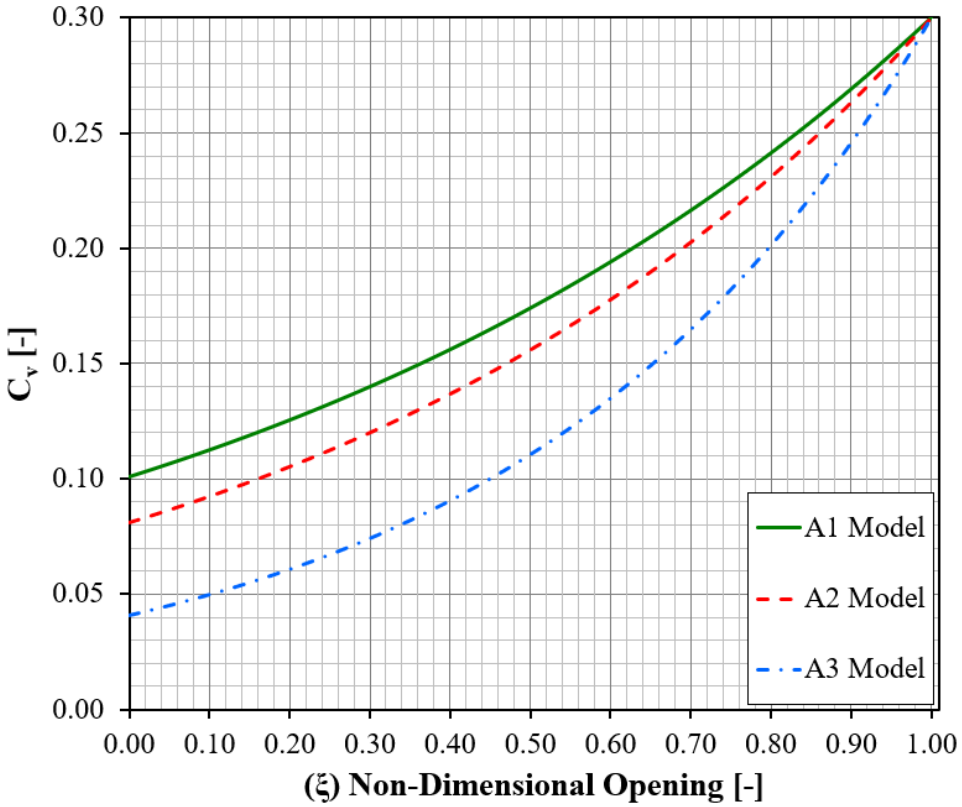

Figure 4.5: 'A-series' Analytical Characterization

4.2 Design of Hybrid Flow Plug

Along with the equal percentage plug profile, a hybrid profile was desired which would provide more precise control at lower flow (say, 0 to 50% open) while allowing for a larger maximum C_v.

The higher maximum C_v allows for easier cool-down of the process line, while maintaining controllability with precise control during low flow conditions. The analytical design of the hybrid flow plug profile is derived from the combination of two equal percent profiles, as shown in *Figure 4.6*, where the two profiles (for instance, $C_{v,m}$ of 0.8 in blue and $C_{v,m}$ of 0.3 in black) are designed to intersect at $\xi = 0.5$.

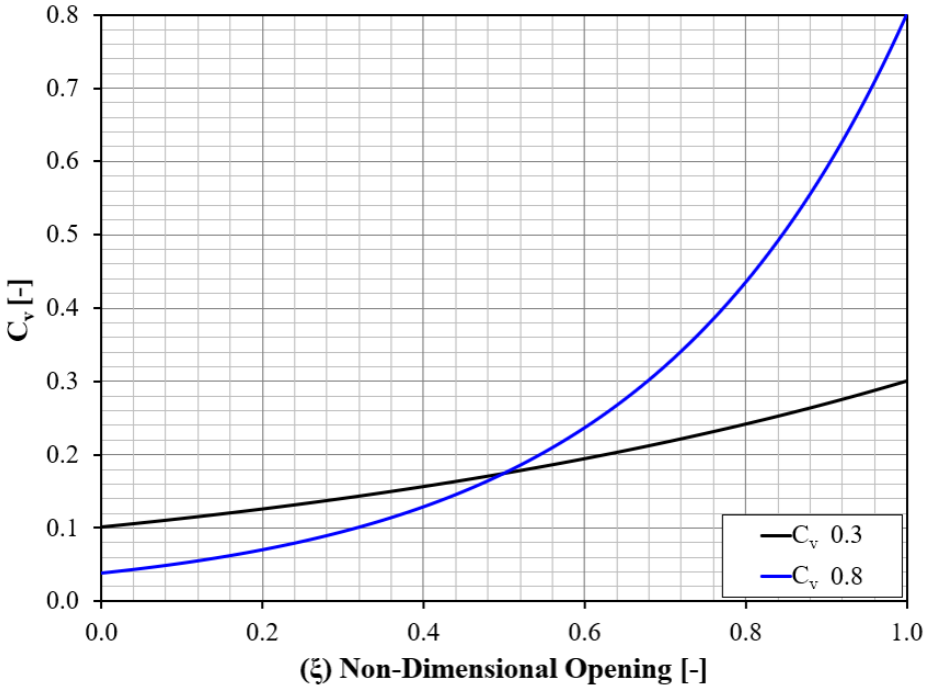

Figure 4.6: Two Equal Percent Profiles

The design of the hybrid profile proceeds as follows:

1. Identify maximum flow coefficient ($C_{v,m}$) needed at full open ($C_{v,(\xi=1)}$)
2. Determine the intersection point at a non-dimensional stroke length (ξ =X), where the lower and upper profiles are selected to meet
3. Design the low flow profile ($0< \xi <X$), selecting $C_{v,m}$ of the low flow profile less than the maximum flow coefficient needed at full open ($C_{v,(\xi=1)}$) using D_{Base}, $C_{v,m}$ of the low flow profile, D_o, and K.
4. At the designated intersection point, let the C_v or D at $\xi = X$ of the lower flow profile match with the C_v or D of the higher flow profile by varying rangeability and base diameter of

the high flow profile curve, since Base Diameter of the 0.8 curve is not applicable. Therefore, by letting R and D_{Base} vary to match the flow coefficient or diameter of the profile of the $C_{v,m} = 0.3$ curve at $\xi = 0.5$, the intersecting $C_{v,m} = 0.8$ curve can be generated.

5. These combined profiles of the lower flow profile from $0 < \xi < X$, and the higher flow profile from $X < \xi < 1$ establish a hybrid plug profile

The analytical hybrid plug profile was generated following the design procedure above, and the generated profile is provided in

Figure 4.7. The dotted line represents the low flow plug profile ($C_{v,m} = 0.3$, also seen in *Figure 4.3*).

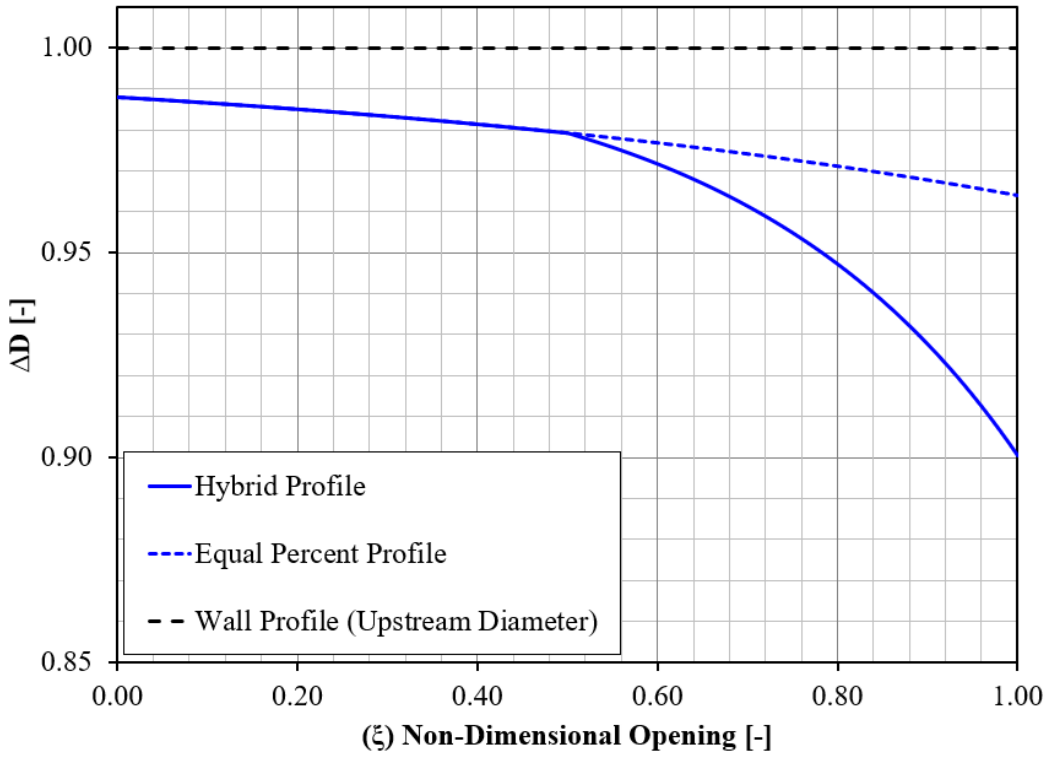

Figure 4.7: Analytical Hybrid Plug Profile

The combination of profiles as seen in *Figure 4.6*, were then combined into a single hybrid flow coefficient versus opening. *Figure 4.8* details this.

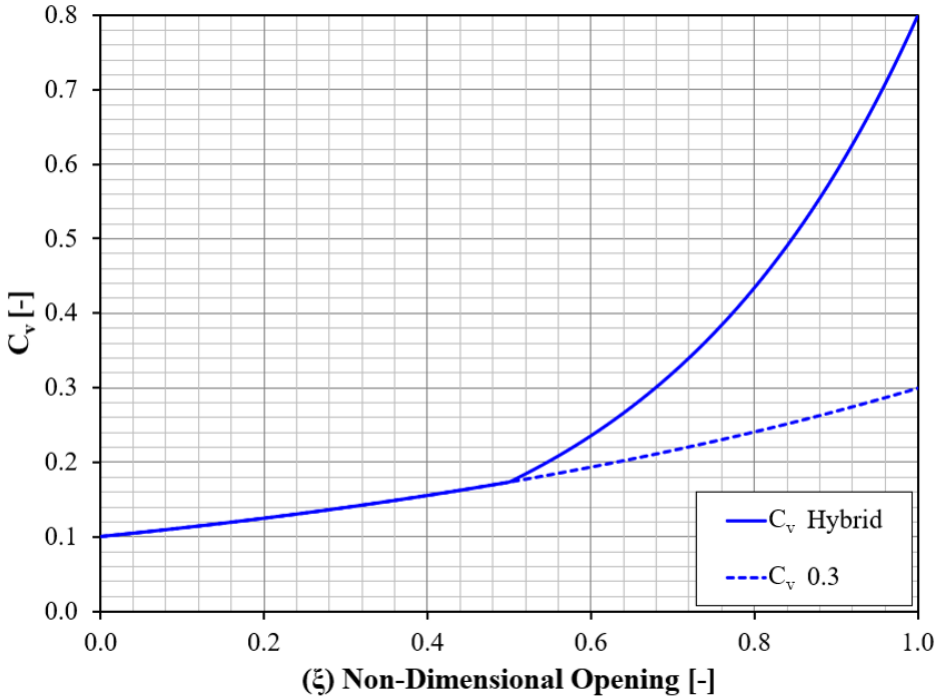

Figure 4.8: Hybrid Flow Coefficient

The plugs B1-B3, denoted as 'B-series', consisting of hybrid plug profiles with a maximum C_v of 0.8 and a low flow profile of $C_{v,m} = 0.3$, while varying the base diameter within reason, like the 'A-series'. The values of maximum flow coefficient and rangeability are the desired values for each plug based upon the above analytical model and procedures for hybrid profile generation, with each geometry generated presented in *Table 4.2*.

Table 4.2: Hybrid Valve Plug Analytical Parameters

Part ID	$C_{v,m}$	R	ℓ_{stroke}	ℓ_{plug}	D_{Base}	Character
[-]	[-]	[-]	[in.]	[in.]	[in.]	[-]
B1	0.8	7.9	0.75	0.948	0.411	Hybrid
B2	0.8	9.9	0.75	0.946	0.414	Hybrid
B3	0.8	19.7	0.75	1.000	0.412	Hybrid

The generated characterization curves of the 'B-series' are shown in *Figure 4.9*, where the non-dimensional opening, representing the stroke (lift) of the valve plug, is plotted against the flow coefficient (C_v). These characterization curves detail the relationship between plug displacement and flow capacity, providing insight into the performance characteristics of the equal percent analytical valve plug models.

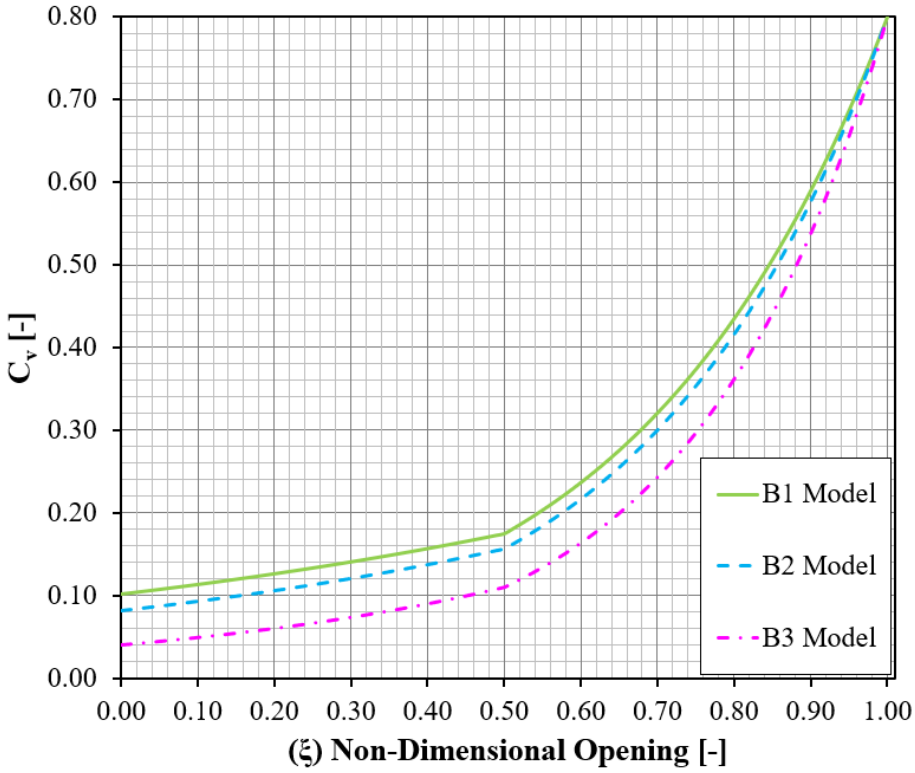

Figure 4.9: 'B-series' Analytical Characterization

4.3 CFD Simulation of Analytical Model

A CFD simulation was used to validate the analytical model's anticipated maximum flow coefficient ($C_{v,m}$). The geometry of the analytical model was based upon the vendor information for the OEM cryogenic control valve body geometry. To effectively model the nitrogen flow through the control valve and across plug, the fluid flow region was modeled between the valve plug and valve body. The flow area of the downstream section was modeled based on the cross-sectional height of the outlet, adjusted for flow area of the real outlet piping. Proper meshing techniques and solver settings were selected to obtain accurate solutions of the OEM plug as well as the equal percent 'A-series' plugs. Given the accuracy of the 'A-series' results, the 'B-series' or hybrid plugs, which were the combination of two equal percent profiles, were assumed to be sufficiently validated based on the results from the 'A-series'. The OEM geometry is shown when detailing specific geometry, mesh, and visual results; however, all settings and methods apply to all plugs numerically simulated unless otherwise stated.

Geometry

The geometry callouts listed in *Figure 4.10* detail the model height from the centerline and length along the centerline, the "S" represent lengths not able to be shown to scale (*i.e.* L1 and L5). The values H3, H5, L8, and L9 correspond to the interface diameter, base diameter, length of plug profile(ℓ_{stroke}), and length of tip, respectively. L10 can be adjusted to bring the valve plug body farther in or out of the upstream area. Therefore, these position values change based upon the valve plug being modeled. All other values will remain consistent, contingent on use of the same cryogenic control valve model. All values for the OEM plug geometry model are listed in *Table 4.3* .

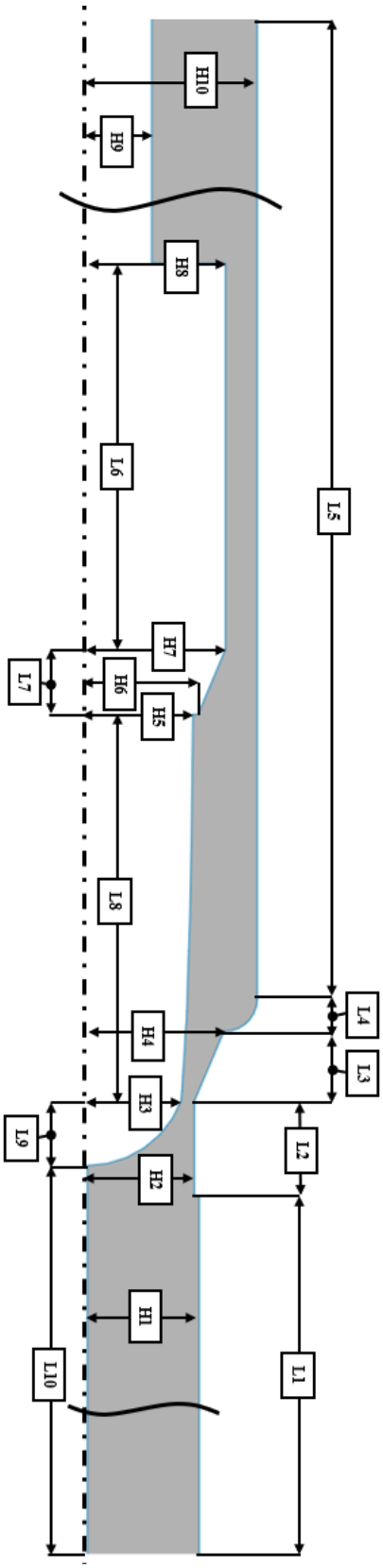

Figure 4.10: OEM Geometry Callout

Table 4.3: OEM Geometry Callout Chart

H1	0.218	[in.]
H2	0.208	[in.]
H3	0.182	[in.]
H4	0.265	[in.]
H5	0.205	[in.]
H6	0.215	[in.]
H7	0.268	[in.]
H8	0.268	[in.]
H9	0.125	[in.]
H10	0.330	[in.]
L1	2.500	[in.]
L2	0.185	[in.]
L3	0.135	[in.]
L4	0.063	[in.]
L5	6.427	[in.]
L6	0.749	[in.]
L7	0.126	[in.]
L8	0.750	[in.]
L9	0.125	[in.]
L10	2.560	[in.]

Meshing Techniques

The mesh generation technique begins with determining the ‘named selections’ to allow ANSYS Fluent to identify the inlet, axis, wall, and outlet boundaries, as seen in *Figure 4.11*. The inlet and outlet boundaries are needed to identify flow direction through the flow region [34]. The wall identifies the boundaries of the flow region which, based upon mesh settings, assist in boundary layer resolution. The center axis is necessary, as this was an axisymmetric numerical simulation and therefore required an axis of rotation along the centerline. It was necessary to put breaks in the inlet and outlet regions of the figure, as the entire length of the geometry was too long for page fitment.

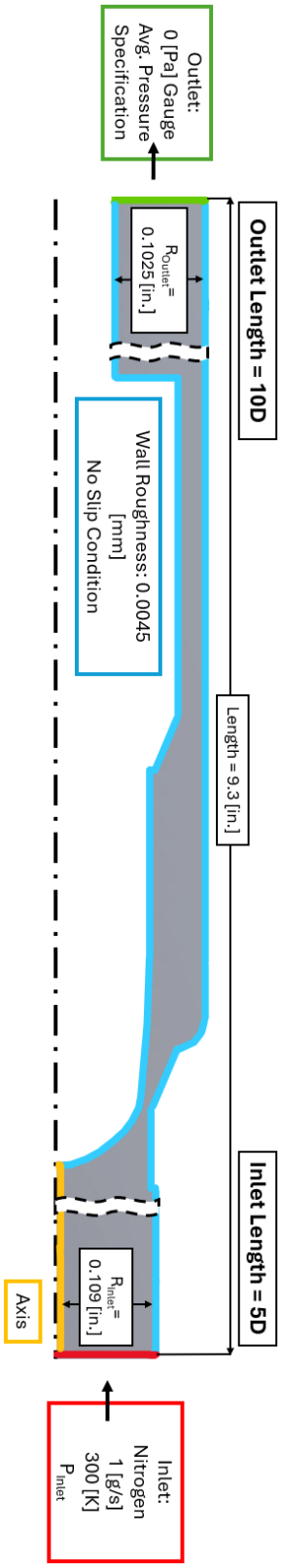

Figure 4.11: OEM Named Selections (Boundary Condition Callouts)

To resolve the boundary layer near the wall, a small element size was introduced [34] while employing inflation layering along the 'named selection' designated in blue, *i.e.* the wall. Once again, the "S" breaks are shown, as the lengths of L1 and L5 are not to scale. The settings of the mesh are shown below in *Table 4.4*, and an example of the near-wall mesh inflation layering is provided in *Figure 4.10.*

Table 4.4: Mesh Settings

Element Size	0.035	[mm]
Inflation Layer	4	[N]
Inflation Growth Rate	1.075	[-]
Inflation Boundary	Wall	[Named Selection]

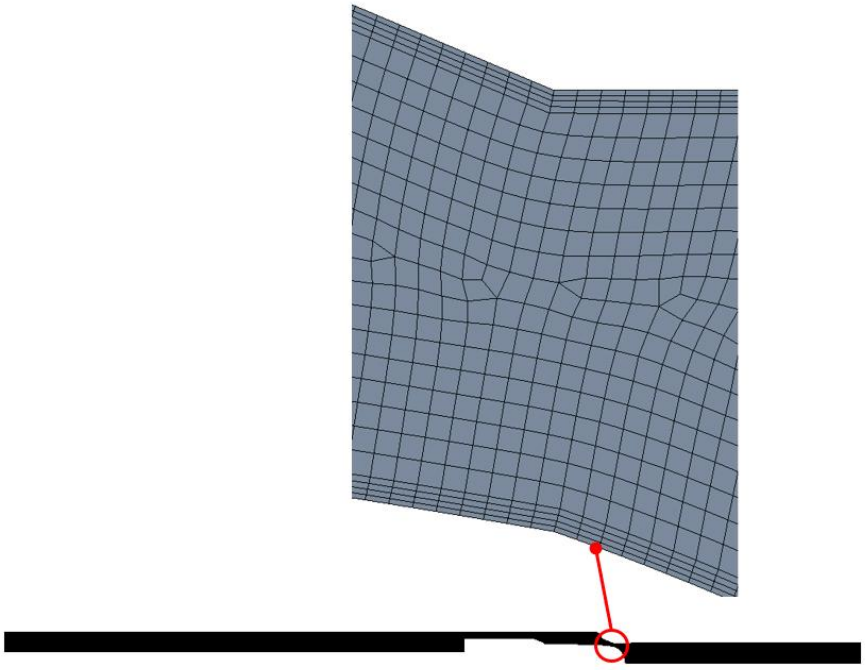

Figure 4.12: CFD Mesh of OEM

Solver Settings

Once the mesh was generated, the Fluent solver was employed using the mesh to converge to a solution. The axisymmetric geometry was chosen to reduce computational time and mesh complexity. The fundamental equations for solving consisted of mass conservation (Eqn. (4.31) [35]), which was applied in the axisymmetric form (Eqn. (4.32) [35]), where S_m is an additional flow effect if required, but for this application it was equated to zero:

$$\frac{\partial \rho}{\partial t} + \nabla \cdot (\rho \vec{v}) = S_m \tag{4.31}$$

$$\frac{\partial \rho}{\partial t} + \frac{\partial}{\partial x}(\rho v_x) + \frac{\partial}{\partial r}(\rho v_r) + \frac{\rho v_r}{r} = S_m \tag{4.32}$$

The general momentum conservation equation (Eqn. (4.33) [35]) was also extended and applied in the axial (Eqn. (4.34) [35]) and radial (Eqn. (4.35) [35]) forms for the axisymmetric model:

$$\frac{\partial}{\partial t}(\rho \vec{v}) + \nabla \cdot (\rho \vec{v}\vec{v}) = -\nabla \mathrm{p} + \nabla \cdot (\bar{\bar{\tau}}) + \rho \vec{g} + \vec{F} \tag{4.33}$$

$$\begin{aligned} &\frac{\partial}{\partial t}(\rho v_x) + \frac{1}{r}\frac{\partial}{\partial x}(r\rho v_x v_x) + \frac{1}{r}\frac{\partial}{\partial r}(r\rho v_r v_x) \\ &\quad = -\frac{\partial p}{\partial x} + \frac{1}{r}\frac{\partial}{\partial x}\left[r\mu\left(2\frac{\partial v_x}{\partial x} - \frac{2}{3}(\nabla \cdot \vec{v})\right)\right] \\ &\quad + \frac{1}{r}\frac{\partial}{\partial r}\left[r\mu\left(\frac{\partial v_x}{\partial r} + \frac{\partial v_r}{\partial x}\right)\right] + F_x \end{aligned} \tag{4.34}$$

$$\begin{aligned} &\frac{\partial}{\partial t}(\rho v_r) + \frac{1}{r}\frac{\partial}{\partial x}(r\rho v_x v_r) + \frac{1}{r}\frac{\partial}{\partial r}(r\rho v_r v_r) \\ &\quad = -\frac{\partial p}{\partial r} + \frac{1}{r}\frac{\partial}{\partial r}\left[r\mu\left(\frac{\partial v_r}{\partial x} + \frac{\partial v_x}{\partial r}\right)\right] \\ &\quad + \frac{1}{r}\frac{\partial}{\partial r}\left[r\mu\left(2\frac{\partial v_r}{\partial r} - \frac{2}{3}(\nabla \cdot \vec{v})\right)\right] - 2\mu\frac{v_r}{r^2} \\ &\quad + \frac{2}{3}\frac{u}{r}(\nabla \cdot \vec{v}) + \rho\frac{v_z^2}{r} + F_r \end{aligned} \tag{4.35}$$

The real gas equation of state was utilized in Fluent for a compressible nitrogen flow, where compressibility effects are enabled in the transport model:

$$P = \frac{RT}{V - b + c} - \frac{\alpha}{(V^2 + \delta V + \varepsilon)} \tag{4.36}$$

The energy equation (Eqn. (4.37)[35]) is enabled to ensure that proper energy and heat transfer is accounted for with viscous heating, if applicable, and the compressibility effects are

then substituted with ρ from Eqn. (4.36)[35]. Additionally, the Brinkman number (Eqn. (4.38)[35]) is enabled for the pressure-based solver when using compressible fluid and viscous heating, and is automatically enabled for a density-based solver approach. Although the Brinkman number may be greater than unity, generally for compressible flows, the pressure-based solver doesn't automatically assume this and therefore 'viscous heating' and 'compressibility effects' must be enabled for a realistic solution within the k-ω turbulence model settings:

$$\frac{\partial}{\partial t}\left(\rho\left(e+\frac{v^2}{2}\right)\right)+\nabla\cdot\left(\rho\vec{v}\left(h+\frac{v^2}{2}\right)\right) = \nabla\cdot\left(k_{eff}\nabla T-\sum_j h_j\vec{J}_j+\bar{\bar{\tau}}_{eff}\cdot\vec{v}\right)+S_h \tag{4.37}$$

$$Br=\frac{\mu U_e^2}{k\Delta T} \tag{4.38}$$

Next, the SST (Shear Stress Transport) k-ω was chosen as the transport model. Originally, the standard k-ω model was formulated as a better predictor than the k-ε model. The standard k-ω model is shown below. The BSL k-ω and SST k-ω models both follow Eqns. (4.39)[35] and (4.40)[35]:

$$\frac{\partial}{\partial t}(\rho k)+\frac{\partial}{\partial x_i}(\rho k u_i)=\frac{\partial}{\partial x_j}\left(\Gamma_k\frac{\partial k}{\partial x_j}\right)+G_k-Y_k+S_k+G_b \tag{4.39}$$

$$\frac{\partial}{\partial t}(\rho\omega)+\frac{\partial}{\partial x_i}(\rho\omega u_i)=\frac{\partial}{\partial x_j}\left(\Gamma_\omega\frac{\partial \omega}{\partial x_j}\right)+G_\omega-Y_\omega+S_\omega+G_{\omega b} \tag{4.40}$$

The primary reason for using the SST k-ω over the BSL or standard model lies in Eqn. (4.41) [35], which is an eddy viscosity limiter. This term corrects the overprediction of eddy viscosity and swirling present in the standard k-ω model, leading to more accurate solutions.

Additionally, the following settings within the transport model were enabled: compressibility effects, viscous heating, and the Kato Launder Production limiter enabled as a byproduct of selecting the gamma-algebraic transition model. The 'compressibility effects' and 'viscous heating' parameters discussed previously are enabled and incorporated through the energy equation as described above.

The transition model used was the gamma-algebraic model, which uses Eqn. (4.42)[35] and (4.43)[35] to calculate turbulence parameters based on local flow characteristics. These equations are essential for defining the turbulence production term, in conjunction with the 'Production Kato Laudner' being enabled. As shown in Eqn. (4.44) [36] , Kato Laudner is necessary, as the 2-equation model (k-ω) overpredicts turbulence in high velocity regions, replacing a strain rate with a vorticity magnitude [36].

$$\mu_t = \frac{\rho k}{\omega} \frac{1}{max\left[\frac{1}{a^*}, \frac{SF_2}{a_1 \omega}\right]} \tag{4.41}$$

$$P_k \rightarrow \gamma P_k \tag{4.42}$$

$$\gamma = tanh(Rat_{Re}^2) \tag{4.43}$$

$$P = \mu_t S\Omega \tag{4.44}$$

The setup of boundary conditions, previously categorized as 'named selections' in the preprocessing phase, ensures that the solver correctly interprets and applies the physical constraints of the problem.

The inlet boundary condition selected was a 'mass-flow-inlet', which is defined using a mass flow rate of 1 g/s to ensure an appropriate resolution of the boundary layer, particularly in the laminar flow region near the inlet. The choice of a mass-based inlet, rather than a velocity-based or pressure inlet, allows for precise control of mass conservation, making it ideal for simulations involving compressible flow. By defining the mass flow rate, Fluent automatically adjusts velocity based on the local density and area, ensuring consistency within the conservation laws.

The outlet boundary condition was selected as 'pressure-outlet', and was set to a 0 [Pa] gauge pressure, representing atmospheric conditions. This indicates that the static pressure at the outlet is equal to the reference atmospheric pressure, allowing flow to exit the domain freely without artificial constraints. The 'Average Pressure Specification' was enabled to ensure that the

mean outlet pressure is maintained at the specified value (*e.g.,* 0-gauge pressure for atmospheric conditions), smoothing out potential numerical oscillations.

The axis boundary condition is used in axisymmetric simulations to specify the axis about which the geometry is revolved. This setting informs Fluent that the problem is two-dimensional but physically represents a 3D axisymmetric flow field.

The wall boundary condition is crucial in defining surface interactions, particularly roughness effects and velocity constraints. Surface roughness at the wall was imposed, with a value of 0.045 mm chosen based on data available in literature [2, 5]. A no-slip boundary condition was applied at the walls, enforcing zero velocity relative to the surface.

These boundary conditions were chosen to properly simulate the pressure drop (ΔP) across the flow region between plug body and upstream valve wall. The constraints allowed for the pressure to 'float up', given a mass flow inlet and an outlet pressure, and solve for the pressure at the inlet and across the fluid flow region. The wall settings were needed to increase accuracy of transport phenomena near the wall. Boundary conditions settings implemented are summarized in *Table 4.5*.

Table 4.5: Boundary Condition Settings

Boundary Condition	**Specification**	**Purpose**
Inlet	Mass flow rate = 1 g/s	Sets inlet mass flow parameter
Outlet	0 [Pa] gauge pressure w/ 'Average Pressure Specification' enabled	Prevents artificial pressure buildup, allows free outflow
Axis	Axis of rotation	Defines the rotational reference for axisymmetric calculations
Wall	Roughness = 0.045 mm, No-slip condition	Models real-world surface effects, ensures velocity adherence

Solver methods utilized in Fluent are detailed in *Table 4.6*. The solving scheme implemented was the SIMPLE-Consistent (SIMPLEC) algorithm, which is an efficient solver for pressure-velocity coupling in steady-state simulations, particularly in cases where convergence is hindered by weak coupling between pressure and velocity fields. Compared to the SIMPLE algorithm, SIMPLEC modifies Eqn. (4.45) [35], the flux correction equation, with a revised d_f term (Eqn. (4.46)[35]). This modification accelerates convergence while maintaining numerical

stability. Additionally, SIMPLEC incorporates a skewness correction step, which enhances its performance on highly non-orthogonal or skewed meshes, where conventional pressure correction methods may struggle to maintain accuracy.

$$J_f = J_f^* + d_f(p'_{c0} - p'_{c1}) \tag{4.45}$$

$$d_f = \left(\overline{\frac{}{a_P - \sum_{nb} a_{nb}}}\right) \tag{4.46}$$

The least-squares gradient method provides accuracy similar to the node-based gradient method while outperforming the cell-based gradient method [35]. As a result, it has been designated as the default gradient calculation method in the ANSYS Fluent solver.

Second-order upwind method (Eqn. (4.47) [35]) estimates the variable at a control volume face by extrapolating from the cell center using a higher-order approximation. This method improves spatial accuracy by reducing numerical diffusion, which is a common issue in first-order schemes.

The second order settings are used due to implementing the central differencing method (Eqn. (4.48) [35]), which uses central differencing for spatial discretization. Central differencing is a symmetric interpolation method that estimates variable values at control volume faces by averaging neighboring cell values. This scheme is preferred in second-order methods because it reduces truncation errors and enhances accuracy [35].

$$\varphi_{f,SOU} = \varphi + \nabla\varphi \cdot \vec{r} \tag{4.47}$$

$$\varphi_{f,CD} = \frac{1}{2}(\varphi_0 + \varphi_1) + \frac{1}{2}(\nabla\varphi_0 \cdot \overrightarrow{r_0} + \nabla\varphi_1 \cdot \overrightarrow{r_0}) \tag{4.48}$$

Table 4.6: Solver Method Settings

Pressure-Velocity Coupling	
Scheme	SIMPLEC
Skewness Correction	0
Flux Type	Rhie-Chow: distance based
Spatial Discretization	
Gradient	Least Squares Cell Based
Pressure	Second Order
Density	Second Order Upwind
Momentum	Second Order Upwind
Turbulent Kinetic Energy	Second Order Upwind
Specific Dissipation Rate	Second Order Upwind
Energy	Second Order Upwind

The standard initialization approach was used specifying the simulation to 'compute from inlet', allowing it to use the inlet boundary condition as the simulations initial calculation point [34]. The standard convergence values, as well as all other inputs, were standard except for the above settings mentioned. Once initialized, the simulation is numerically solved until convergence is achieved.

Solver Results

Results for the numerical simulation of the OEM plug profile are displayed in *Figure 4.13* and *Figure 4.14*. *Figure 4.13* describes the pressure gradient across the flow area, and *Figure 4.14* provides the streamlines through the valve opening. The valve behaves similarly to an orifice or venturi, with a significant pressure drop across the smallest gap between the valve plug and valve wall, increasing the flow velocity (as is evident from the streamlines). The red streamlines of *Figure 4.14* indicate the highest velocity, corresponding to the pressure drop along the pressure gradients.

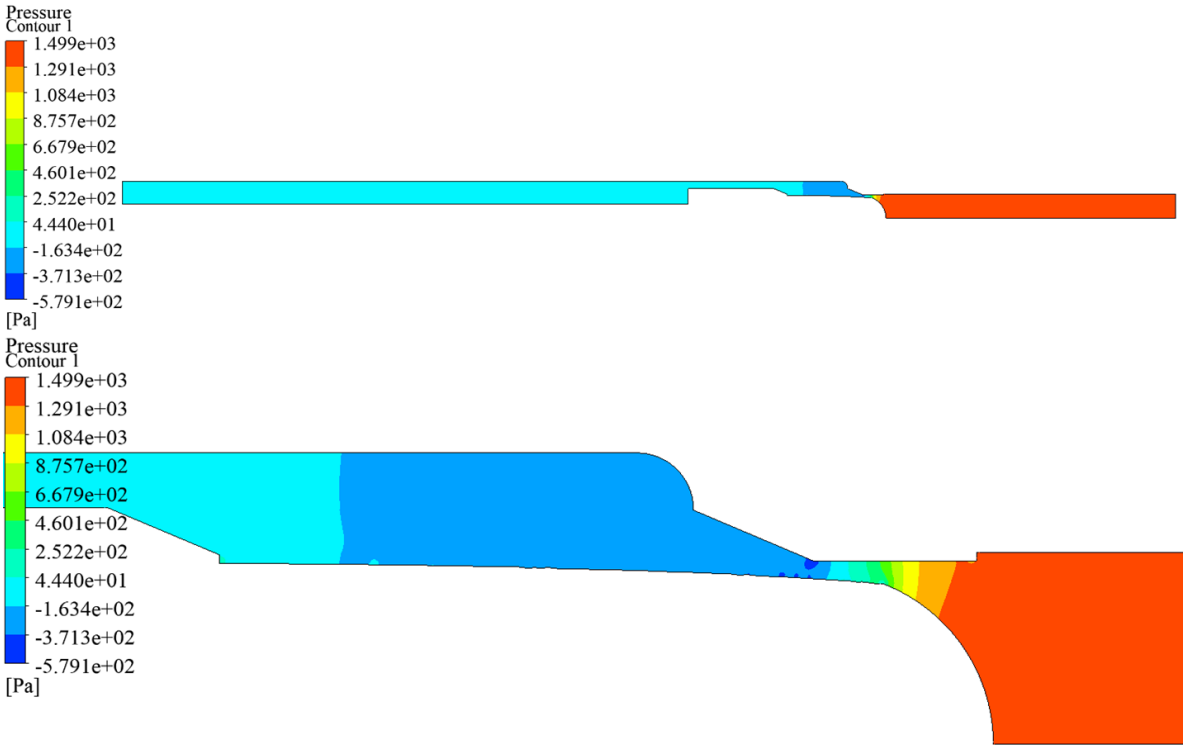

Figure 4.13: Pressure Gradient of Axisymmetric Valve Flow Area Cross-section (OEM)

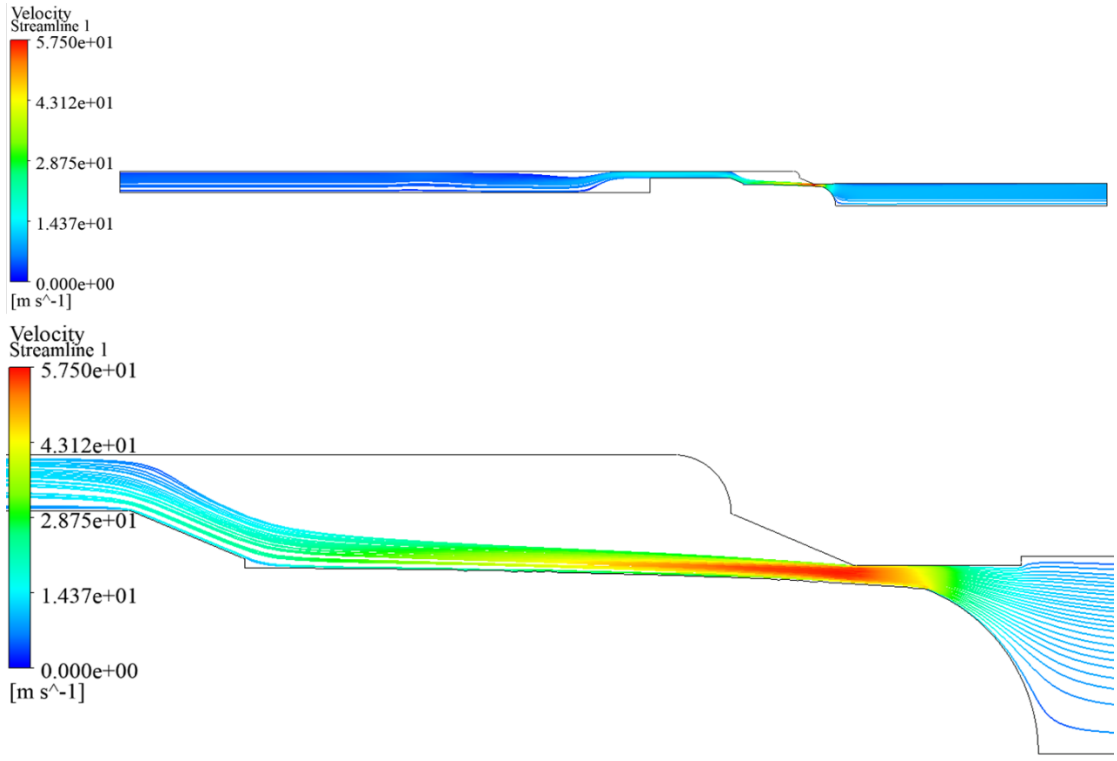

Figure 4.14: Streamline of Axisymmetric Valve Flow Area Cross-section (OEM)

Table 4.7 details the maximum flow coefficient and parameter changes such as length of plug (ℓ_{plug}), analytical flow coefficient ($C_{v,m}$), and base diameter (D_{Base}). The flow coefficient was calculated based on the pressure drop across the valve from the inlet to outlet boundary conditions, mass flow rate (which was constrained to 1g/s), the temperature, and the inlet pressure, which was solved for by ANSYS Fluent. Specifically, given the mass flow and pressure at the outlet, Fluent converged to an inlet pressure which satisfied the conservation equations.

Each valve plug geometry considered in the analysis showed excellent agreement between analytical maximum flow coefficient ($C_{v,m}$) and calculated maximum flow coefficient ($C_{v,m,CFD}$), with maximum relative error being approximately 7%. All plug geometries modeled used equivalent boundary conditions, including mass flow and outlet pressure allowing for the simulation to solve the pressure across the flow region. Given that the hybrid flow plugs are a combination of two equal percent profiles, it was assumed that CFD analysis is not required to verify the analytical model results, as it would yield similar trends as the 'A-series' plugs.

Table 4.7: Analytical and CFD Comparison (Nitrogen at 300K)

Part ID	$C_{v,m}$	$C_{v,m,CFD}$	Relative error between Analytical and CFD	ℓ_{stroke}	ℓ_{plug}	D_{Base}	Character
[-]	[-]	[-]	[%]	[in.]	[in.]	[in.]	[-]
OEM	1.0	1.03	3.0	0.75	0.875	0.4105	Eq %
A1	0.3	0.300	0.19	0.75	0.948	0.4110	Eq %
A2	0.3	0.297	0.99	0.75	0.948	0.4120	Eq %
A3	0.3	0.280	6.65	0.75	0.946	0.4140	Eq %
A4	0.3	0.295	1.62	0.75	1.000	0.4120	Eq %

Modeling of Cryogenic Helium Flow

To further validate the applicability of the designed plugs under cryogenic conditions, the ANSYS Fluent simulations were repeated using helium gas at 50 K. This temperature closely reflects the actual operating environment of cryogenic thermal intercepts (as discussed in Chapter 5) such as those used in FRIB. All simulations used the same mesh geometry and boundary conditions (apart from temperature and fluid) as previous runs (with gaseous nitrogen at room temperature), but real-gas helium properties based on REFPROP [37] were applied to capture compressibility and thermal property effects. The results, summarized in *Table 4.8*, show that plug

designs based on incompressible flow assumptions still achieve close agreement with targeted maximum flow coefficients under real gas conditions for cryogenic helium. Across all 'A-series' plugs and the OEM design, the relative between analytical and CFD-predicted maximum flow coefficients remained under 5.1%. These helium-based CFD results reinforce the validity of the original plug design approach and provide further confidence in performance under cryogenic operation.

Table 4.8: Analytical and CFD Comparison (Helium at 50K)

Part ID	$C_{v,m}$	$C_{v,m,CFD}$	Relative error between Analytical and CFD	ℓ_{stroke}	ℓ_{plug}	D_{Base}	Character
[-]	[-]	[-]	[%]	[in.]	[in.]	[in.]	[-]
OEM	1.0	1.051	5.1	0.75	0.875	0.4105	Eq %
A1	0.3	0.299	0.33	0.75	0.948	0.4110	Eq %
A2	0.3	0.31	3.33	0.75	0.948	0.4120	Eq %
A3	0.3	0.296	1.33	0.75	0.946	0.4140	Eq %
A4	0.3	0.31	3.33	0.75	1.000	0.4120	Eq %

Chapter 5: MODEL VALIDATION AND VALVE FLOW CHARACTERIZATION

5.1 Characterization of Equal Percent Plugs

The equal percent valve plugs tested experimentally consisted of the OEM and 'A-series', as seen in *Figure 5.1*, which were designed for a desired maximum flow coefficient ($C_{v,m}$) of 1.0 and 0.3, respectively. The 'A-series' designs that were fabricated consisted of four unique geometries, designated A1-A4, each with a target maximum flow coefficient of 0.3. Plugs A1-A3 had rounded tips and varied in rangeability through adjustment of the base diameter (D_{Base}). The A4 valve plug was designed to investigate the effects of increasing the overall length of the plug, maintaining the A2 plug base diameter and extending its tip length, therefore sharpening the tip end. The analytical parameters for the individual plugs are outlined in *Table 5.1,* where D_{Base}, $C_{v,m}$, and the length of the plug (based on tip shape) were varied.

Table 5.1: Equal Percent Analytical Parameters of Study

Part ID	$C_{v,m}$	R	ℓ_{stroke}	ℓ_{plug}	D_{Base}	Character
[-]	[-]	[-]	[in.]	[in.]	[in.]	[-]
OEM	1.0	9.1	0.75	0.875	0.4105	Eq %
A1	0.3	3.0	0.75	0.948	0.4110	Eq %
A2	0.3	3.7	0.75	0.948	0.4120	Eq %
A3	0.3	7.4	0.75	0.946	0.4140	Eq %
A4	0.3	3.7	0.75	1.000	0.4120	Eq %

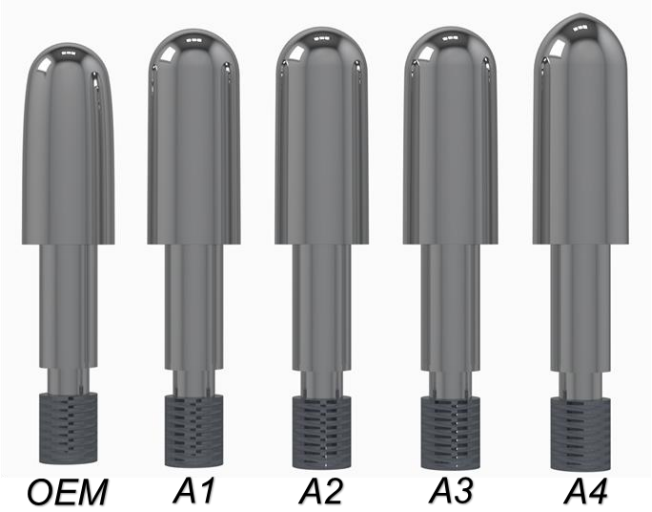

Figure 5.1: 'A-series' Valve Plugs

The geometry of the OEM plug that was tested was not fully captured in the analytical model, mainly due to the OEM design process, design specifications (such as rangeability), and manufacturing tolerances not being available from the vendor. Therefore, an analytical model was applied based upon the same processes to design the 'A-series', with the goal of trying to approximate the OEM plug's characteristics. Relative error between the analytical model results and the actual OEM plug geometry was expected to be somewhat significant due to the lack of design information available.

On the test bench, the control valve was calibrated with respect to valve stem positioning, ensuring the valve stem and actuator were properly positioned before and after each experiment. Pressure sensor offsets were recorded to accurately corrected pressure and differential pressure measurements. To verify the plug was installed properly, the fully closed position (0% stroke) was tested to ensure there was no leakage across the installed valve plug, *i.e.* the Kel-F seated fully into the upstream valve body wall. The stroke measurement was also calibrated to enable consistent and accurate measurements from 0-100% range, verifying that at 0% stroke the valve position corresponded to a 0.00mm reading on the caliper. For validation and characterization of the valve plug, data points were collected from 5% stroke to 100% stroke in 5% increments, and then returning to 5% stroke, ending with another full seal position (0%) to verify the final caliper measurement settled to 0.00mm.

Experimental Performance of Designed Plugs

The valve plugs designed using the incompressible flow assumption were initially designed based on simplified fluid behavior. While this approach was effective for shaping the general flow characteristic (e.g., equal percent), and therefore a geometry of the plug profile, real operating environments may deviate from these assumptions. To assess performance validity, these plug designs were evaluated, and the flow coefficient was calculated with respect to the ANSI/ISA S75.01 standards. Where the model deviates from the experimental results may be due to compressibility effects coming into play, as well as inconsistencies in manufacturing tolerancing of the geometric plug profile.

Experimental Validation

The OEM plug was the first flow plug to be validated experimentally, and as anticipated the middle range of predicted flow coefficient varies from the analytical estimation, while the maximum and minimum flow coefficients are reasonably accurate. As mentioned previously, this

is due to the design and manufacturing process (as well as tolerancing) being unknown when re-designing the plug profile.

The variability between the OEM plug analytical model and experimental data was a maximum of 37% at a valve position of 60% open and a minimum of 0.31% at 5% open. The average variability between the analytical model and experimental data was 21.75%. The experimental measurement uncertainty was a maximum of 1.53% at a valve position of 5% open and minimum of 0.42% at 100% open. The average experimental uncertainty across the data was 0.73%. Comparison between the OEM plug measured data and the analytical estimation is shown in *Figure 5.1*.

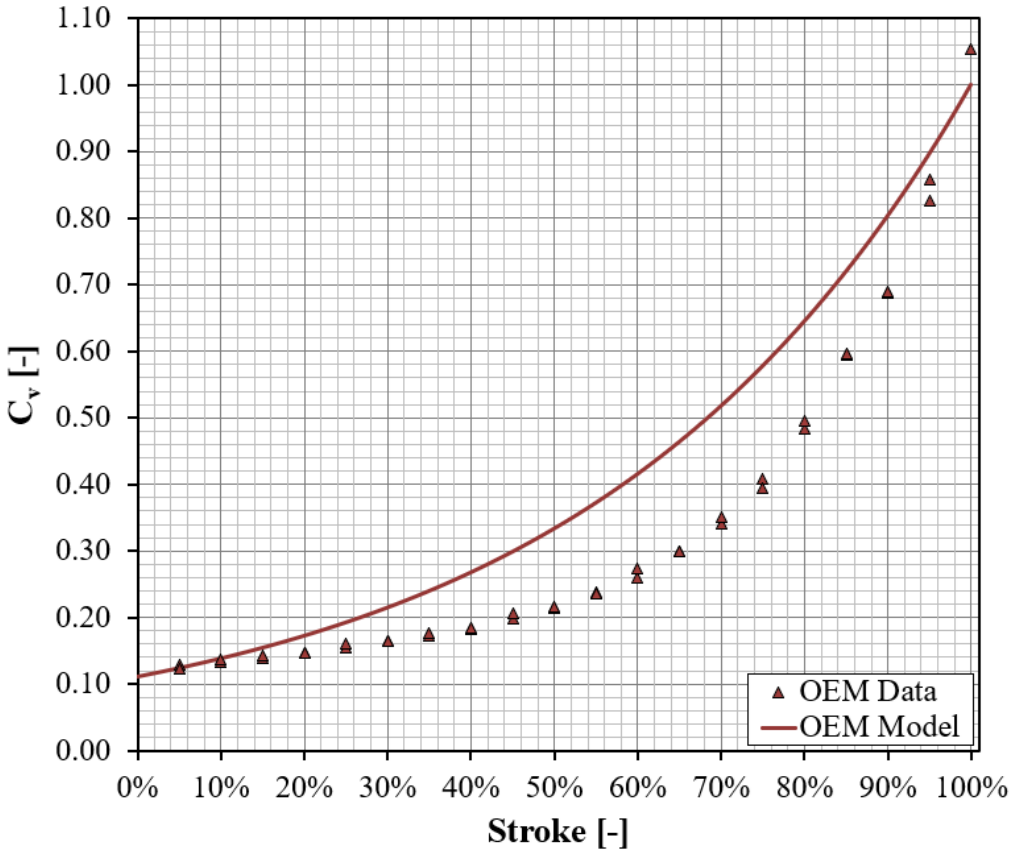

Figure 5.2: OEM Plug Experimental Characterization

The variability between the A1 analytical model and experimental data was a maximum of 14.42% at a valve position of 100% open and a minimum of 3.18% at 55% open. The average variability between the analytical model and experimental data was 7.54%. The experimental uncertainty was a maximum of 1.86% at 5% open and minimum of 0.44% at 100% open. The

average experimental uncertainty across the data was 0.88%. A comparison between the A1 measured data and the analytical estimation is shown in *Figure 5.2*.

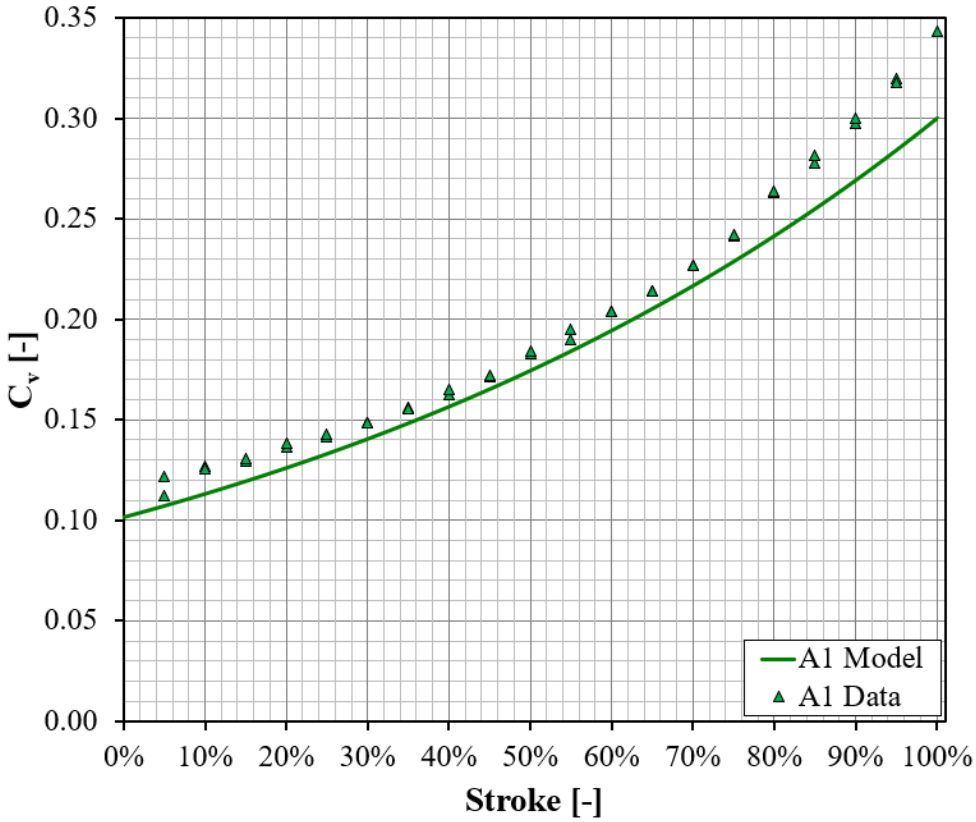

Figure 5.3: A1 Plug Experimental Characterization

The variability between the A2 analytical model and experimental data was a maximum of 14.57% at a valve position of 100% open and a minimum of 2.64% at 45% open. The average variability between the analytical model and experimental data was 7.46%. The experimental uncertainty was a maximum of 2.43% at 5% open and minimum of 0.45% at 100% open. The average experimental uncertainty across the data was 1.13%. Comparison between the A2 measured data and the analytical estimation is shown in *Figure 5.3*.

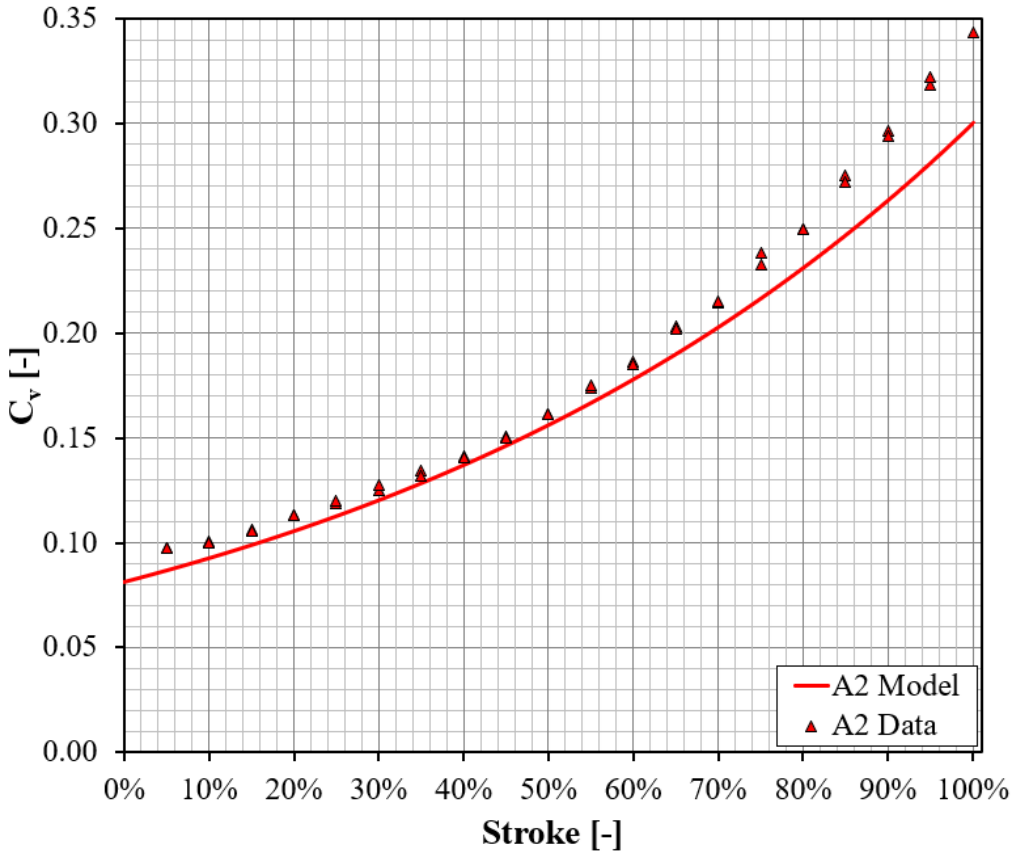

Figure 5.4: A2 Plug Experimental Characterization

The variability between the A3 analytical model and experimental data was a maximum of 15.35% at a valve position of 100% open and a minimum of 0.58% at 55% open. The average variability between the analytical model and experimental data was 6.98%. The experimental uncertainty was a maximum of 11.14% at 5% open and minimum of 0.44% at 100% open. The average experimental uncertainty across the data was 3.41%. Comparison between the A3 measured data and the analytical estimation is shown in *Figure 5.4*.

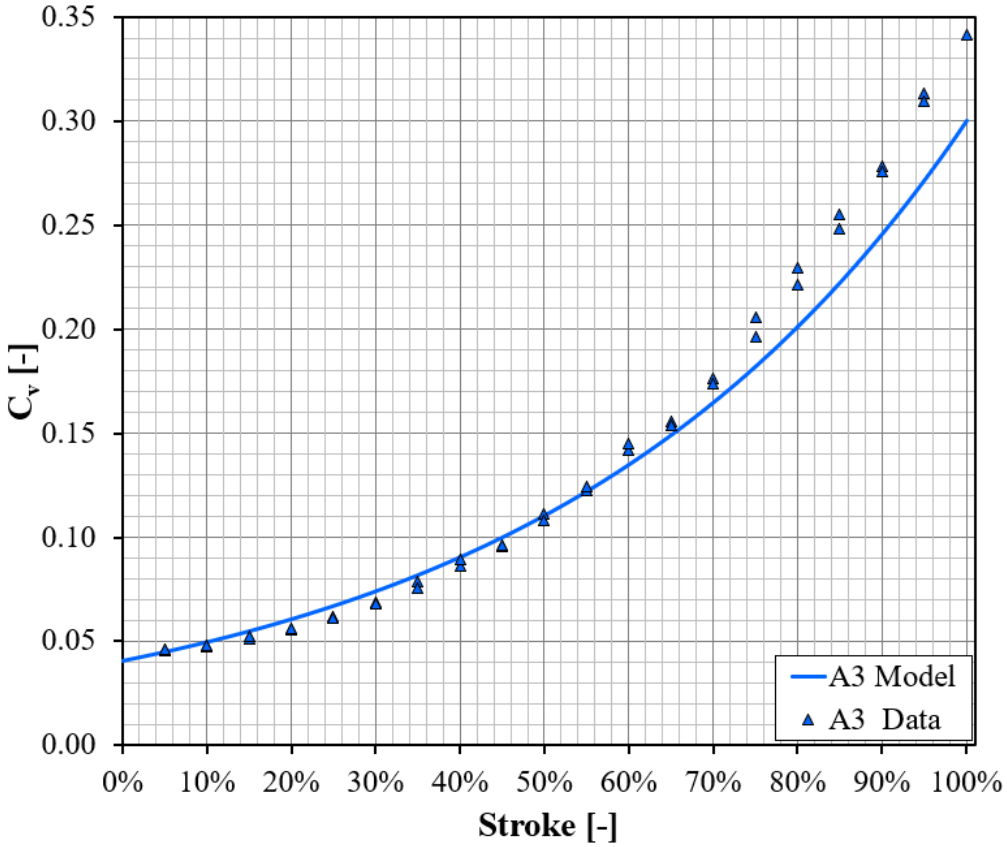

Figure 5.5: A3 Plug Experimental Characterization

The variability between the A4 analytical model and experimental data was a maximum of 16.33% at a valve position of 100% open and a minimum of 4.08% at 55% open. The average variability between the analytical model and experimental data was 9.13%. The experimental uncertainty was a maximum of 2.42% at 5% open and minimum of 0.44% at 100% open. The average experimental uncertainty across the data was 1.10%. Comparison between the A4 measured data and the analytical estimation is shown in *Figure 5.5*.

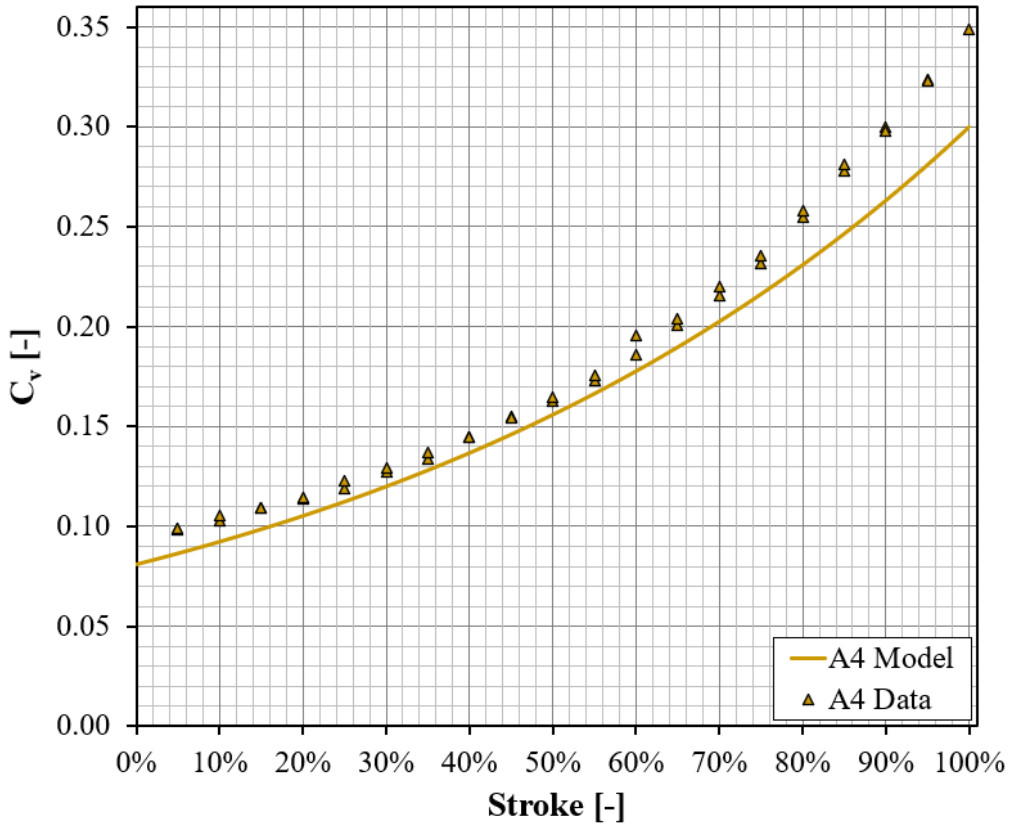

Figure 5.6: A4 Plug Experimental Characterization

Table 5.2 details the intended analytical design values versus the experimentally validated values. The maximum analytically designed flow coefficient ($C_{v,m}$) matched reasonably well with the experimental maximum flow coefficient ($C_{v,m,exp}$) for each of the designs tested. Slight variation in the experimental stroke was observed between tests due to measurement calibration as well as accurate repeatability of the positioner/actuator.

Table 5.2: Equal Percent Plug Experimental Validation Results

Part ID	$C_{v,m}$	R	ℓ_{stroke}	$C_{v,m,exp}$	R_{exp}	$\ell_{stroke,\ exp}$	ℓ_{plug}	D_{Base}	Character
[-]	[-]	[-]	[in.]	[-]	[-]	[in.]	[in.]	[in.]	[-]
OEM	1.0	9.1	.75	1.04	10.7	0.671	0.875	0.4105	Eq %
A1	0.3	3.0	.75	0.34	2.9	0.674	0.948	0.411	Eq %
A2	0.3	3.7	.75	0.34	3.5	0.676	0.948	0.412	Eq %
A3	0.3	7.4	.75	0.34	7.5	0.676	0.946	0.414	Eq %
A4	0.3	3.7	.75	0.35	3.5	0.675	1.000	0.412	Eq %

For the plugs A1-A3, the base diameter increased sequentially from 0.411” to 0.412” and .414”, respectively. Increasing the base diameter lowered the minimum flow coefficient, however it had negligible effect on flow coefficient near 100% valve position, as designed. Similar trends were presented in Chapter 4, where increasing the D_{Base} of the analytical model reduced the flow coefficient near the closed position but had negligible effect on the maximum C_v. This is confirmed in *Figure 5.6*, where no noticeable effect was perceived at the top end of the stroke when increasing the D_{Base} parameter.

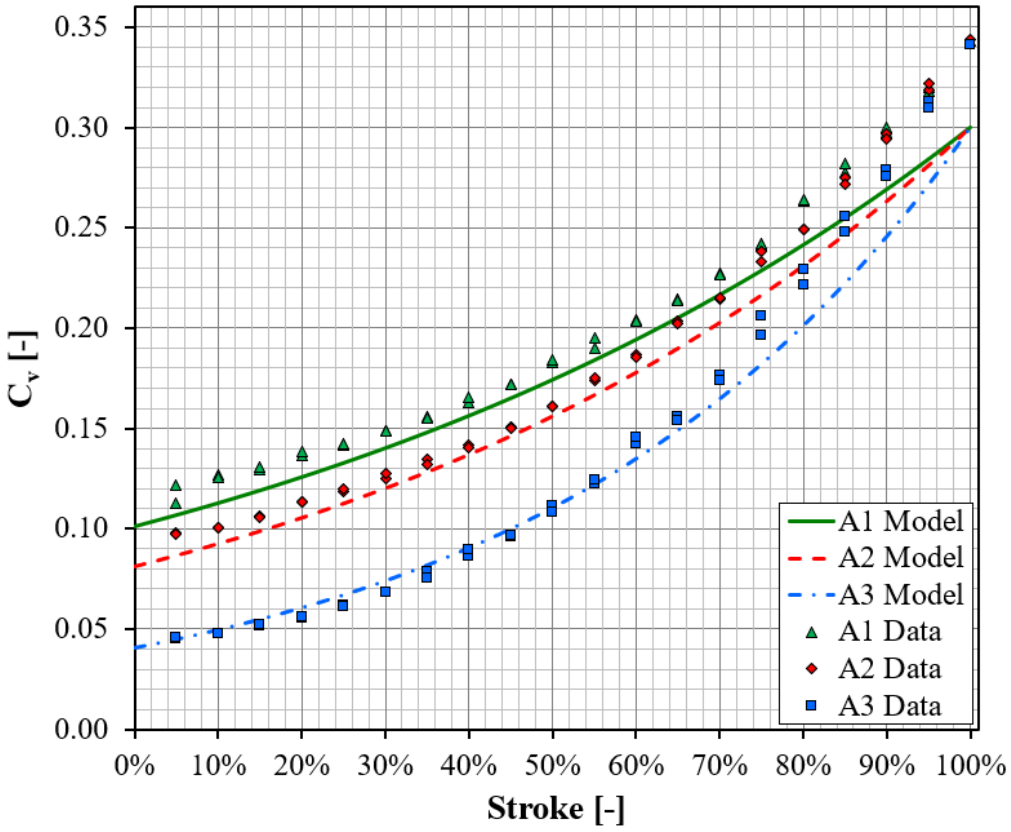

Figure 5.7: A1-A3 Plug Comparison

The designs for A2 and A4 had the same base diameter and plug profile, but the overall plug length was increased by lengthening of the plug tip by 0.05”, creating a sharper and more elongated tip. The overall plug length, consisting of the 0.75” active profile and the tip length, increasing from 0.95” to 1”. Results from the CFD simulation predicted minimal effect on flow coefficient at 100% stroke, which was validated from experimental testing, as shown in *Figure 5.8* and *Table 5.3*.

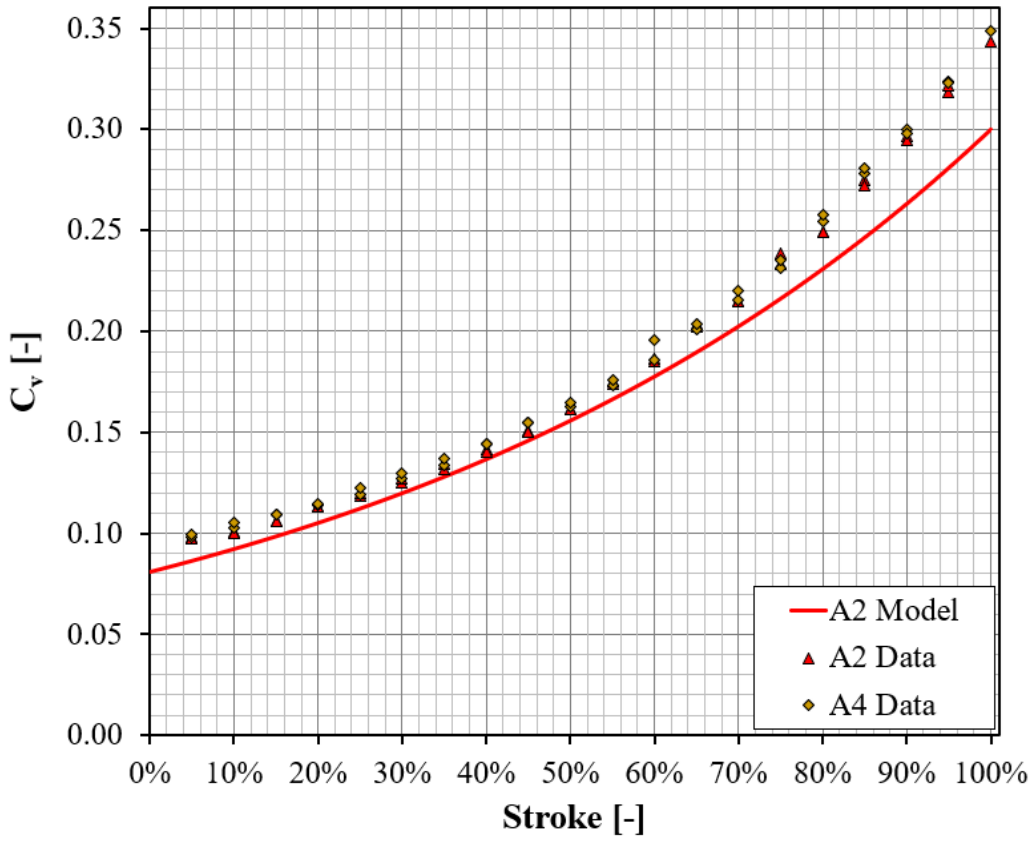

Figure 5.8: A2 and A4 Plug Comparison

The CFD validation presented in Chapter 4 is also applicable to compare with the experimental results. Both A2 and A4 exhibit a negligible decrease in the CFD-derived flow coefficient, consistent with experimental observations. Furthermore, both the experimental and CFD calculations were performed in accordance with ISA standards [6]. Overall, the OEM and 'A-series' both experimentally and using CFD are within reasonable accuracy to their analytical counterparts, as seen in *Table 5.3*.

Table 5.3: Equal Percentage CFD Validation

Part ID	$C_{v,m}$	$C_{v,m,exp}$	$C_{v,m,CFD}$	ℓ_{stroke}	$\ell_{stroke,exp}$	ℓ_{plug}	D_{Base}	Character
[-]	[-]	[-]	[-]	[in.]	[in.]	[in.]	[in.]	[-]
OEM	1	1.04	1.03	0.75	0.671	0.875	0.4105	Eq %
A1	0.3	0.34	0.3	0.75	0.674	0.948	0.411	Eq %
A2	0.3	0.34	0.297	0.75	0.676	0.948	0.412	Eq %
A3	0.3	0.34	0.28	0.75	0.676	0.946	0.414	Eq %
A4	0.3	0.35	0.295	0.75	0.675	1.000	0.412	Eq %

Tip Shape Variation Analysis

To anticipate the effects of plug tip geometry variance, a computational fluid dynamics (CFD) analysis was conducted which considered three different tip configurations for the A2 equal percent plug: flat tip, rounded tip, and sharp (extended) tip, as seen in *Figure 5.9* and *Figure 5.10* . The A2 profile was selected for these tests due to the tip variance experimentally tested with the identical A4 profile, ensuring that only the effects of tip shape were examined without modification of other geometric factors. Descriptions for the tip modifications considered in the CFD study are:

1. Flat Tip (Solid Black Line) – At the end of the generated profile of the A2 equal percent plug, the tip is a flattened with a vertical extension down to the centerline.
2. Rounded Tip (Small Dotted Red Line) – The tip is smoothly tangent to the end of the A2 plug's active profile and transitions to intersect perpendicularly with the centerline, creating a rounded shape.
3. Sharp Tip (Thick Dotted Blue Line) – The tip is also tangent to the end of the A2 plug's active profile, and is constrained at a specified extended total tip length, forming a sharpened point at the center line

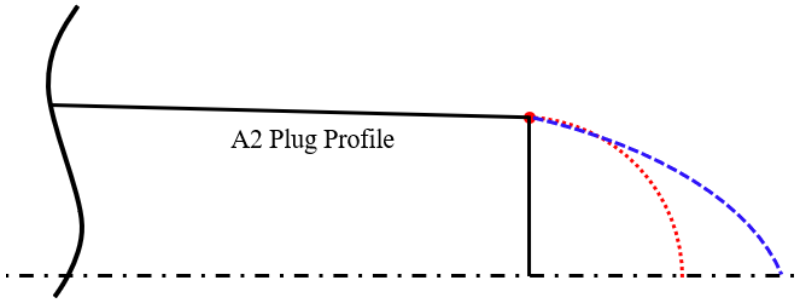

Figure 5.9: A2 Tip Callouts Cross-Section

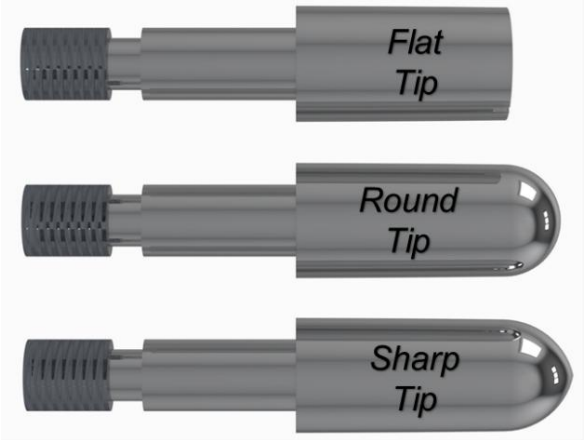

Figure 5.10: Tip Variation of A2 Profile

The flat tip configuration was found to result in a reduction of the maximum flow coefficient by approximately 0.02. The experimental validation of A2 (Round Tip) versus A4 (A2 Profile w / Sharp Tip) along with the CFD validation support that extending the length of the tip beyond the perpendicular end configuration has negligible effect on maximum flow coefficient. Results from the CFD study is provided in *Table 5.4*.

Table 5.4: Valve Plug Tip CFD Analysis

Descriptor [-]	$C_{v,m}$ [-]	$C_{v,m,CFD}$ [-]	ℓ_{stroke} [in.]	ℓ_{plug} [in.]	ℓ_{tip} [in.]	D_{Base} [in.]	Character [-]
Flat Tip	0.3	0.279	0.75	0.75	0.00	0.412	Eq %
Round Tip	0.3	0.297	0.75	0.95	0.20	0.412	Eq %
Sharp Tip	0.3	0.295	0.75	1.00	0.25	0.412	Eq %

Given the impact of tip shape on flow characteristics, a rounded tip (with a perpendicular end with respect to the center line) appears to be the most practical choice. Both experimental results (A2 vs. A4) and CFD simulations indicate that the sharp tip does not provide an advantage and uses more material in the fabrication process. Additionally, the flat tip is not ideal as it creates a flow stagnation point, which can negatively affect flow performance (as seen by the reduction in maximum C_v). This flow stagnation point can be clearly seen in the pressure contour and velocity contour produced using CFD, as shown in the comparison between the plug tip variation in *Figure 5.11* through *Figure 5.13*.

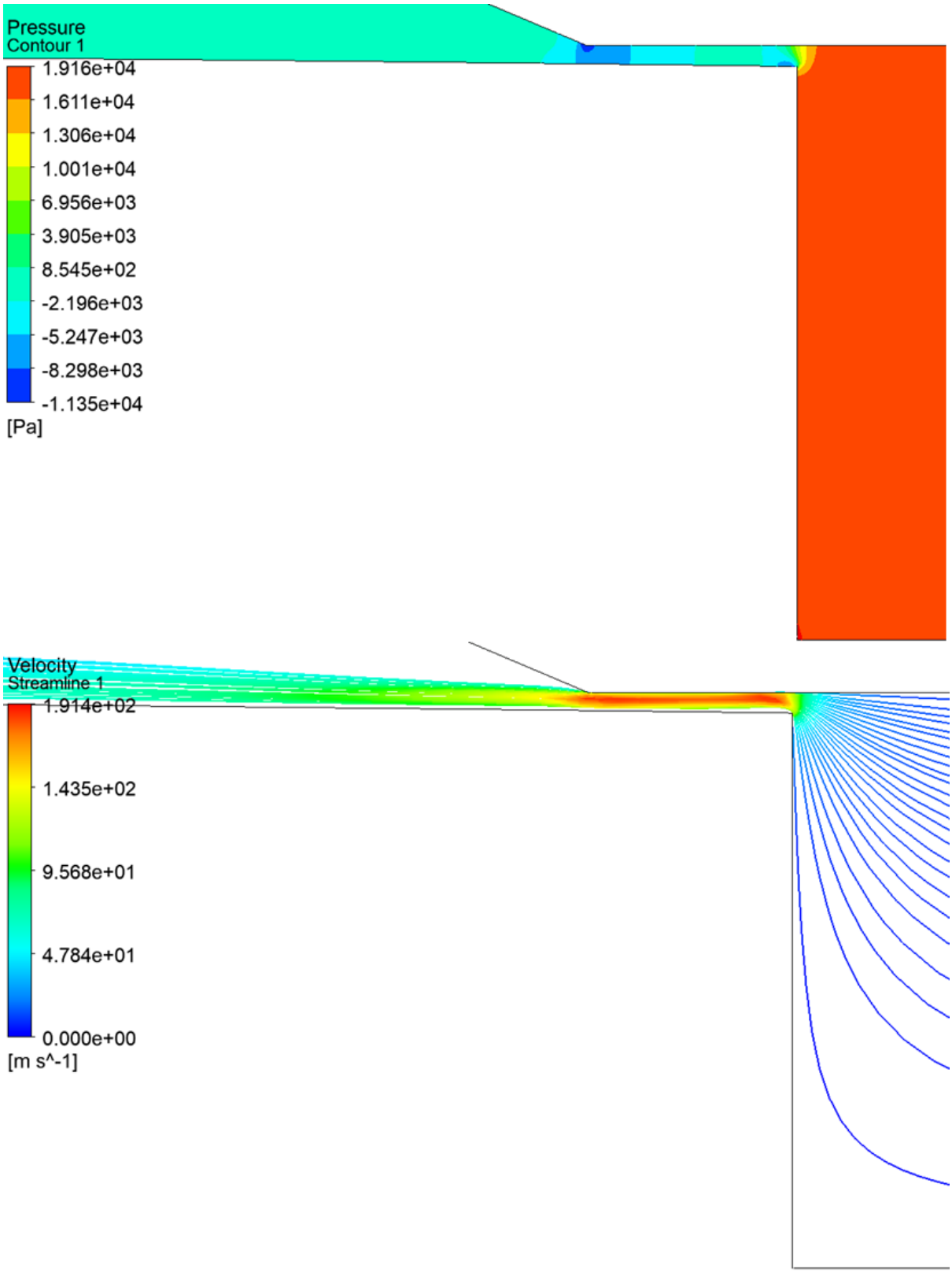

Figure 5.11: A2 Profile – Flat Tip | Pressure Contour (Left) and Streamlines (Right)

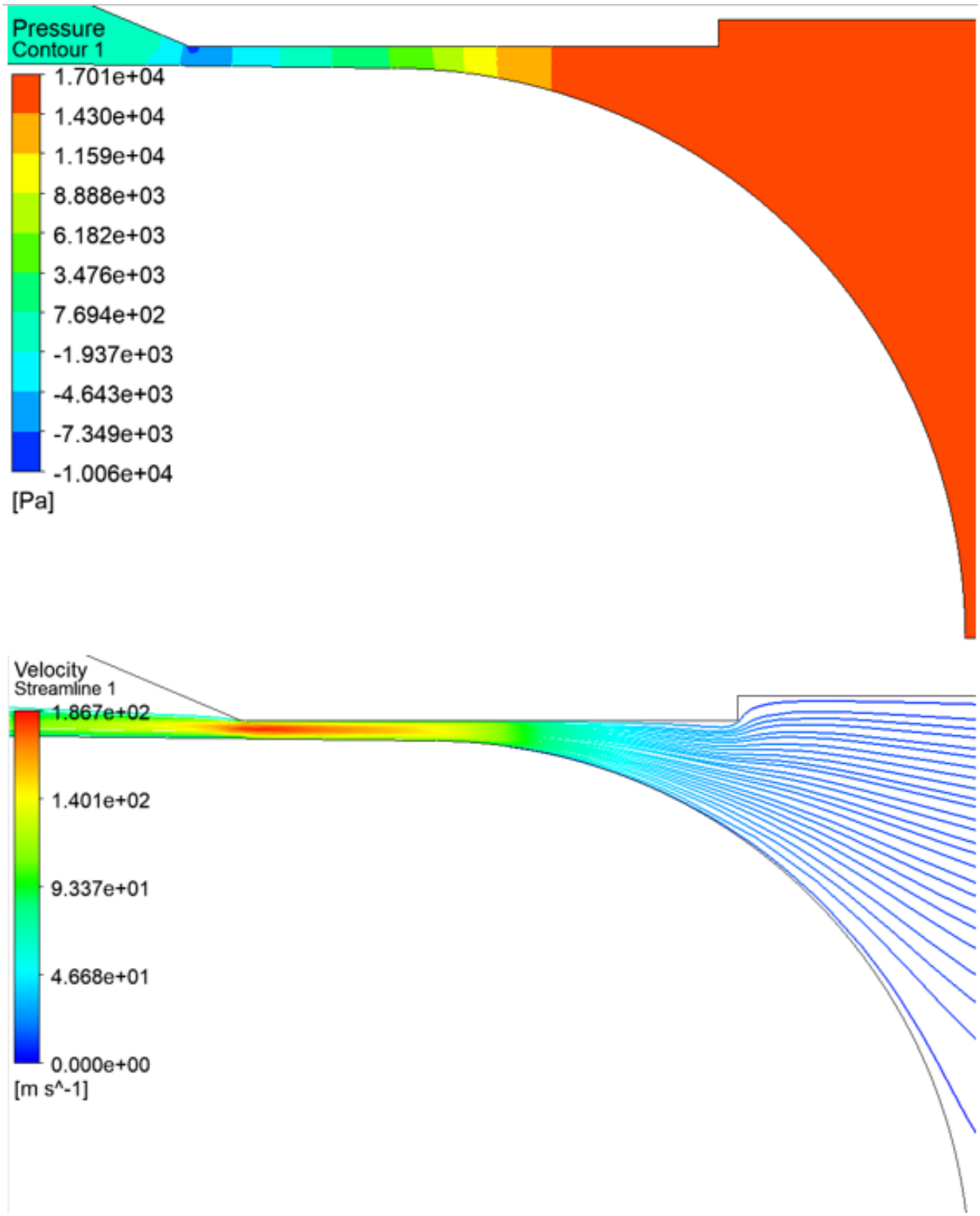

Figure 5.12: A2 Profile – Round Tip | Pressure Contour (Left) and Streamlines(Right)

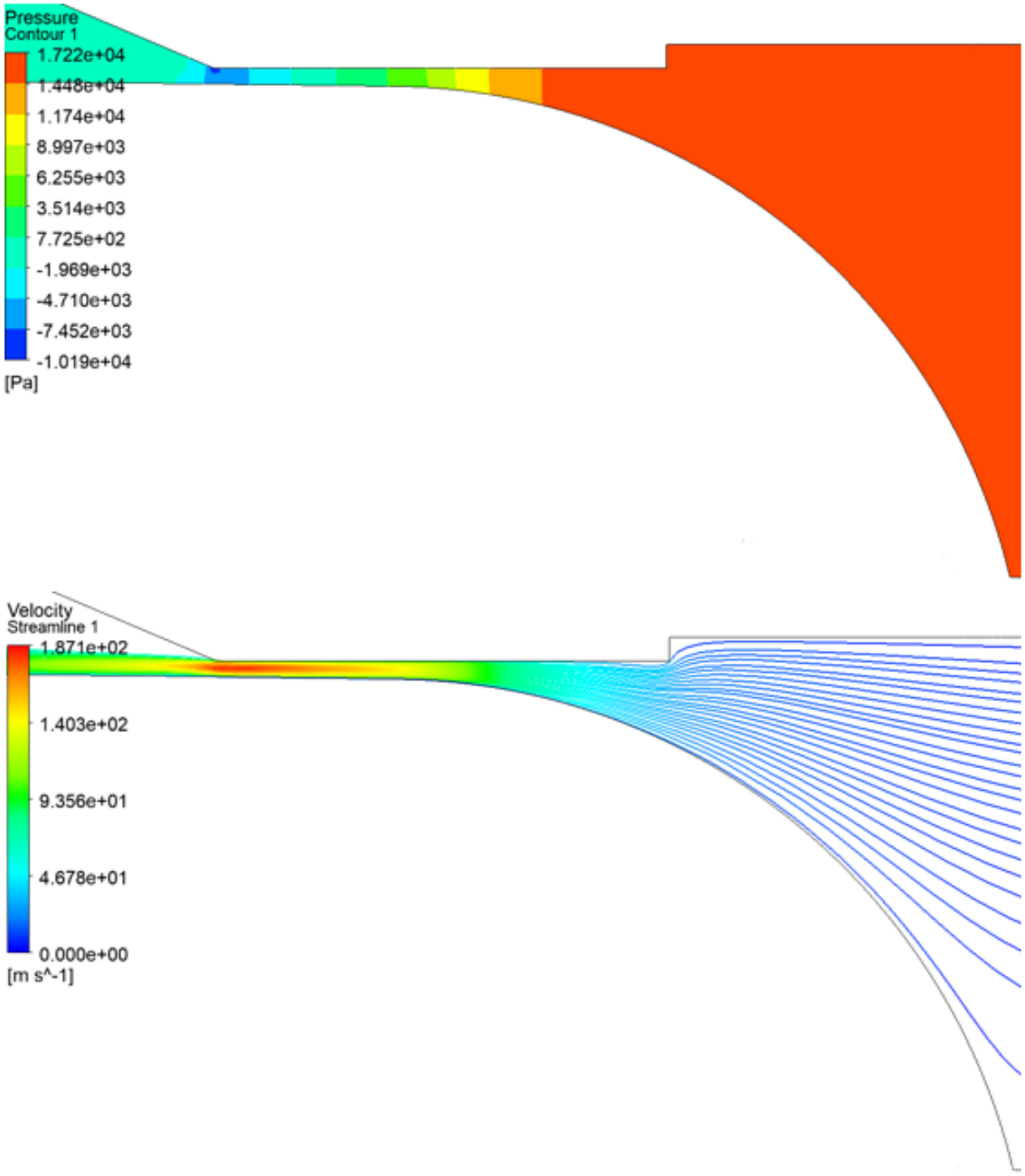

Figure 5.13: A2 Profile – Sharp Tip | Pressure Contour (Left) and Streamlines(Right)

5.2 Characterization of Hybrid Plugs

The hybrid valve plug characterization was experimentally validated in the same manner as the OEM and A1-A4. The geometry of the plugs tested is provided in *Table 5.5*, and denoted as B1-

B3. The ‘B-series’ plugs, as seen in *Figure 5.14*, were fabricated with the same tolerancing on their respective profiles as used for the ‘A-series’. The base diameters (D_{Base}) were chosen in the same fashion as the ‘A-series’, where the upstream diameter (D_o) was known as 0.416”. Each installation process consisted of ensuring full seal of the installed valve plug at full close, as well as calibrated stroke caliper to ensure accurate stroke reading.

Table 5.5: Hybrid Plug Parameters of Study

Part ID	$C_{v,m}$	R	ℓ_{stroke}	ℓ_{plug}	D_{Base}	Character
[-]	[-]	[-]	[in.]	[in.]	[in.]	[-]
B1	0.8	7.9	0.75	0.948	0.411	Hybrid
B2	0.8	9.9	0.75	0.946	0.414	Hybrid
B3	0.8	19.7	0.75	1.000	0.412	Hybrid

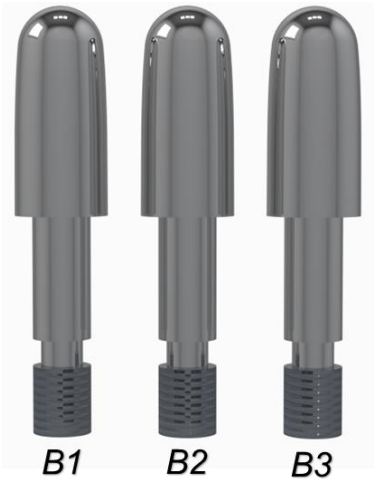

Figure 5.14: ‘B-series’ Valve Plugs

The variability between the B1 analytical model and experimental data was a maximum of 16.08% at a valve position of 55% open and a minimum of 1.99% at 100% open. The average variability between the analytical model and experimental data was 8.37%. The experimental uncertainty was a maximum of 1.65% at 5% open and minimum of 0.41% at 100% open. The average experimental uncertainty across the data was 1.10%. Comparison between the B1 measured data and the analytical estimation is shown in *Figure 5.15*.

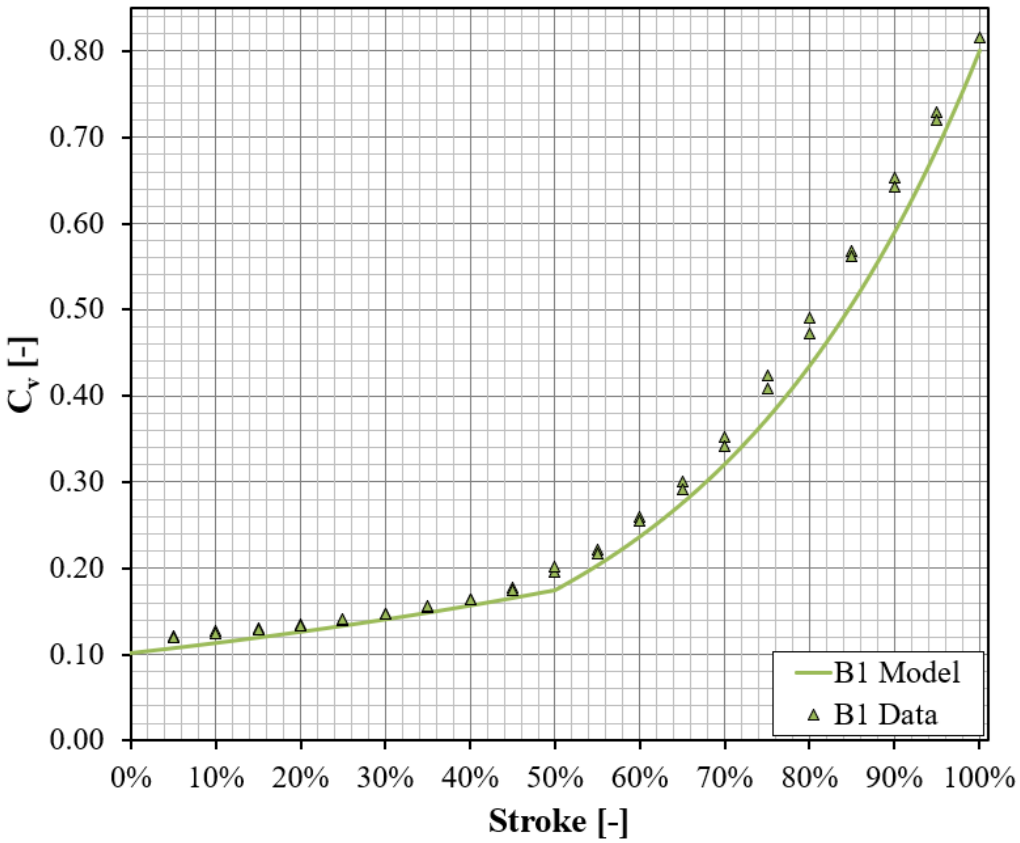

Figure 5.15: B1 Plug Experimental Characterization

The variability between the B2 analytical model and experimental data was a maximum of 25.04% at a valve position of 5% open and a minimum of 0.36% at 100% open. The average variability between the analytical model and experimental data was 14.78%. The experimental uncertainty was a maximum of 2.03% at 5% open and minimum of 0.41% at 100% open. The average experimental uncertainty across the data was 0.89%. Comparison between the B2 measured data and the analytical estimation is shown in *Figure 5.16*.

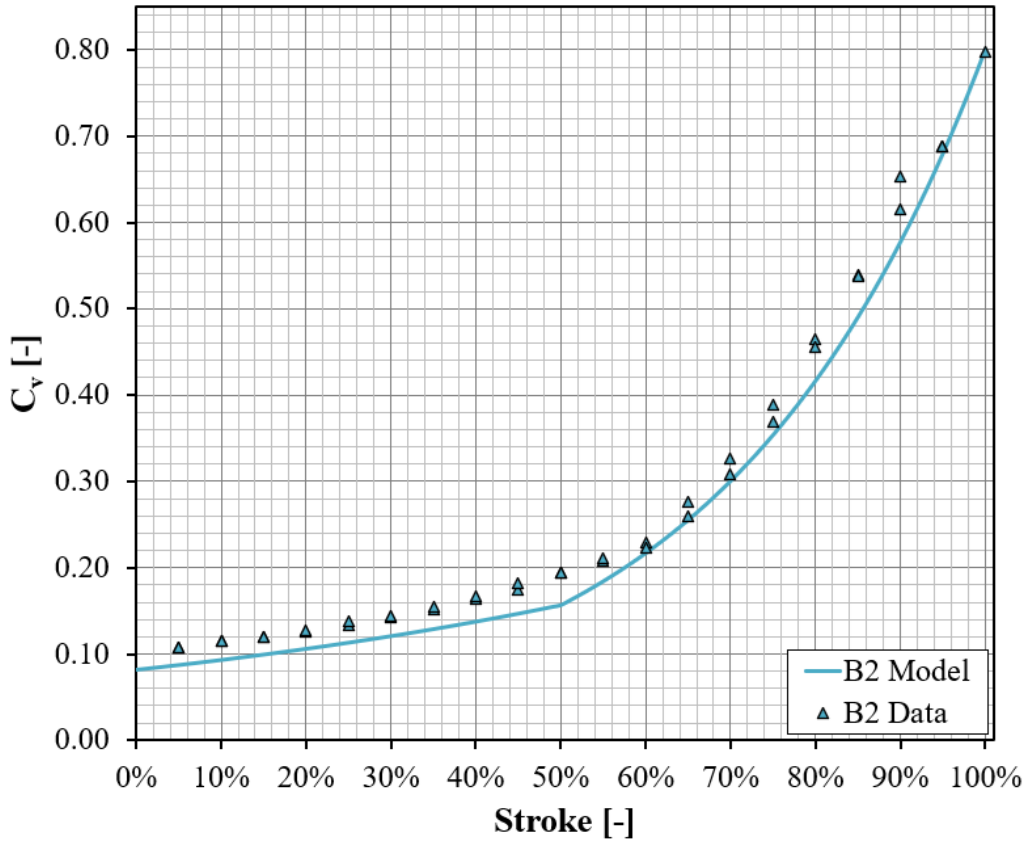

Figure 5.16: B2 Plug Experimental Characterization

The variability between the B3 analytical model and experimental data was a maximum of 36.87% at a valve position of 50% open and a minimum of 1.63% at 15% open. The average variability between the analytical model and experimental data was 13.95%. The experimental uncertainty was a maximum of 9.97% at 5% open and minimum of 0.41% at 100% open. The average experimental uncertainty across the data was 2.59%. Comparison between the B3 measured data and the analytical estimation is shown in *Figure 5.17*.

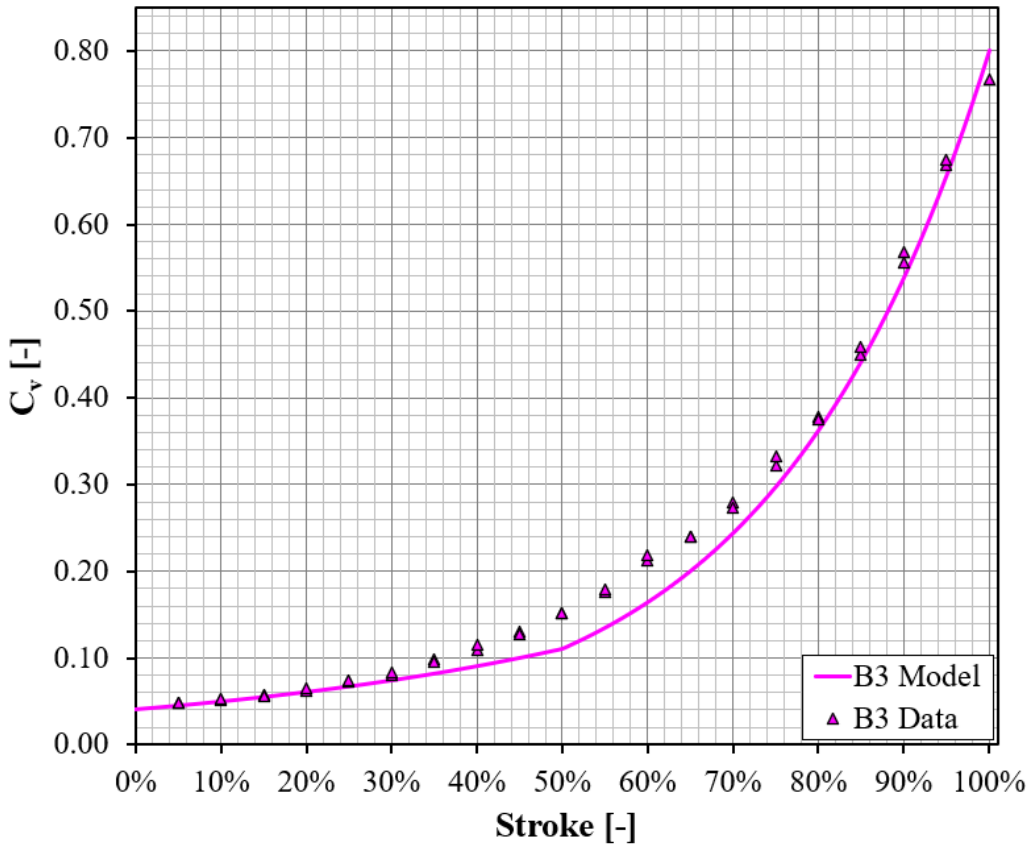

Figure 5.17: B3 Plug Experimental Characterization

Table 5.6 details the target analytical design values versus the experimentally measured values. The maximum analytically designed flow coefficient of the hybrid plugs ($C_{v,m}$) compared to the experimental maximum flow coefficient ($C_{v,m,exp}$) observed were seen to follow the same trends as the 'A-series'. Like previous experimental testing, the measured stroke was found to have minor variation between tests due to measurement calibration as well as accurate repeatability of the positioner/actuator.

Table 5.6: Hybrid Plug Characteristics against Analytical Model

Part ID	$C_{v,m}$	R	ℓ_{stroke}	$C_{v,m,exp}$	R_{exp}	$\ell_{stroke,\ exp}$	ℓ_{plug}	D_{Base}	Character
[-]	[-]	[-]	[in.]	[-]	[-]	[in.]	[in.]	[in.]	[-]
B1	0.8	7.9	0.75	0.82	6.8	0.674	0.920	0.411	Hybrid
B2	0.8	9.9	0.75	0.80	7.4	0.671	0.919	0.412	Hybrid
B3	0.8	19.7	0.75	0.77	16.0	0.674	0.915	0.414	Hybrid

Overall, the 'B-series' follows the same trend as the 'A-series', where an increase in base diameter results in a lower minimum flow coefficient. This follows the same trends as anticipated in Chapter 4.1, where an equal percent profile with the same maximum flow coefficient can reduce the minimum flow coefficient by increasing the base diameter (and therefore increasing the rangeability). The effect of raising the base diameter is evident in the comparison between the 'B-series' plugs shown in *Figure 5.18*.

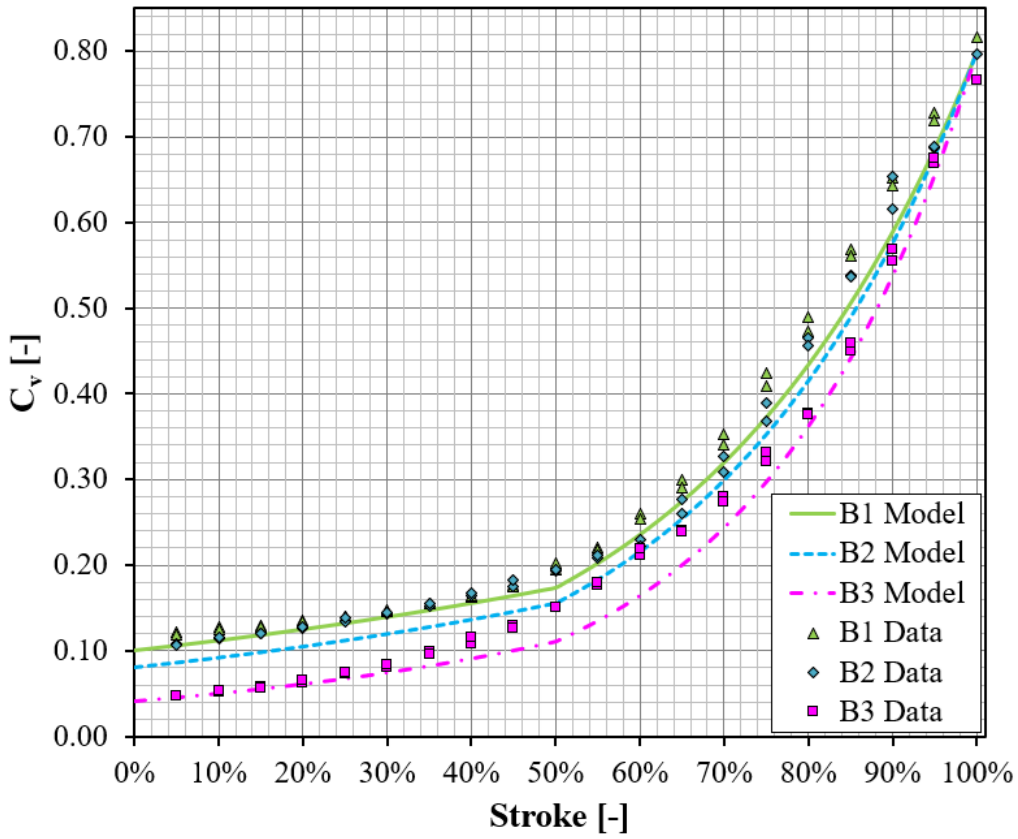

Figure 5.18: B1-B3 Comparison

As previously mentioned in Chapter 4, the CFD simulation of the A-series was conducted to validate the flow characteristics. Similarly, the 'B-series', which consists of two equal percent profiles, follows the same methodology for analysis and therefore it was not considered necessary to validate experimental results against CFD results.

5.3 Control Valve Plug as a Flowmeter Method

For a known and calibrated control valve with a proper installation of the control valve plug, the flow characteristics can be measured and utilized to estimate mass flow rate through the valve. After accurately measuring the flow coefficient versus stroke (valve position), the control valve can be used as a flow meter if pressure drop across the valve, inlet pressure, and inlet temperature to the valve are measured.

The following parameters must be measured or known to enable mass flow estimation:

- Valve characteristic flow profile (C_v vs stroke)
- Valve position (current stroke %)

- Pressure drop across the valve
- Inlet Pressure
- Inlet temperature

With these values, and given their known uncertainties, a mass flow can be estimated based upon the mean experimental flow coefficient profile. For a demonstration of this technique, the A2 plug profile was chosen. With an experimental stroke range of 5% to 100% and then back down to 5%, a 3rd order polynomial curve fit was used via Excel to be able to reasonably calculate the C_v at any stroke position between 5% to 100%. Using the curve fit flow coefficient ($C_{v,cf}$), along with the pressure drop, inlet pressure and inlet temperature measured at the valve, a mean mass flow can be estimated based on the characteristic flow profile.

First, it is noted that although the test bench used gaseous nitrogen, and the characterization curve (flow coefficient vs stroke) is independent of process fluid and conditions. Seen in *Figure 1.10,* the two-phase region (red) is shown and the ideal gas region(blue) where $Z > 0.99$. This is to understand why ideal gas assumptions are valid for both helium and nitrogen as given their reduced pressure and volumes both are within the ideal gas region based on the compressibility factor(Z). Therefore, the following procedure and methodology will be using ideal gas assumptions with a single-phase fluid at the specified operating conditions.

The mean characterization curve, seen in *Figure 5.19*, shows the mean experimentally curve fitted flow coefficient versus stroke in green, with its upper and lower bound of uncertainty shown as the grey dotted lines. The uncertainty using this method was approximately 6% between the upper and lower bound of uncertainty.

From this, given process conditions as seen in *Figure 5.19*, given the curve-fitted characterization curve, inlet temperature at 300K, inlet pressure at 1.5 Bar, and a pressure drop of 0.4 Bar. A mass flow rate of nitrogen along the stroke percentage between 5%-100% can be calculated via ISA standards.

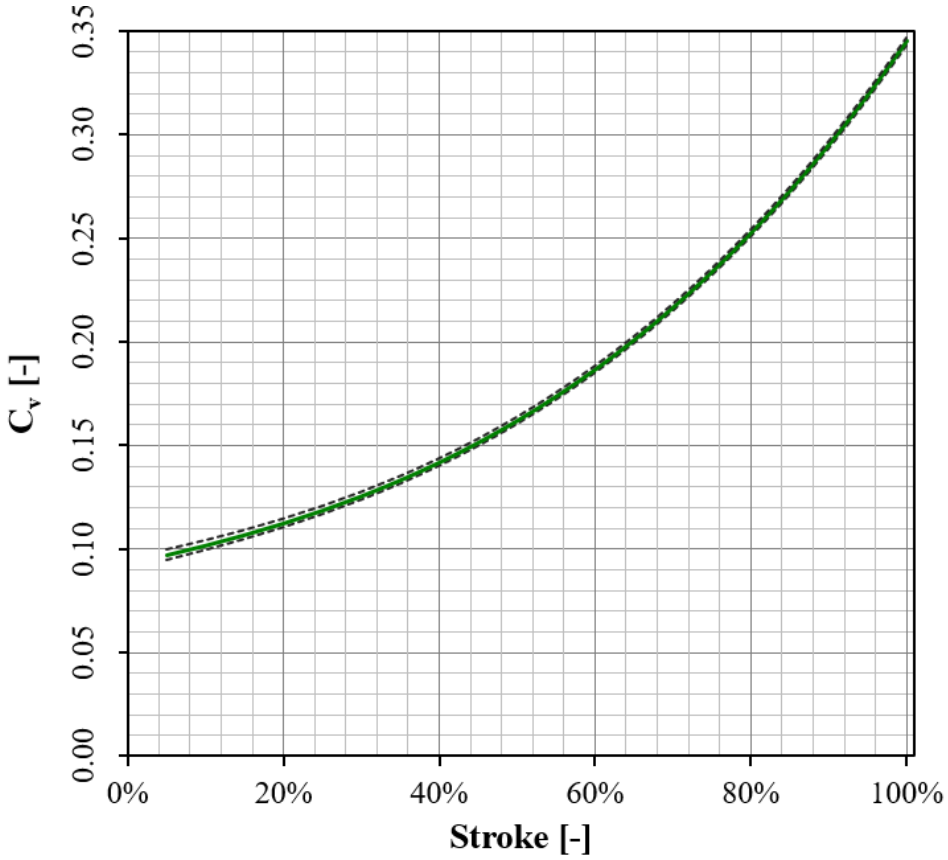

Figure 5.19: A2 Plug Experimental Flow Coefficient Curve Fit

From this, given process conditions as seen in Figure 5.20, given the curve-fitted characterization curve, inlet temperature at 300K, inlet pressure at 1.5 Bar, and a pressure drop of 0.4 Bar. A mass flow rate of nitrogen along the stroke percentage between 5%-100% can be calculated via ISA standards.

Figure 5.20: Nitrogen Process Conditions for Mass Flow Rate Calculation

As seen below, the pink line denotes the mass flow of nitrogen at the specified process conditions with the upper and lower bounds of uncertainty denoted as the grey dashed lines with a similar approximate uncertainty of 6%. The error is propagated from the curve-fitting technique as if this was experimentally calculated the uncertainty of the mass flow measurement would be likely be lower based on the A2 plug's experimental uncertainty analysis.

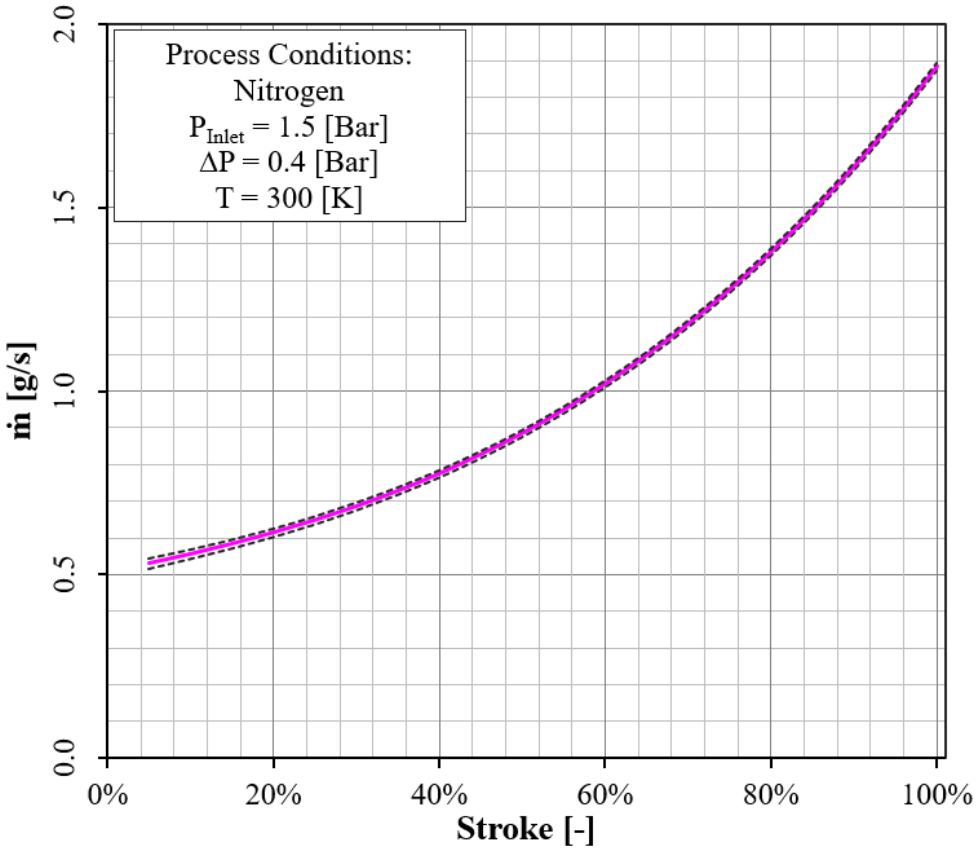

Figure 5.21: Nitrogen Mass Flow from Curve-Fitted A2 Characterization Curve

At the Facility for Rare Isotope Beams (FRIB), superconducting magnets are maintained in a liquid helium bath at 4.5 K. To minimize heat in-leak to the liquid helium, thermal radiation shielding is maintained at an elevated temperature (~40-100 K). This shielding is essential in reducing the amount of heat transferred from the surrounding environment to the cryogenic system. Additionally, several cryogenic components must be thermally intercepted at this temperature to ensure stable operation.

In such systems, it is crucial to evaluate the refrigeration load along the thermal intercept and radiation shielding circuit to maintain stable and efficient performance. Accurate knowledge of the mass flow is vital for calculating the heat load associated with these components. A fully characterized control valve, with precise flow measurement capabilities, can provide an accurate estimate of mass flow without adding additional resistance through a traditional mass flowmeter.

For a series of superconducting magnets, installing traditional flow measurement devices to estimate individual heat in-leak is both cost-prohibitive and impractical. In these cases, the methodology described earlier offers a practical alternative for estimating mass flow and heat in-

leak. While it may not provide extremely high fidelity, especially when uncertainties in measurements (e.g., temperature, pressure, and differential pressure) are unknown, it offers a relative estimation that can be useful for assessing a range of similar magnets.

Given process conditions for a heat shield, as seen in *Figure 5.22*, one can estimate the helium mass flow, and from that helium mass flow, identify the heat load (Q) as a function of valve stroke. Using the method above and the process conditions described below this can be achieved as seen in *Figure 5.23*.

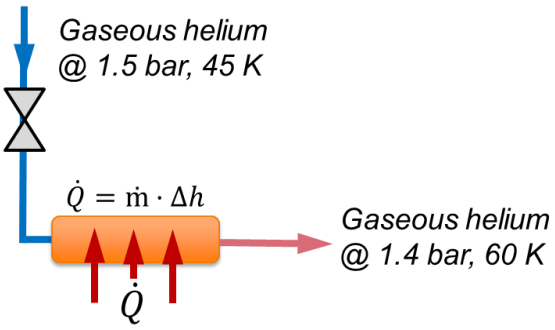

Figure 5.22: Helium Process Conditions

The helium mass flow based upon process conditions above, result in the light blue curve denoting this specific helium mass flow as a function of valve stroke. The uncertainty of this mass flow is approximately 6%, however this will be increased due to subsequent measurements of pressure, temperature, and differential pressure needed for measured process conditions. This calculated mass flow only accounts for uncertainty due to the uncertainty in the mean characterization curve.

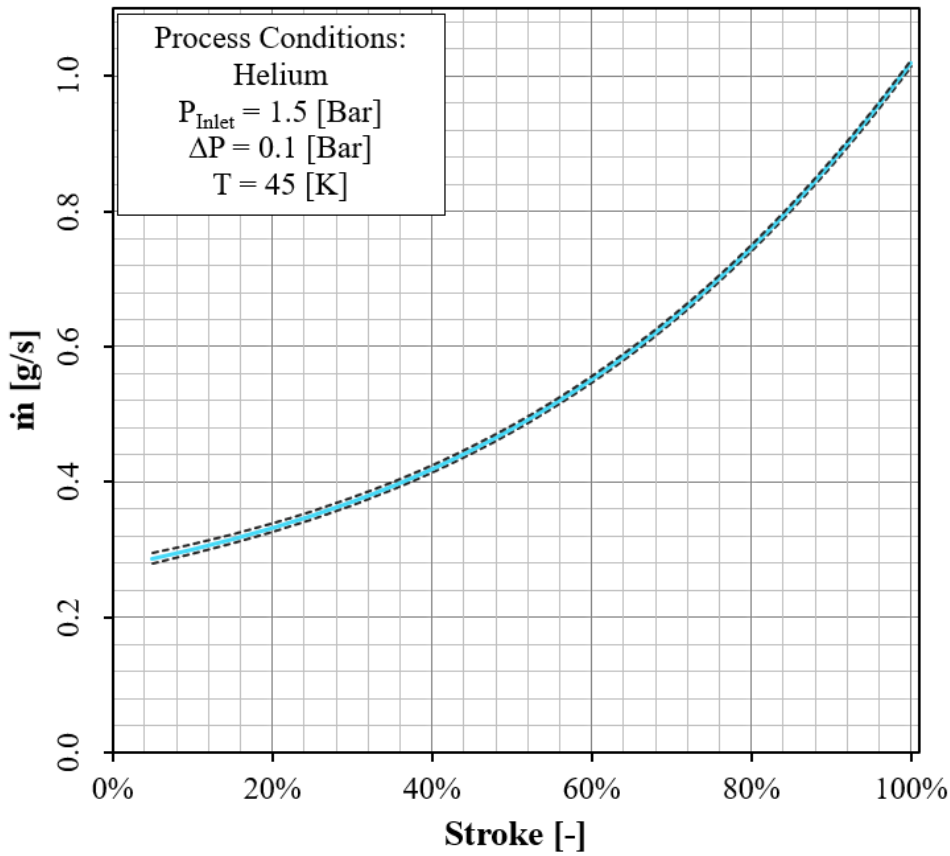

Figure 5.23: Helium Mass Flow from Curve-Fitted A2 Characterization Curve

With the mass flow rate of the helium vapor at the estimated process conditions of the heat shield, the heat load entering the shield can be estimated using the mass flow rate and specific enthalpy change due to the temperature difference between the inlet and outlet.

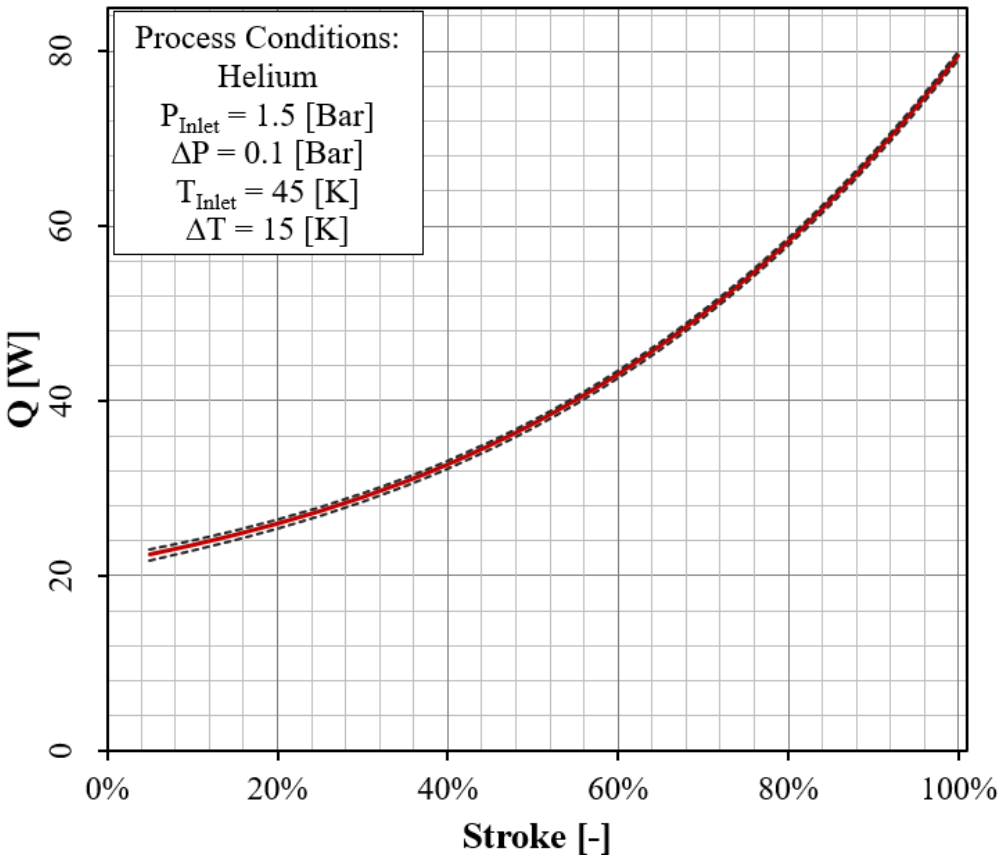

Figure 5.24: Heat Load Estimation

Using a control valve as a flowmeter can reduce equipment costs, and heat-in leak at cryogenic conditions. Likewise, control valves that are installed in areas which a flow meter cannot easily be integrated in the system can be used to estimate flow rates of interest. But it should be noted that the mass flow rates calculated from the control valve are estimates based on valve characterization and therefore will have larger error as compared to traditionally used mass flow measurement devices.

Chapter 6: CONCLUSIONS AND FUTURE WORK

The present study focused on the design and characterization of a cryogenic control valve plug with equal percent characteristics, addressing the critical need for precise flow control in cryogenic applications. Through an approach encompassing analytical modeling, computational fluid dynamics (CFD) simulation, and experimentation, a systematic methodology for designing cryogenic control valve plugs was developed and validated. The findings contribute to improving the design process of cryogenic control valve plug performance and overall cryogenic system efficiency.

A test bench for experimental validation was designed based on necessary parameters to calculate the flow coefficient, namely the mass flow rate through the valve, the differential pressure across the valve (ΔP [Bar]), and the inlet pressure and temperature of the fluid. Experimental validation was conducted through the fabrication and testing of valve plugs using the custom-built test bench designed for precise characterization of flow coefficients versus stroke (lift). The results confirmed the general trends predicted by the analytical and CFD models, with slight variation attributed to manufacturing tolerances, accuracy of the valve actuator and fluid dynamics effects which were not captured in the analysis. The validation process emphasized the importance of incorporating real-world performance data into the iterative design cycle. The flow coefficient calculations for both CFD and experimental validation utilized the ISA: Flow Equations for Sizing Control Valve standard [6]. The study examined multiple plug designs, as seen in *Figure 6.1*, including the 'A-series' and 'B-series' which were equal percent and hybrid plugs, respectively. The OEM plug served as an initial benchmark, understanding how the test bench valve must be calibrated, however due to its tolerancing and design practices not known a best attempt at recreating the OEM plug's profile was made.

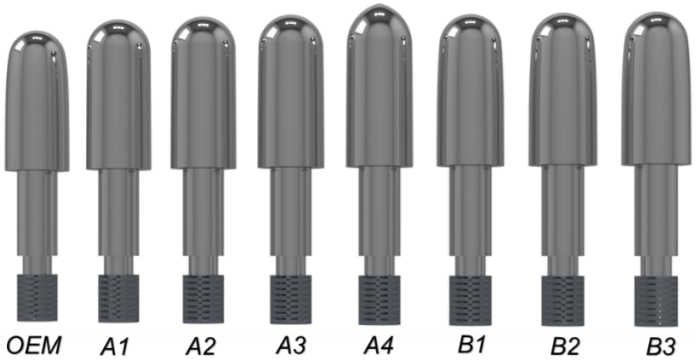

Figure 6.1: Seven Novel Valve Plugs

The analytical model was developed based upon the characteristic valve design equations [4, 11] and orifice sizing [30], particularly the diameter of the throat (D_t) which is akin to an annular diameter. This diameter corresponds with the throat (flow) area, A_t. The analytical model successfully generated non-dimensional plug profile(s) in terms of ratio of diameter of the plug compared to the upstream wall diameter of the valve body, ΔD. The profile started at the base diameter (D_{Base}) and generated the geometry along the length of the active profile, ending at the interface diameter (D_{Int}). Therefore, the non-dimensional ratio of diameters versus a non-dimensional opening from (0-1) or (0%-100%) generated the full valve plug profile. Additionally, the fundamental equations were modified to create a flow coefficient (C_v) versus stroke (lift %) characteristic curve. These analytical models then were able to be dimensionalized into coordinates, after which the analytical model characterization process was complete.

After successfully testing the developed and manufactured valve plugs, the A2 plug, corresponding to the D_{Base} of 0.412" and a desired maximum flow coefficient ($C_{v,m}$) of 0.3, was installed in three separate cryogenic control valves as seen in *Figure 6.2*. These control valves serviced both liquid nitrogen (PVN52122) and liquid helium (PVN52121 & PVN52321). These valves have been operating as intended under process conditions, validating the design process and improving the controllability of the cryogenic system.

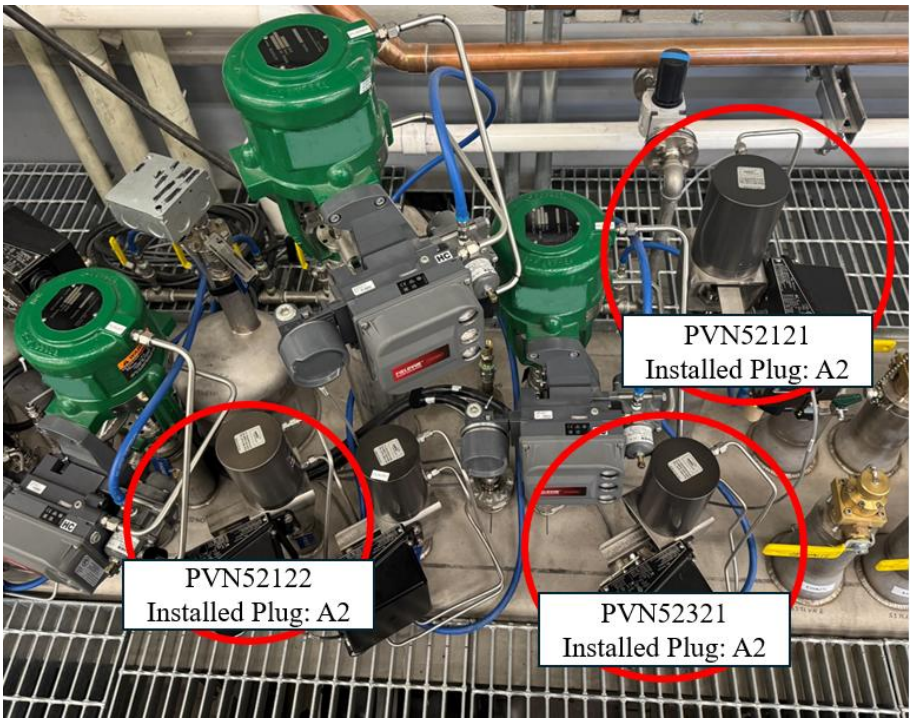

Figure 6.2: A2 Plugs Installed in FRIB Cryogenic System(s)

Although advancements have been made in this study and allowed for physical implementation of the A2 valve plug into a pre-existing system, several limitations must be acknowledged. The analytical model does not fully capture the effects of tip geometry and overall length of plug, leading to slight deviations from experimental results. CFD simulations, while useful for predicting flow behavior and pressure drop, remain limited by the accuracy of turbulence modeling and computational constraints (*i.e*. mesh element size, inflation layering, and computational cost). Future research should focus on refining the analytical model to incorporate additional geometric parameters. Furthermore, enhancing CFD methodologies by utilizing higher-resolution meshing and incorporating alternative boundary conditions derived from experimental data would be worthwhile. Investigating alternative plug geometries, including multi-profile hybrid designs, could further optimize performance across a broader range of operational conditions.

This study successfully developed and validated a methodology for designing cryogenic control valve plugs with equal percent characteristics. By integrating analytical, computational, and experimental approaches, a comprehensive framework for cryogenic valve plug design was established, contributing to advancements in cryogenic fluid control. The insights gained from this research pave the way for further innovation in control valve plug design, ultimately enhancing the efficiency and reliability of cryogenic process systems. Continued development in this field will support a wide range of applications where precise fluid control at extremely low temperatures is essential.

REFERENCES

1. Towler, G. and R. Sinnott, *Chemical Engineering Design - Principles, Practice and Economics of Plant and Process Design (3rd Edition)*. 2022, Elsevier.
2. American Society of Plumbing, E., *Plumbing Engineering Design Handbook*. 2012, American Society of Plumbing Engineers (ASPE).
3. Barron, R.F., *Cryogenic Systems*. 1985: Oxford University Press.
4. Smith, P. and R.W. Zappe, *2 - Fundamentals*, in *Valve Selection Handbook (Fifth Edition)*, P. Smith and R.W. Zappe, Editors. 2004, Gulf Professional Publishing: Burlington. p. 7-45.
5. Idel′chik, I.E. and M.O. Steinberg, *Handbook of Hydraulic Resistance*. 1996: Begell House.
6. (ISA), I.S.o.A., *Flow Equations for Sizing Control Valves* in *ANSI/ISA-S75.01-2007*. 2007.
7. (ISA), I.S.o.A., *Control Valve Capacity Test Procedures*, in *ANSI/ISA-S75.02-1996*. 1996.
8. Bruckner, N., S. Backhaus, and R. Packard, *An improved low temperature valve.* Czechoslovak Journal of Physics, 1996. **46**(5): p. 2741-2742.
9. Jha, A.R., *Cryogenic Technology and Applications*. Elsevier.
10. Sotoodeh, K., *Chapter Three - Cryogenic valve design features*, in *Cryogenic Valves for Liquefied Natural Gas Plants*, K. Sotoodeh, Editor. 2022, Gulf Professional Publishing. p. 111-174.
11. Rohani, S., *Coulson and Richardson's Chemical Engineering, Volume 3B - Process Control (4th Edition)*. Elsevier.
12. Wiedmann, J. and W. Rowan, *Control-Valve Plug Design.* Transactions of the American Society of Mechanical Engineers, 1956. **78**(6): p. 1367-1372.
13. Patal, U., et al., *Mathematical Method for Designing the Profile of the Plug of Horizontal Glove Valve for Required Inherent Flow Characteristics.* IOSR J. Mech. Civ. Eng, 2017. **14**: p. 31-40.
14. Chandar, E. and A. Sai, *Design and flow coefficient analysis of globe valve as control valve using MATLAB.* International Journal of Innovative Science and Research Technology, 2022. **7**(1): p. 279-283.
15. Geng, S., et al., *Analysis and experimental study on flow characteristic and rangeability of plug control valve.* Journal of Physics: Conference Series, 2024. **2691**(1): p. 012039.
16. Davis, J.A. and M. Stewart, *Predicting Globe Control Valve Performance—Part I: CFD Modeling.* Journal of Fluids Engineering, 2002. **124**(3): p. 772-777.
17. Davis, J.A. and M. Stewart, *Predicting Globe Control Valve Performance—Part II: Experimental Verification.* Journal of Fluids Engineering, 2002. **124**(3): p. 778-783.

18. Aumanand, M.A. and M. Konnur, *A novel method of using a control valve for measurement and control of flow.* IEEE Transactions on Instrumentation and Measurement, 1999. **48**(6): p. 1224-1226.

19. Choi, J., *Flow control system design without flow meter sensor.* Sensors and Actuators A: Physical, 2012. **185**: p. 127-131.

20. Mu, Y., M. Liu, and Z. Ma, *Research on the measuring characteristics of a new design butterfly valve flowmeter.* Flow Measurement and Instrumentation, 2019. **70**: p. 101651.

21. Leephakpreeda, T., *Flow-sensorless control valve: neural computing approach.* Flow Measurement and Instrumentation, 2003. **14**(6): p. 261-266.

22. Mitutoyo Absolute Digimatic Scale Units. Catalog No. E316-572R, F.

23. McMaster-Carr. *Cleaned and Bagged Pressure-Regualting Valve for Air and Inert Gas, 1NPT Female.* Available from: https://www.mcmaster.com/products/argon-regulators/high-purity-tank-mount-pressure-regulating-valves-for-inert-gas/.

24. McMaster-Carr. *Stainless Steel Pressure Gauge with 1/4 NPT Connection, 0-100 psi, 2-1/2" Dial Diameter.* Available from: https://www.mcmaster.com/catalog/130/655/4088K6.

25. Swagelok. *MS-01-164, RevO October 2021 Stainless Steel On/Off Valve with Lever Handle, 1/2 NPT Female*. Available from: https://www.swagelok.com/downloads/webcatalogs/EN/MS-01-164.pdf.

26. McMaster-Carr. *High-Pressure Compact 316 Stainless Steel On/Off Valve with Lever Handle, 1/2 NPT Female*. Available from: https://www.mcmaster.com/products/argon-regulators/high-purity-tank-mount-pressure-regulating-valves-for-inert-gas/

27. Druck. *UNIK 5000 Pressure Sensing Platform*. Available from: https://www.bakerhughesds.com/pressure-sensors/unik-5000-pressure-sensing-platform.

28. Emerson. *Micro Motion ELITE Coriolis Flow and Density Meters Product Data Sheet*. September 2016.

29. Rosemount 3051 Pressure Transmitter Product Data Sheet. Revision SB, A.

30. Nakayama, Y., *Introduction to Fluid Mechanics (2nd Edition)*. Elsevier.

31. ISO 5167-4: Venturi Tubes. International Organization for Standardization.

32. Holman, J.P., *Experimental Methods for Engineers (7th ed.)*. McGraw-Hill Education. 2000.

33. Rudnev, V. and G.E. Totten, *ASM Handbook, Volume 04C - Induction Heating and Heat Treatment*. ASM International.

34. Ansys, *Ansys Fluent 2024 R2: Fluent User's Guide.* Ansys Inc., USA, 2024.

35. Ansys, *Ansys Fluent 2024 R2: Fluent Theory Guide.* Ansys Inc., USA, 2024.

36. Kato, M. *The modeling of turbulent flow around stationary and vibrating square cylinders*. 1993.

37. E. W. Lemmon, I.H.B., M. L. Huber, M. O. McLinden, *NIST Standard Reference Database 23: Reference Fluid Thermodynamic and Transport Properties-REFPROP, Version 10.0, National Institute of Standards and Technology.* 2018.

APPENDIX A: ANSI/ISA-S75.01 CONTROL VALVE SIZING EQUATIONS

All following material, parameters, and equational definitions were adapted from [6].

Table A.1: Valve Geometry Sizing Parameters, adapted from [6]

Valve type	Trim type	Flow direction [2]	F_L	x_T	F_d
Globe, single port	3 V-port plug	Open or close	0.9	0.70	0.48
	4 V-port plug	Open or close	0.9	0.70	0.41
	6 V-port plug	Open or close	0.9	0.70	0.30
	Contoured plug (linear and equal percentage)	Open Close	0.9 0.8	0.72 0.55	0.46 1.00
	60 equal diameter hole drilled cage	Outward [3] or inward [3]	0.9	0.68	0.13
	120 equal diameter hole drilled cage	Outward [3] or inward [3]	0.9	0.68	0.09
	Characterized cage, 4-port	Outward [3] Inward [3]	0.9 0.85	0.75 0.70	0.41 0.41
Globe, double port	Ported plug	Inlet between seats	0.9	0.75	0.28
	Contoured plug	Either direction	0.85	0.70	0.32
Globe, angle	Contoured plug (linear and equal percentage)	Open Close	0.9 0.8	0.72 0.65	0.46 1.00
	Characterized cage, 4-port	Outward [3] Inward [3]	0.9 0.85	0.65 0.60	0.41 0.41
	Venturi	Close	0.5	0.20	1.00
Globe, small flow trim	V-notch	Open	0.98	0.84	0.70
	Flat seat (short travel)	Close	0.85	0.70	0.30
	Tapered needle	Open	0.95	0.84	$N_{19}\frac{(CF_L)^{0.5}}{D_o}$
Rotary	Eccentric spherical plug	Open Close	0.85 0.68	0.60 0.40	0.42 0.42
	Eccentric conical plug	Open Close	0.77 0.79	0.54 0.55	0.44 0.44
Butterfly (centered shaft)	Swing-through (70°)	Either	0.62	0.35	0.57
	Swing-through (60°)	Either	0.70	0.42	0.50
	Fluted vane (70°)	Either	0.67	0.38	0.30
High Performance Butterfly (eccentric shaft)	Offset seat (70°)	Either	0.67	0.35	0.57
Ball	Full bore (70°)	Either	0.74	0.42	0.99
	Segmented ball	Either	0.60	0.30	0.98

1) These values are typical only; actual values shall be stated by the valve manufacturer.

2) Flow tends to open or close the valve, i.e. push the closure device (plug, ball, or disc) away from or towards the seat.

3) Outward means flow from center of cage to outside, and inward means flow from outside of cage to center.

Table A.2: ISA Constants, adapted from [6]

Constant	Flow coefficient C		Formulae unit						
	K_v	C_v	W	Q	P, ΔP	ρ	T	d, D	ν
N_1	1×10^{-1}	8.65×10^{-2}	–	m^3/h	kPa		–	–	–
	1	8.65×10^{-1}	–	m^3/h	bar		–	–	–
		1	–	gpm	psia		–	–	–
N_2	1.60×10^{-3}	2.14×10^{-3}	–	–	–	–	–	mm	–
		8.90×10^{2}	–	–	–	–	–	in	–
N_4	7.07×10^{-2}	7.60×10^{-2}	–	m^3/h	–	–	–	–	m^2/s
		1.73×10^{4}	–	gpm	–	–	–	–	cS
		2.153×10^{3}	–	scfh	–	–	–	–	cS
N_5	1.80×10^{-3}	2.41×10^{-3}	–	–	–	–	–	mm	–
		1.00×10^{3}	–	–	–	–	–	in	–
N_6	3.16	2.73	kg/h	–	kPa	kg/m^3	–	–	–
	3.16×10^{1}	2.73×10^{1}	kg/h	–	bar	kg/m^3	–	–	–
		6.33×10^{1}	lbm/h	–	psia	lbm/ft^3	–	–	–
N_7	4.82	4.17	–	m^3/h	kPa	–	–K	–	–
($t = 15.6°C$)	4.82 x 10^{2}	4.17×10^{2}	–	m^3/h	bar	–	–K	–	–
		1.36×10^{3}	–	scfh	psia	–	–R	–	–
N_8	1.10	9.48×10^{-1}	kg/h	–	kPa	–	K	–	–
	1.10×10^{2}	9.48×10^{1}	kg/h	–	bar	–	K	–	–
		1.93×10^{1}	lbm/h	–	psia	–	R	–	–
N_9	2.46×10^{1}	2.12×10^{1}	–	m^3/h	kPa	–	K	–	–
($t = 0°C$)	2.46×10^{3}	2.12×10^{3}	–	m^3/h	bar	–	K	–	–
		6.94×10^{3}	–	scfh	psia	–	R	–	–
N_9	2.60×10^{1}	2.25×10^{1}	–	m^3/h	kPa	–	K	–	–
($t_s = 15°C$)	2.60×10^{3}	2.25×10^{3}	–	m^3/h	bar	–	K	–	–
		7.32×10^{3}	–	scfh	psia	–	R	–	–
N_{18}	8.65×10^{-1}	1.00	–	–	–	–	–	mm	–
		6.45×10^{2}	–	–	–	–	–	in	–
N_{19}	2.5	2.3	–	–	–	–	–	mm	–
		9.06×10^{-2}	–	–	–	–	–	in	–
N_{22}	1.73×10^{1}	1.50×10^{1}	–	m^3/h	kPa	–	K	–	–
($t_s = 0°C$)	1.73×10^{3}	1.50×10^{3}	–	m^3/h	bar	–	K	–	–
		4.92×10^{3}	–	scfh	psia	–	R	–	–
N_{22}	1.84×10^{1}	1.59×10^{1}	–	m^3/h	kPa	–	K	–	–
($t_s = 15°C$)	1.84×10^{3}	1.59×10^{3}	–	m^3/h	bar	–	K	–	–
		5.20×10^{3}	–	scfh	psia	–	R	–	–
N_{27}	7.75×10^{-1}	6.70×10^{-1}	kg/h	–	kPa	–	K	–	–
($t_s = 0°C$)	7.75×101	$6.70 \times 10^{+1}$	kg/h	–	bar	–	K	–	–
		1.37×10^{1}	lbm/h	–	psia	–	R	–	–
N_{32}	1.40 x 10^{2}	1.27×10^{2}	–	–	–	–	–	mm	–
		1.70 x 10^{1}	–	–	–	–	–	in	–

NOTE Use of the numerical constants provided in this table together with the practical metric and US units specified in the table will yield flow coefficients in the units in which they are defined.

Incompressible Flow Coefficient Calculation

- Select F_L using valve type and size (if there is uncertainty in sizing, use inlet pipe size as valve size)
- Calculate F_F using Eqn. (A.1)

$$F_F = 0.96 - 0.28\sqrt{\frac{P_v}{P_c}} \tag{A.1}$$

- If ΔP is less than $F_L^2(P_1 - F_F P_V)$ using Eqn. (A.2), using the non-choked flow coefficient Eqn. (A.3).
- If ΔP is greater than or equal to $F_L^2(P_1 - F_F P_V)$ using Eqn. (A.2), using the choked flow coefficient Eqn. (A.4).

$$\Delta P < F_L^2(P_1 - F_F P_V) \tag{A.2}$$

$$C_v = \left(\frac{Q}{N_1}\right)\sqrt{\frac{\rho_1}{\Delta P \rho_o}} \tag{A.3}$$

$$C_v = \left(\frac{Q}{N_1 F_L}\right)\sqrt{\frac{\rho_1/\rho_o}{P_1 - F_F P_V}} \tag{A.4}$$

- Calculate Re_v using Eqn. (A.5), using C_v (in place of C_i from the above equations) and F_d

$$Re_v = \frac{N_4 F_d Q}{v\sqrt{C_i F_L}}\left(\frac{F_L^2 F C_i^2}{N_2 D^4} + 1\right)^{1/4} \tag{A.5}$$

- If $Re_v \leq 10{,}000$, proceed with calculation in the *Non-Turbulent Flow Calculation* section
- If $Re_v > 10{,}000$, proceed with calculation in the *Turbulent Flow Calculation* section

Turbulent Flow Calculation ($Re_v > 10{,}000$)

- If $Re_v > 10{,}000$, and *valve size = pipe size*, use the calculated C_v. The calculation is finished
- If $Re_v > 10{,}000$, but if *valve size ≠ pipe size*, use $F_P = 1$ and $C_i = C_v$. The following iterative routine will be necessary to calculate an accurate C_v
- From here, there is an iterative routine by first calculating F_P and F_{LP} as a function of C_i as seen below using Eqns. (A.6) and (A.7)

$$F_P = \frac{1}{\sqrt{1 + \frac{\Sigma\zeta}{N_2}\left(\frac{C_i}{d^2}\right)^2}} \tag{A.6}$$

$$F_{LP} = \frac{F_L}{\sqrt{1 + \frac{F_L^2}{N_2}(\Sigma\zeta_1)\left(\frac{C_i}{d^2}\right)^2}} \tag{A.7}$$

- If $\Delta P \geq \left(\frac{F_{LP}}{F_P}\right)^2 (P_1 - F_F P_V)$, then calculate C_v using Eqn. (A.8)
- If $\Delta P < \left(\frac{F_{LP}}{F_P}\right)^2 (P_1 - F_F P_V)$, then calculate C_v using Eqn. (A.9)

$$C_v = \left(\frac{Q}{N_1 F_{LP}}\right)\sqrt{\frac{\rho_1/\rho_o}{P_1 - F_F P_V}} \tag{A.8}$$

$$C_v = \left(\frac{Q}{N_1 F_P}\right)\sqrt{\frac{\rho_1/\rho_o}{\Delta P}} \tag{A.9}$$

- If $\frac{C_i}{C_v} < 0.99$, then let $C_i = C_v$, and recalculate the routine starting with $F_P(C_i)$ad $F_{LP}(C_i)$ using the newly calculated C_v from either Eqn. (A.8) or Eqn. (A.9)
- If $\frac{C_i}{C_v} \geq 0.99$, then the flow coefficient has been calculated, there is no need for further iteration. The calculation is finished.

Non-Turbulent Flow Calculation ($Re_v \leq 10{,}000$)

- Let $C_i = 1.3C_v$ from the initial calculation
- Now Re_v can be recalculated from Eqn. (A.5)
- From here, there is an iterative routine for the flow coefficient
- If $\frac{C}{d^2} > 0.016N_{18}$, then F_R must be calculated as both Eqn. (A.10)F.1a and (A.11)F.2 and taken as the lower value.
- If $\frac{C}{d^2} \leq 0.016N_{18}$, then F_R must be calculated as both Eqn. (A.12)F.3a and (A.13) F.4 and taken as the lower value.

$$F_R = 1 + \left(\frac{0.33F_L^{1/2}}{n_1^{1/4}}\right)\log_{10}\left(\frac{Re_v}{10{,}000}\right) \tag{A.10}$$

$$F_R = \frac{0.026}{F_L}\sqrt{n_1 Re_v} \tag{A.11}$$

$$F_R = 1 + \left(\frac{0.33F_L^{1/2}}{n_2^{1/4}}\right)\log_{10}\left(\frac{Re_v}{10{,}000}\right) \tag{A.12}$$

$$F_R = \frac{0.026}{F_L}\sqrt{n_2 Re_v} \tag{A.13}$$

- If $\frac{C}{F_R} > C_i$, C_i must be increased by 30% and the iterative routine must restart at the calculation of $\frac{C}{d^2}$
- If $\frac{C}{F_R} \leq C_i$, then there is no need for further iteration, and $C_i$is the calculated flow coefficient. The calculation is finished.

Compressible Flow Coefficient Calculation

- Select x_T using valve type and size (if there is uncertainty in sizing, use inlet pipe size as valve size)
- Calculate F_γ using Eqn. (A.14)

$$F_\gamma = \frac{\gamma}{1.40} \tag{A.14}$$

- If x is less then $F_\gamma x_T$, use the non-choked flow coefficient Eqn. (A.16), and calculate Y via Eqn. (A.15)
- If x is greater than or equal to $F_\gamma x_T$, use the choked flow coefficient Eqn. (A.17) , where Y = 0.667

$$Y = \frac{x}{3F_\gamma x_T} \tag{A.15}$$

$$C_v = \frac{W}{N_6 Y\sqrt{xP_1\rho_1}} \tag{A.16}$$

$$C_v = \frac{W}{0.667N_6\sqrt{F_\gamma x_T P_1\rho_1}} \tag{A.17}$$

- Calculate Re_v using Eqn. (A.18), using C_v (in place of C_i from the above equations) and F_d

$$Re_v = \frac{N_4 F_d Q}{\upsilon\sqrt{C_i F_L}}\left(\frac{F_L^2 F C_i^2}{N_2 D^4} + 1\right)^{1/4} \quad \text{(A.18)}$$

- If $Re_v \leq 10{,}000$, proceed with calculation in the *Non-Turbulent Flow Calculation* section
- If $Re_v > 10{,}000$, proceed with calculation in the *Turbulent Flow Calculation* section

Turbulent Flow Calculation ($Re_v > 10{,}000$)

- If $Re_v > 10{,}000$, and *valve size = pipe size*, use the calculated C_v. The calculation is finished
- If $Re_v > 10{,}000$, but if *valve size ≠ pipe size*, use $F_P = 1$ and $C_i = C_v$. The following iterative routine will be necessary to calculate an accurate C_v
- From here, there is an iterative routine by first calculating F_P and x_{TP} as a function of C_i as seen below using Eqns. (A.19) and (A.20)

$$F_P = \frac{1}{\sqrt{1 + \frac{\Sigma\zeta}{N_2}\left(\frac{C_i}{d^2}\right)^2}} \quad \text{(A.19)}$$

$$x_{TP} = \frac{\frac{x_T}{F_P^2}}{1 + \frac{x_T \zeta_i}{N_5}\left(\frac{C_i}{d^2}\right)^2} \quad \text{(A.20)}$$

- If $x \geq F_\gamma x_T$, then calculate C_v using Eqn. (A.21)
- If $x < F_\gamma x_T$ then calculate C_v using Eqn. (A.22)

$$C_v = \frac{W}{0.667 N_6 F_P \sqrt{F_\gamma x_{TP} P_1 \rho_1}} \quad \text{(A.21)}$$

$$C_v = \frac{W}{N_6 F_P Y \sqrt{x P_1 \rho_1}} \quad \text{(A.22)}$$

- If $\frac{C_i}{C_v} < 0.99$, then let $C_i = C_v$, and recalculate the routine starting with $F_P(C_i)$ad $x_{TP}(C_i)$ using the newly calculated C_v from either Eqn. (A.21) or Eqn. (A.22)
- If $\frac{C_i}{C_v} \geq 0.99$, then the flow coefficient has been calculated, there is no need for further iteration. The calculation is finished

Non-Turbulent Flow Calculation ($Re_v \leq 10{,}000$)

- Let $C_i = 1.3C_v$ from the initial calculation

- Now Re_v can be recalculated from Eqn. (A.18)
- From here, there is an iterative routine for the flow coefficient.
- If $\frac{C}{d^2} > 0.016N_{18}$, then F_R must be calculated as both Eqn. (A.23)F.1aand (A.24)F.2 and taken as the lower value
- If $\frac{C}{d^2} \leq 0.016N_{18}$, then F_R must be calculated as both Eqn. (A.25) F.3a and (A.26) F.4 and taken as the lower value

$$F_R = 1 + \left(\frac{0.33F_L^{1/2}}{n_1^{1/4}}\right)\log_{10}\left(\frac{Re_v}{10{,}000}\right) \quad \text{(A.23)}$$

$$F_R = \frac{0.026}{F_L}\sqrt{n_1 Re_v} \quad \text{(A.24)}$$

$$F_R = 1 + \left(\frac{0.33F_L^{1/2}}{n_2^{1/4}}\right)\log_{10}\left(\frac{Re_v}{10{,}000}\right) \quad \text{(A.25)}$$

$$F_R = \frac{0.026}{F_L}\sqrt{n_2 Re_v} \quad \text{(A.26)}$$

- If $\frac{C}{F_R} > C_i$, C_i must be increased by 30% and the iterative routine must restart at the calculation of $\frac{C}{d^2}$.
- If $\frac{C}{F_R} \leq C_i$, then there is no need for further iteration, and $C_i$is the calculated flow coefficient. The calculation is finished.

APPENDIX B: UNCERTAINTY ANALYSIS FOR FLOW COEFFICIENT, VALVE PLUG AS FLOWMETER, AND ISA STANDARDS ITERATIVE ROUTINE MATLAB CODE

Main Uncertainty Analysis (ValveExpUncertainty)

3/6/25 12:47 PM E:\Grake\MATLAB\ValveExpUncertainty.m 1 of 4

```
FID = 'Nitrogen';
%----------------------------------------
% Test Variables

%Arrays for MATLAB -Valve Test-Datasheet
%----------------------------------------
%OEM Plug
stroke_trials = [5, 10, 15, 20, 25, 30, 35, 40, 45, 50,...
    55, 60, 65, 70, 75, 80, 85, 90, 95, 100, 95, 90, ...
    85, 80, 75, 70, 65, 60, 55, 50, 45, 40, 35, 30, 25,...
    20, 15, 10, 5];

P1_trials = [1.6160338,1.6116466,1.6103763,1.6072824,...
    1.620321,1.6183326,1.6116066,1.6136584,1.6115765,...
    1.6102781,1.6130185,1.6136768,1.6147637,1.612905,...
    1.6281588,1.6251719,1.6430692,1.5598662,1.3761623,...
    1.26445,1.3970103,1.5580041,1.6351847,1.6251452,...
    1.6176657,1.6232247,1.6127951,1.6152303,1.6166737,...
    1.6187691,1.614207,1.6153352,1.6168105,1.617289,...
    1.6122182,1.6170189,1.614917,1.6153319,1.617094];

T_trials = [288.9,288.9,288.9,288.9,288.9,288.9,288.9,...
    288.9,288.9,288.9,288.9,288.9,288.9,288.9,288.9,...
    288.9,288.9,288.9,288.9,288.9,288.9,288.9,288.9,...
    288.9,288.9,288.9,288.9,288.9,288.9,288.9,288.9,...
    288.9,288.9,288.9,288.9,288.9,288.9,288.9];

dP_trials = [603.7,598.8,597.7,594.9,606.3,604.4,598.3,...
    600.0,597.4,594.6,596.7,597.4,596.9,593.9,604.6,597.7,...
    602.6,520.5,338.5,228.7,360.2,519.5,601.9,601.2,596.3,...
    602.8,595.0,598.6,602.9,604.9,600.5,602.4,603.2,604.7,...
    598.5,604.8,602.8,603.1,605.3] ./1000;

P2_trials  = [1.01491533,1.0146576,1.01497255,1.0150877,...
    1.0151292,1.01508103,1.01540504,1.0159708,1.01637755,...
    1.0164882,1.01736556,1.01811634,1.0194913,1.02076016,...
    1.0242871,1.0289372,1.0367819,1.0400091,1.03898154,...
    1.03825,1.0387617,1.0395883,1.03635536,1.0288647,...
    1.02349053,1.02125345,1.0193437,1.01832805,1.0175148,...
    1.0166415,1.01582347,1.01543103,1.0153476,1.0150236,...
    1.01517115,1.0145577,1.01454016,1.0142103,1.01411];

dPven_trials  = [2.29,2.44,2.66,2.94,3.35,3.82,4.15,4.61,...
    5.41,6.28,7.85,9.35,12.40,16.09,23.86,33.28,52.10,59.53,...
    58.13,58.36,57.71,59.78,51.93,35.21,21.86,17.45,12.35,...
    10.38,7.82,6.57,5.85,4.78,4.32,3.82,3.56,3.03,2.84,2.61,2.10] ./1000;

mdot_trials =[0,0,0,0,0,0,0,0,0,0,0,0,0,0,0,0,0,0,0,0,0,0,0,0,0,0,0,...
    0,0,0,0,0,0,0,0,0,0,0,0,0,0]
```

```
% Initialize results storage
venturi_results = [];
coriolis_results = [];

% Initialize arrays for plotting
strokes = [];
Cv_values = [];
total_unc = [];

% Iterate through trials
venturi_index = 1; % Index for accessing venturi_results
coriolis_index = 1; % Index for accessing coriolis_results

for i = 1:length(mdot_trials)
    mdot = mdot_trials(i);
    stroke = stroke_trials(i); % Get the corresponding stroke value

    if mdot == 0
        % Venturi scenario
        P1 = P1_trials(i);
        P2 = P2_trials(i);
        dPven = dPven_trials(i);
        dP = dP_trials(i);
        T = T_trials(i);

        % Call Venturi function
        result = Venturi_Call(FID, P1, P2, dPven, dP, T);
        result.stroke = stroke; % Add stroke measurement to result
        venturi_results = [venturi_results; result];

        % Collect data for plotting
        strokes = [strokes, stroke];
        Cv_values = [Cv_values, result.Cv];
        total_unc = [total_unc, result.total_unc];
        venturi_index = venturi_index + 1; % Increment Venturi index
    elseif mdot > 0
        % Coriolis scenario
        P1 = P1_trials(i);
        dP = dP_trials(i);
        T = T_trials(i);

        % Call Coriolis function
        result = Coriolis_Call(FID, mdot, P1, dP, T);
        result.stroke = stroke; % Add stroke measurement to result
        coriolis_results = [coriolis_results; result];

        % Collect data for plotting
        strokes = [strokes, stroke];
        Cv_values = [Cv_values, result.Cv];
        total_unc = [total_unc, result.total_unc];
        coriolis_index = coriolis_index + 1; % Increment Coriolis index
```

```
    else
        error('Unexpected mdot value at trial %d: %f', i, mdot);
    end
end

% Display Results
disp('----- Combined Results -----');
venturi_index = 1; % Reset Venturi index
coriolis_index = 1; % Reset Coriolis index
trial_counter = 1; % Single counter for all trials

for i = 1:length(mdot_trials)
    stroke = stroke_trials(i); % Get the corresponding stroke value

    if mdot_trials(i) == 0
        % Venturi scenario
fprintf('Trial %d (Stroke = %d%%): Venturi\n', trial_counter, stroke);
       fprintf('    m_ven: %.4f\n', venturi_results(venturi_index).m_ven);
       fprintf('    v_inst_err: %.4f\n', venturi_results(venturi_index).v_inst_err);
        fprintf('    P1: %.4f bar\n', venturi_results(venturi_index).P1);
        fprintf('    dP: %.4f bar\n', venturi_results(venturi_index).dP);
        fprintf('    T: %.2f K\n', venturi_results(venturi_index).T);
        fprintf('    Cv: %.4f\n', venturi_results(venturi_index).Cv);
        fprintf('    m_unc: %.4f\n', venturi_results(venturi_index).m_unc);
         fprintf('    P1_unc: %.4f\n', venturi_results(venturi_index).P1_unc);
           fprintf('    dP_unc: %.4f\n', venturi_results(venturi_index).dP_unc);
            fprintf('    T_unc: %.4f\n', venturi_results(venturi_index).T_unc);
       fprintf('    total_unc: %.4f\n\n', venturi_results(venturi_index).total_unc);
        fprintf('    prc_error_Cv: %.4f%%\n\n', venturi_results(venturi_index).↙
prc_error);
        venturi_index = venturi_index + 1;
    elseif mdot_trials(i) > 0
        % Coriolis scenario
        fprintf('Trial %d (Stroke = %d%%): Coriolis\n', trial_counter, stroke);
        fprintf('    mdot: %.4f g/s\n', coriolis_results(coriolis_index).mdot);
        fprintf('    P1: %.4f bar\n', coriolis_results(coriolis_index).P1);
        fprintf('    dP: %.4f bar\n', coriolis_results(coriolis_index).dP);
        fprintf('    T: %.2f K\n', coriolis_results(coriolis_index).T);
        fprintf('    Cv: %.4f\n', coriolis_results(coriolis_index).Cv);
        fprintf('    m_unc: %.4f\n', coriolis_results(coriolis_index).m_unc);
        fprintf('    total_unc: %.4f\n', coriolis_results(coriolis_index).total_unc);
        fprintf('    prc_error_Cv: %.4f%%\n\n', coriolis_results(coriolis_index).↙
prc_error);
        coriolis_index = coriolis_index + 1;
    end

    trial_counter = trial_counter + 1; % Increment the global trial counter
end
```

Coriolis Call Function for Main Uncertainty Analysis (Coriolis_Call)


```
function results = Coriolis_Call(FID, mdot_trials, P1_trials, dP_trials, T_trials)
% COMPUTE_CORIOLIS

% Arguments:
% - FID: Fluid ID string (e.g., 'Nitrogen')
% - mdot_trials: Array of mass flow rates [g/s]
% - P1_trials: Array of inlet pressures [bar]
% - dP_trials: Array of pressure drops [bar]
% - T_trials: Array of temperatures [K]

    % Fixed parameters
    Delta = [0.9, 1.0, 1.1]; % Perturbation factors
    xT = 0.72; % Valve Pressure Differential Ratio Factor
    FL = 0.9; % Liquid Pressure Recovery Factor
    Fd_0 = 0.46; % Valve Style Modifier
    d = 0.5; % Valve Size [in.]
    D1 = 0.5; % Inlet Pipe ID [in.]
    D2 = 0.5; % Outlet Pipe ID [in.]
    Do = 0; % Valve Orifice Diameter [in.]
    Ctype = 0; % Compressible Fluid [1 if Incompressible]

    % Instrumentation errors
    inst_err.mdot = 0.001; % [g/s]
    inst_err.P1 = 7 * 0.0004; % [bar]
    inst_err.dP = 0.621 * 0.001; % [bar]
    inst_err.T = 0.005; % Temperature [% of reading]

    % Initialize results storage
    results = struct();

    % Iterate through trials
    for trial = 1:length(mdot_trials)
        % Extract trial-specific nominal values
        mdot = mdot_trials(trial);
        P1 = P1_trials(trial);
        dP = dP_trials(trial);
        T = T_trials(trial);

        % uncertainty storage
        Cv_values_mdot = zeros(size(Delta));
        Cv_values_P1 = zeros(size(Delta));
        Cv_values_dP = zeros(size(Delta));
        Cv_values_T = zeros(size(Delta));

        % Mass flow uncertainty
        mass_flows = mdot .* Delta;
        for i = 1:length(Delta)
            Cv_values_mdot(i) = Valve_Cv_Dp_Replacement(FID, mass_flows(i), P1, dP, T,↙
xT, FL, Fd_0, d, D1, D2, Do, Ctype);
        end
        dCv_dm = (Cv_values_mdot(3) - Cv_values_mdot(1)) / (3.6 * (mass_flows(3) -↙
```

```
mass_flows(1))); % g/s to kg/hr
        m_unc = inst_err.mdot * 3.6 * mdot * dCv_dm;

        % P1 uncertainty
        P1_values = P1 .* Delta;
        for i = 1:length(Delta)
            Cv_values_P1(i) = Valve_Cv_Dp_Replacement(FID, mdot, P1_values(i), dP, T, xT,↙
FL, Fd_0, d, D1, D2, Do, Ctype);
        end
        dCv_dP1 = (Cv_values_P1(3) - Cv_values_P1(1)) / (100 * (P1_values(3) - P1_values↙
(1))); % bar to kPa
        P1_unc = inst_err.P1 * 100 * dCv_dP1;

        % dP uncertainty
        dP_values = dP .* Delta;
        for i = 1:length(Delta)
            Cv_values_dP(i) = Valve_Cv_Dp_Replacement(FID, mdot, P1, dP_values(i), T, xT,↙
FL, Fd_0, d, D1, D2, Do, Ctype);
        end
        dCv_ddP = (Cv_values_dP(3) - Cv_values_dP(1)) / (100 * (dP_values(3) - dP_values↙
(1))); % bar to kPa
        dP_unc = inst_err.dP * 100 * dCv_ddP;

        % Temperature uncertainty
        T_values = T .* Delta;
        for i = 1:length(Delta)
            Cv_values_T(i) = Valve_Cv_Dp_Replacement(FID, mdot, P1, dP, T_values(i), xT,↙
FL, Fd_0, d, D1, D2, Do, Ctype);
        end
        dCv_dT = (Cv_values_T(3) - Cv_values_T(1)) / (T_values(3) - T_values(1));
        T_unc = inst_err.T * T * dCv_dT;

        % Cumulative uncertainty (RSS)
        total_unc = sqrt(m_unc^2 + P1_unc^2 + dP_unc^2 + T_unc^2);

        % Original Cv without perturbation
        original_Cv = Valve_Cv_Dp_Replacement(FID, mdot, P1, dP, T, xT, FL, Fd_0, d, D1,↙
D2, Do, Ctype);

        % Percent error
        prc_error = (total_unc / original_Cv) * 100;

        % Store results
        results(trial).mdot = mdot;
        results(trial).P1 = P1;
        results(trial).dP = dP;
        results(trial).T = T;
        results(trial).Cv = original_Cv;
        results(trial).m_unc = m_unc;
        results(trial).m_unc = P1_unc;
        results(trial).m_unc = dP_unc;
```

```
        results(trial).m_unc = T_unc;
        results(trial).total_unc = total_unc;

        results(trial).prc_error = prc_error;
         % Return all results in a struct


end
```

Venturi Call Function for Main Uncertainty Analysis (Venturi_Call)

2/28/25 9:29 AM E:\Grake\MATLAB\Cv Pack\Venturi_Call.m 1 of 3

```
function results = Venturi_Call(FID, P1_trials, P2_trials, dPven_trials, dP_trials,↙
T_trials)
% COMPUTE_VENTURI
%
%  # :
% - FID: Fluid ID string (e.g., 'Nitrogen')
% - P1_trials: Array of inlet pressures [bar]
% - P2_trials: Array of outlet pressures [bar]
% - dPven_trials: Array of Venturi pressure drops [bar]
% - dP_trials: Array of valve pressure drops [bar]
% - T_trials: Array of temperatures [K]


    % Constants
    d1 = 0.674 * 0.0254; % Inlet diameter [m]
    d2 = 0.270 * 0.0254; % Outlet diameter [m]
    z1 = 0.995; % Flow coefficient
    B = d2 / d1; % Diameter ratio
    g = 1.4; % Specific heat ratio
    R = 296.8; % Gas constant [Pa·m³/(kg·K)]
    xT = 0.72; FL = 0.9; Fd_0 = 0.46; d = 0.5; D1 = 0.5; D2 = 0.5; Do = 0; Ctype = 0;

    % Instrumentation errors
    inst_err.P1 = 7 * 0.0004; % [bar]
    inst_err.P2 = 7 * 0.0004; % [bar]
    inst_err.dP = 0.621 * 0.001; % [bar]
    inst_err.dPven = 0.06221 * 0.001; % [bar]
    inst_err.T = 0.005; % [% of reading]


    Delta = [0.9, 1.0, 1.1];

    % Initialization
    results = struct();

    %  Venturi flow rates and uncertainties for each trial
    for trial = 1:length(P1_trials)
        %  trial-specific inputs
        P1 = P1_trials(trial);
        P2 = P2_trials(trial);
        dPven = dPven_trials(trial);
        dP = dP_trials(trial);
        T = T_trials(trial);


        % Density calculations
        rho = P2 * 1e5 / (R * T); % [kg/m³]
        drhodP = 1 / (R * T); % [kg/m³ per Pa]
        drhodT = -P2 * 1e5 / (R * T^2); % [kg/m³ per K]
        sigma_rho = sqrt((drhodP * inst_err.P2 * 1e5)^2 + (drhodT * inst_err.T * T)^2); %↙
[kg/m³]
```

```
        % Venturi flow rate calculation
        t_ven = 1 - (dPven / P2);
        E = sqrt(((g * t_ven^(2 / g)) / (g - 1)) * ...
                 ((1 - B^4) / (1 - B^4 * t_ven^(2 / g))) * ...
                 ((1 - t_ven^((g - 1) / g)) / (1 - t_ven)));
        m_ven = E * z1 * pi * 0.25 * d2^2 * sqrt(2 * (dPven * 1e5) * rho / (1 - B^4)) *↙
1e3; % [g/s]

        % Partial derivatives for uncertainty propagation
        dmdrho = 0.5 * E * z1 * pi * 0.25 * d2^2 * sqrt(2 * dPven * 1e5) * 1e3 * (1 /↙
sqrt(rho)) / sqrt(1 - B^4); % [g/s per kg/m³]
        dmddPven = 0.5 * E * z1 * pi * 0.25 * d2^2 * sqrt(2 * rho) * 1e3 * (1 / sqrt↙
(dPven * 1e5)) / sqrt(1 - B^4); % [g/s per Pa]
        vmass_unc = 3.6 * sqrt((dmdrho * sigma_rho)^2 + (dmddPven * inst_err.dPven * 1e5)↙
^2); % [kg/hr]

        % Cv calculations with perturbations
        mass_flows = m_ven .* Delta; % Adjusted mass flows
        Cv_values = zeros(size(Delta));
        for i = 1:length(Delta)
            mdot_adjusted = mass_flows(i);
            Cv_values(i) = Valve_Cv_Dp_Replacement(FID, mdot_adjusted, P1, dP, T, xT, FL,↙
Fd_0, d, D1, D2, Do, Ctype);
        end

        % Numerical differentiation for Cv uncertainty
        dCv_dm = (Cv_values(3) - Cv_values(1)) / (3.6 * (mass_flows(3) - mass_flows(1)));↙
% [kg/hr]
        m_unc = vmass_unc .* dCv_dm; % [g/s to kg/hr]
        P1_values = P1 .* Delta;
        T_values = T .* Delta;
        dP_values = dP .* Delta;

        % Cv uncertainties for P1, dP, and T
        Cv_values_P1 = arrayfun(@(P1_adj) Valve_Cv_Dp_Replacement(FID, m_ven, P1_adj, dP,↙
T, xT, FL, Fd_0, d, D1, D2, Do, Ctype), P1_values);
        dCv_dP1 = (Cv_values_P1(3) - Cv_values_P1(1)) / (100 * (P1_values(3) - P1_values↙
(1)));
        P1_unc = inst_err.P1 * 100 * dCv_dP1;

        Cv_values_dP = arrayfun(@(dP_adj) Valve_Cv_Dp_Replacement(FID, m_ven, P1, dP_adj,↙
T, xT, FL, Fd_0, d, D1, D2, Do, Ctype), dP_values);
        dCv_ddP = (Cv_values_dP(3) - Cv_values_dP(1)) / (100 * (dP_values(3) - dP_values↙
(1)));
        dP_unc = inst_err.dP * 100 * dCv_ddP;

        Cv_values_T = arrayfun(@(T_adj) Valve_Cv_Dp_Replacement(FID, m_ven, P1, dP,↙
T_adj, xT, FL, Fd_0, d, D1, D2, Do, Ctype), T_values);
        dCv_dT = (Cv_values_T(3) - Cv_values_T(1)) / (T_values(3) - T_values(1));
        T_unc = inst_err.T * T * dCv_dT;
```

```
        % Total uncertainty (RSS)
        total_unc = sqrt(m_unc^2 + P1_unc^2 + dP_unc^2 + T_unc^2);
        prc_error = (total_unc / Cv_values(2)) * 100;

        % Storage callout

        results(trial).m_ven = m_ven;
        results(trial).v_inst_err = vmass_unc;
        results(trial).P1 = P1;
        results(trial).dP = dP;
        results(trial).T = T;
        results(trial).Cv = Cv_values(2); % Nominal Cv
        results(trial).m_unc = m_unc;
        results(trial).P1_unc = P1_unc;
        results(trial).dP_unc = dP_unc;
        results(trial).T_unc = T_unc;
        results(trial).total_unc = total_unc;
        results(trial).prc_error = prc_error;
        %results(trial).uncertainties = struct('m_unc', m_unc, 'P1_unc', P1_unc,↙
'dP_unc', dP_unc, 'T_unc', T_unc, 'total', total_unc);
    end


end
```

Valve Plug as Flowmeter (Cv to Mass Backout Uncertainty)


```
%↙
----------------------------------------------------------------------------↙
----
%Mass Flow from CurveFitted Flow Coefficient

cv_curvefit = [0.1185153,0.1244274,0.1303506,0.1363992,0.1426875,0.1493298...
         ,0.1564404,0.1641336,0.1725237,0.181725,0.1918518,0.2030184,0.2153391...
         ,0.2289282,0.2439,0.2603688,0.2784489,0.2982546,0.3199002,0.3435]

cv_experimental_trials = [0.112471163580358,0.126884025982945,0.129590209917242,...
     0.136491169070485,0.141861925581628,0.148494404457524,0.156175803022491,...
     0.162789227060784,0.171806298573977,0.182884352544710,0.189797470076128,...
     0.204096625720836,0.214178705327708,0.227069569590723,0.241450419544518,...
     0.26311559399254,0.277680859104482,0.297395310160913,0.319776034535442,...
     0.343260843120563]

stroke_trials = [5, 10, 15, 20, 25, 30, 35, 40, 45, 50, 55, 60,...
     65, 70, 75, 80, 85, 90, 95, 100]
%
P1_trials = [1.6116348, 1.6099179, 1.6157687, 1.6196058, 1.6169787, 1.6131118, ...
        1.6142068, 1.6157136, 1.6176572, 1.6147054, 1.6293328, 1.6164454, ...
        1.617409, 1.6161771, 1.6154886, 1.6139718, 1.6161538, 1.6134885, ...
        1.6206077, 1.6205211]

T_trials = [294.0841, 293.93024, 293.9092, 293.96085, 293.87976, 293.93045, ...
        293.79272, 293.85416, 293.82883, 293.82892, 293.7782, 293.8038, ...
        293.77924, 293.77823, 293.70728, 293.75375, 293.70218, 293.67706, ...
        293.70218, 293.60712]

dP_trials = [596.49310, 594.58716, 599.99540, 603.20874, 600.54320, 596.98206, ...
        596.87540, 598.32620, 599.98130, 597.70355, 597.57380, 599.63370, ...
        599.48050, 598.27170, 596.56824, 594.91223, 596.86835, 592.37116, ...
        598.30330, 597.67490] ./1000

%↙
----------------------------------------------------------------------------↙
----

% Valve Plug : A1
FID = 'Nitrogen';

% Valve parameters
Delta = [0.9, 1.0, 1.1]; % Perturbation factors
xT = 0.72; % Valve Pressure Differential Ratio Factor
FL = 0.9; % Liquid Pressure Recovery Factor
Fd_0 = 0.46; % Valve Style Modifier
d = 0.5; % Valve Size [in.]
D1 = 0.5; % Inlet Pipe ID [in.]
D2 = 0.5; % Outlet Pipe ID [in.]
Do = 0; % Valve Orifice Diameter [in.]
Ctype = 0; % Compressible Fluid [1 if Incompressible]
```

```
% Initialize results
mdot_curvefit = zeros(1, length(cv_curvefit));
mdot_experimental = zeros(1, length(cv_experimental_trials));

% Compute mass flow for curve-fitted Cv values
for trial = 1:length(cv_curvefit)
    targetCv = cv_curvefit(trial);
    P1 = P1_trials(trial);
    dP = dP_trials(trial);
    T = T_trials(trial);

    mdot_curvefit(trial) = SolveForMdot(targetCv, FID, P1, dP, T, xT, FL, Fd_0, d, D1,↙
D2, Do, Ctype);
end

% Compute mass flow for experimental Cv values
for trial = 1:length(cv_experimental_trials)
    targetCv = cv_experimental_trials(trial);
    P1 = P1_trials(trial);
    dP = dP_trials(trial);
    T = T_trials(trial);

    mdot_experimental(trial) = SolveForMdot(targetCv, FID, P1, dP, T, xT, FL, Fd_0, d,↙
D1, D2, Do, Ctype);
end
```

Mass Flow Backout using ISA standards(Valve_Cv_Dp_Replacement)

3/6/25 1:30 PM E:\Grake\MATLAB\SolveForMdot.m 1 of 1

```
function mdot = SolveForMdot(targetCv, FID, P1, dP, T, xT, FL, Fd_0, d, D1, D2, Do,↙
Ctype)
% SolveForMdot calculates the mass flow rate (mdot, in g/s) that produces a valve
% Cv equal to targetCv. It uses fsolve to find the mdot that zeros the difference
% between the computed Cv (using Valve_Cv_Dp_Replacement) and the targetCv.
%
% Inputs:
%   targetCv : Desired valve Cv value.
%   FID      : Fluid ID (see CoolProps documentation).
%   P1       : Inlet Pressure [bar].
%   dP       : Pressure Drop [bar].
%   T        : Inlet Temperature [K].
%   xT       : Valve Pressure Differential Ratio Factor [-].
%   FL       : Liquid Pressure Recovery Factor [-].
%   Fd_0     : Valve Style Modifier [-] (or 0 if the orifice diameter is known).
%   d, D1, D2: Valve/Pipe dimensions [in].
%   Do       : Valve Orifice Diameter [in] (set to 0 if unknown).
%   Ctype    : 0 for compressible fluid, 1 for incompressible fluid.
%
% Output:
%   mdot     : Mass flow rate [g/s] that yields a valve Cv ≈ targetCv.
%
% Example usage:
%   targetCv = .3;
%   mdot = SolveForMdot(targetCv, 'Nitrogen', 1.6, 0.6, 300,.72 , 0.9,.46 ,.5, .5, .5,↙
0,0);

    % Set an initial guess for mdot (in g/s)
    mdot0 = 1;

    % Options for fsolve (set 'Display' to 'off' to suppress output)
    options = optimset('Display','iter');

    % Define the residual function: the difference between the computed Cv and targetCv.
    % f(mdot) = Valve_Cv_Dp_Replacement(...) - targetCv should be zero.
    residual = @(mdot) Valve_Cv_Dp_Replacement(FID, mdot, P1, dP, T, xT, FL, Fd_0, d, D1,↙
D2, Do, Ctype) - targetCv;

    % Use fsolve to find the mdot that makes the residual zero.
    mdot = fsolve(residual, mdot0, options);
end
```

ISA Standards(Valve_Cv_Dp_Replacement)


```
% This function calculates the valve flow coefficients given the inputs
% Calculations are performed based on ANSI/ISA 75.01.01 (2007)

function Cv = Valve_Cv_Dp_Replacement(FID,mdot,P1,dP,T,xT,FL,Fd_0,d,D1,D2,Do,Ctype)

    PEFID = 'CP';

    %--------------------------------------------------------------------
    % Inputs

    % FID                   Fluid ID (See CoolProps Documentation)
    % mdot                  Mass Flow Rate [g/s]
    % P1                    Inlet Pressure [bar]
    % P2                    Outlet Pressure [bar]
    % T                     Inlet Temperature [K]
    % xT                    Valve Pressure Differential Ratio Factor [-] (See ANSI/ISA↙
75.01.01 Table 2 for details)
    % FL                    Liquid Pressure Recovery Factor [-] (See ANSI/ISA 75.01.01↙
Table 2 for details)
    % Fd_0                  Valve Style Modifier [-] (See ANSI/ISA 75.01.01 Table 2 for↙
details, Or Set 0 if valve orifice diameter is known)
    % d                     Valve Size [in.]
    % D1                    Inlet Pipe ID [in.]
    % D2                    Outlet Pipe ID [in.]
    % Do                    Valve Orifice Diameter [in.] (Set 0 if unknown)
    % Ctype                 0 if Compressible, 1 if incompressible
    %--------------------------------------------------------------------

    % Vapor Pressure of Fluid at Test Temperature [bar]
    Pv = psat_T(PEFID,FID,T);
    % Critical Pressure of Fluid [bar]
    Pc = p_crit(PEFID,FID);

    % Inlet Density of Fluid at Test Temperature and Pressure [kg/m3]
    rho = rho_pT(PEFID,FID,P1,T);
    % Density of Fluid at Standard Conditions (1.0 atm and 288K)
    rho_o = rho_pT(PEFID,FID,101.325/100,288);

    %Mass Flow Rate [kg/hr]
    w = mdot*(3600/1000);

    %Volume Flow Rate [m3/hr] at standard conditions
    Q = (mdot/rho_pT(PEFID,FID,101.325/100,288))*(3600/1000);

    % Kinematic Viscosity of Fluid [m2/s]
    nu = visc_pT(PEFID,FID,P1,T)*1e-6/rho;

    % Specific Heat Ratio
    gamma = gamma_pT(PEFID,FID,P1,T);
```

```
    % Molecular Weight of Fluid
    M = mw(PEFID,FID);

    % Compressibility Factor for Fluid
    Z = 1; %Z_pT(PEFID,FID,P1,T);

    % Convert inlet pressure to [kPa]
    P1 = P1*100;
    % Convert pressure drop to [kPa]
    dP = dP*100;
    % Calculate and Convert outlet pressure to [kPa]
    P2 = (P1-dP);

    % Convert Valve/Pipe Dimensions to [mm]
    d = d*25.4;
    D1 = D1*25.4;
    D2 = D2*25.4;
    Do = Do*25.4;

    % Conversion Factors per ANSI/ISA
    N1 = 8.65E-2;
    N2 = 2.14E-3;
    N4 = 7.60E-2;
    N5 = 2.41E-3;
    N6 = 2.73;
    N9 = 2.12e1;
    N18 = 1.0;
    N19 = 2.3;
    N27 = 6.7e-1;
    N32 = 1.27E2;

    i = 0; j = 0;

    Fgma = gamma/1.4;

    dP = (P1-P2);
    FF = 0.96 - 0.28*sqrt(Pv/Pc);
    dP_crit = (FL^2)*(P1-FF*Pv*100);

    x = dP/P1;

if (Ctype == 0)
% Compressible Fluid
    if x < (Fgma*xT)
        Type = 'Non-Choked';
        Y = 1-(x/(3*Fgma*xT));
        C = w/(N6*Y*sqrt(x*P1*rho));
    else
        Type = 'Choked';
        Y = 0.667;
        C = w/(Y*N6*sqrt(Fgma*xT*P1*rho));
```

```
end

C1 = 1.3*C;

if (Fd_0 == 0)
    Fd = (N19*sqrt(C1*FL))/Do;
else
    Fd = Fd_0;
end

Rev = (N4*Fd*Q/(nu*sqrt(C1*FL)))*(((FL*C1)^2/(N2*D1^4))+1)^0.25;

if Rev > 10000
    Flow = 'Turbulent';
    if (d == D1) && (d==D2)
        Cv = C1;
    else
        flag_1 = 1;
        while flag_1
            j = j+1;
            C1 = C;
            za11 = 0.5*(1-(d/D1)^2)^2;
            za12 = (1-(d/D2)^2)^2;
            zaB1 = 1-(d/D1)^4;
            zaB2 = 1-(d/D2)^4;
            sza1 = za11 + za12 + zaB1 - zaB2;
            FP = 1/sqrt(1+(sza1/N2)*(C1/d^2)^2);
            xTP = (xT/FP^2)/(1+(xT*za11/N5)*(C1/d^2)^2);

            if x >= Fgma*xTP
                C = w/(0.667*N6*FP*sqrt(Fgma*xTP*P1*rho));
            else
                C = w/(Y*N6*FP*sqrt(x*P1*rho));
            end

            if C1/C >= 0.99
                flag_1 = 0;
            else
                flag_1 = 1;
            end
        end
        Cv = C;
    end
else
    Flow = 'Laminar / Transition';
    flag_2 = 1;

    while (flag_2) && (1<50)
        1 = 1+1;

        if (C1/d^2)>0.016*N18
```

```
                n1 = N2/(C1/d^2)^2;
                FR1 = 1+(0.33*FL^0.5/n1^0.25)*log10(Rev/10000);
                FR2 = (0.026/FL)*sqrt(n1*Rev);
                FR = min([FR1 FR2 1]);
            else
                n2 = 1+N32*(C1/d^2)^(2/3);
                FR1 = 1+(0.33*FL^0.5/n2^0.25)*log10(Rev/10000);
                FR2 = (0.026/FL)*sqrt(n2*Rev);
                FR = min([FR1 FR2 1]);
            end

            C = (w/(N27*FR))*sqrt(T/(dP*(P1+P2)*M));

            if (C/FR) <= C1
                flag_2 = 0;
            else
                C1 = 1.3*C1;
                if (Fd_0 == 0)
                    Fd = (N19*sqrt(C1*FL))/Do;
                else
                    Fd = Fd_0;
                end

                Rev = (N4*Fd*Q/(nu*sqrt(C1*FL)))*(((FL*C1)^2/(N2*D1^4))+1)^0.25;
            end
        end
    end
    Cv = C;

elseif (Ctype == 1)
% Incompressible Fluid
    if dP< dP_crit
        Type = 'Non-Choked';
        C = (Q/N1)*sqrt((rho/rho_o)/dP);
    else
        Type = 'Choked';
        C = (Q/(N1*FL))*sqrt((rho/rho_o)/(P1-FF*Pv));
    end

    C1 = C;
    Rev = (N4*Fd_0*Q/(nu*sqrt(C1*FL)))*(((FL*C1)^2/(N2*D^4))+1)^0.25;

    if Rev > 10000
        Flow = 'Turbulent';
        if (d == D1) && (d==D2)
            Cv = C1;
        else
            flag_1 = 1;
            while flag_1
                C1 = C;
                za11 = 0.5*(1-(d/D)^2)^2;
```

```
            za12 = (1-(d/D)^2)^2;
            sza1 = za11 + za12;
            FP = 1/sqrt(1+(sza1/N2)*(C1/d^2)^2);
            FLP = FL/sqrt(1+(FL^2*za11/N2)*(C1/d^2)^2);

            if dP >= (FLP/FP)^2*(P1-FF*Pv)
                C = (Q/(N1*FLP))*sqrt((rho/rho_o)/(P1-FF*Pv));
            else
                C = (Q/(N1*FP))*sqrt((rho/rho_o)/dP);
            end

            if C1/C >= 0.99
                flag_1 = 0;
            else
                flag_1 = 1;
            end
        end

        Cv = C;
    end
else
    Flow = 'Laminar / Transitional';
    flag_2 = 1;
    while flag_2
        i = i+1;
        C1 = 1.3*C;
        Rev = (N4*Fd_0*Q/(nu*sqrt(C1*FL)))*(((FL*C1)^2/(N2*D^4))+1)^0.25;
        n1 = N2/(C1/d^2)^2;
        n2 = 1+N32*(C1/d^2)^(2/3);
        if Rev < 10
            FR1 = (0.026/FL)*sqrt(n2*Rev);
            FR = min([FR1 1]);
        else
            if (C/d^2)>0.016*N18
                FR1 = 1+(0.33*FL^0.5/n1^0.25)*log10(Rev/10000);
                FR2 = (0.026/FL)*sqrt(n1*Rev);
                FR = min([FR1 FR2 1]);
            else
                FR1 = 1+(0.33*FL^0.5/n2^0.25)*log10(Rev/10000);
                FR2 = (0.026/FL)*sqrt(n2*Rev);
                FR = min([FR1 FR2 1]);
            end
        end

        %C = (Q/(N1*FR))*sqrt((rho/rho_o)/dP);

        if (C/FR) <= C1
            flag_2 = 0;
            Cv = C;
        else
            flag_2 = 1;
```

```
            end
        end
    end
end

end
```

APPENDIX C: VALVE PLUG NOMENCLATURE AT FRIB

Table C.1: Valve Plug Numbering System for FRIB

Part ID	FRIB PART ID
OEM	[n/a]
A1	T30200-MDE-0002-0041
A2	T30200-MDE-0002-0042
A3	T30200-MDE-0002-0043
A4	T30200-MDE-0002-0047
B1	T30200-MDE-0002-0044
B2	T30200-MDE-0002-0045
B3	T30200-MDE-0002-0046

APPENDIX D: VALVE PLUG TEST DATA

Table D.1: OEM Valve Plug Test Data with Corrected Pressure Offsets

OEM - Measured Data with Corrected Pressure Offsets									
Trial #	Stroke [ξ]	Stroke [ξ]	P100	P101	T101	DPT101	P102	T102	DPT102
	[%]	[mm]	[Bar]	[Bar]	[K]	[mBar]	[Bar]	[K]	[mBar]
1	5%	1.35	0.03	1.62	288.90	603.73	1.01	288.90	2.29
2	10%	2.21	0.03	1.61	288.90	598.79	1.01	288.90	2.44
3	15%	2.71	0.03	1.61	288.90	597.65	1.01	288.90	2.66
4	20%	3.42	0.03	1.61	288.90	594.89	1.02	288.90	2.94
5	25%	4.09	0.03	1.62	288.90	606.29	1.02	288.90	3.35
6	30%	4.81	0.03	1.62	288.90	604.38	1.02	288.90	3.82
7	35%	5.68	0.03	1.61	288.90	598.31	1.02	288.90	4.15
8	40%	6.42	0.03	1.61	288.90	600.03	1.02	288.90	4.61
9	45%	7.20	0.03	1.61	288.90	597.43	1.02	288.90	5.41
10	50%	7.88	0.03	1.61	288.90	594.65	1.02	288.90	6.28
11	55%	8.82	0.03	1.61	288.90	596.69	1.02	288.90	7.85
12	60%	9.58	0.03	1.61	288.90	597.41	1.02	288.90	9.35
13	65%	10.59	0.03	1.61	288.90	596.86	1.02	288.90	12.40
14	70%	11.33	0.03	1.61	288.90	593.86	1.02	288.90	16.09
15	75%	12.35	0.03	1.63	288.90	604.57	1.02	288.90	23.86
16	80%	13.40	0.03	1.63	288.90	597.73	1.03	288.90	33.28
17	85%	14.39	0.03	1.64	288.90	602.65	1.04	288.90	52.10
18	90%	15.40	0.03	1.56	288.90	520.52	1.04	288.90	59.53
19	95%	16.23	0.03	1.38	288.90	338.49	1.04	288.90	58.13
20	100%	17.03	1.39	1.26	288.90	228.71	1.04	288.90	58.36
21	95%	16.24	0.03	1.40	288.90	360.22	1.04	288.90	57.71
22	90%	15.26	0.03	1.56	288.90	519.52	1.04	288.90	59.78
23	85%	14.38	0.03	1.64	288.90	601.89	1.04	288.90	51.93
24	80%	13.49	0.03	1.63	288.90	601.22	1.03	288.90	35.21
25	75%	12.31	0.03	1.62	288.90	596.33	1.02	288.90	21.86
26	70%	11.33	0.03	1.62	288.90	602.77	1.02	288.90	17.45
27	65%	10.55	0.03	1.61	288.90	595.04	1.02	288.90	12.35
28	60%	9.85	0.03	1.62	288.90	598.59	1.02	288.90	10.38
29	55%	8.63	0.03	1.62	288.90	602.88	1.02	288.90	7.82
30	50%	8.18	0.03	1.62	288.90	604.90	1.02	288.90	6.57
31	45%	7.36	0.03	1.61	288.90	600.48	1.02	288.90	5.85
32	40%	6.34	0.03	1.62	288.90	602.39	1.02	288.90	4.78
33	35%	5.77	0.03	1.62	288.90	603.23	1.02	288.90	4.32
34	30%	4.81	0.03	1.62	288.90	604.68	1.02	288.90	3.82
35	25%	4.34	0.03	1.61	288.90	598.52	1.02	288.90	3.56
36	20%	3.43	0.03	1.62	288.90	604.81	1.01	288.90	3.03
37	15%	2.25	0.03	1.61	288.90	602.82	1.01	288.90	2.84
38	10%	0.91	0.03	1.62	288.90	603.12	1.01	288.90	2.61
39	5%	0.91	0.03	1.62	288.90	605.35	1.01	288.90	2.10

Table D.2: A1 Valve Plug Test Data with Corrected Pressure Offsets

A1 - Measured Data with Corrected Data									
Trial #	Stroke [ξ]	Stroke [ξ]	P100	P101	T101	DPT101	P102	T102	DPT102
	[%]	[mm]	[Bar]	[Bar]	[K]	[mBar]	[Bar]	[K]	[mBar]
1	5%	1.30	1.62	1.61	294.08	596.49	1.01	294.08	1.71
2	10%	1.86	1.62	1.61	293.93	594.59	1.01	293.93	2.17
3	15%	2.52	1.62	1.62	293.91	600.00	1.01	293.91	2.29
4	20%	3.21	1.63	1.62	293.96	603.21	1.01	293.96	2.56
5	25%	4.09	1.62	1.62	293.88	600.54	1.01	293.88	2.75
6	30%	4.83	1.62	1.61	293.93	596.98	1.01	293.93	2.99
7	35%	5.64	1.62	1.61	293.79	596.88	1.02	293.79	3.31
8	40%	6.29	1.62	1.62	293.85	598.33	1.02	293.85	3.61
9	45%	7.07	1.63	1.62	293.83	599.98	1.02	293.83	4.04
10	50%	8.05	1.62	1.61	293.83	597.70	1.02	293.83	4.55
11	55%	8.77	1.62	1.63	293.78	597.57	1.02	293.78	4.97
12	60%	9.73	1.63	1.62	293.80	599.63	1.02	293.80	5.69
13	65%	10.51	1.63	1.62	293.78	599.48	1.02	293.78	6.28
14	70%	11.41	1.63	1.62	293.78	598.27	1.02	293.78	7.04
15	75%	12.34	1.63	1.62	293.71	596.57	1.02	293.71	7.95
16	80%	13.58	1.63	1.61	293.75	594.91	1.02	293.75	9.42
17	85%	14.40	1.64	1.62	293.70	596.87	1.02	293.70	10.54
18	90%	15.25	1.64	1.61	293.68	592.37	1.02	293.68	12.01
19	95%	16.27	1.65	1.62	293.70	598.30	1.02	293.70	14.08
20	100%	17.13	1.65	1.62	293.61	597.67	1.02	293.61	16.23
21	95%	16.26	1.65	1.62	293.63	602.58	1.02	293.63	14.01
22	90%	15.41	1.65	1.62	293.59	601.70	1.02	293.59	12.47
23	85%	14.52	1.64	1.62	293.63	601.87	1.02	293.63	10.96
24	80%	13.63	1.64	1.62	293.55	601.19	1.02	293.55	9.57
25	75%	12.35	1.64	1.62	293.57	600.50	1.02	293.57	8.04
26	70%	11.39	1.64	1.62	293.60	603.19	1.02	293.60	7.09
27	65%	10.48	1.63	1.62	293.65	600.70	1.02	293.65	6.28
28	60%	9.97	1.63	1.62	293.58	600.35	1.02	293.58	5.68
29	55%	8.69	1.63	1.62	293.58	601.58	1.02	293.58	5.22
30	50%	7.87	1.63	1.62	293.62	600.54	1.02	293.62	4.65
31	45%	7.28	1.63	1.62	293.58	604.24	1.02	293.58	4.07
32	40%	6.37	1.63	1.62	293.63	602.29	1.02	293.63	3.75
33	35%	5.48	1.62	1.61	293.61	597.22	1.02	293.61	3.28
34	30%	4.75	1.62	1.62	293.62	599.72	1.02	293.62	3.02
35	25%	4.00	1.62	1.61	293.62	598.03	1.02	293.62	2.76
36	20%	3.26	1.62	1.62	293.57	599.75	1.02	293.57	2.60
37	15%	2.56	1.62	1.62	293.58	601.59	1.02	293.58	2.34
38	10%	1.87	1.62	1.61	293.58	598.39	1.01	293.58	2.15
39	5%	1.42	1.62	1.61	293.57	596.57	1.02	293.57	2.00

Table D.3: A2 Valve Plug Test Data with Corrected Pressure Offsets

A2 - Measured Data with Corrected Pressure Offsets									
Trial #	Stroke [ξ]	Stroke [ξ]	P100	P101	T101	DPT101	P102	T102	DPT102
	[%]	[mm]	[Bar]	[Bar]	[K]	[mBar]	[Bar]	[K]	[mBar]
1	5%	1.59	1.62	1.62	294.35	602.72	1.01	294.35	1.31
2	10%	2.08	1.62	1.62	294.38	602.43	1.01	294.38	1.39
3	15%	2.77	1.62	1.61	294.33	597.93	1.01	294.33	1.53
4	20%	3.50	1.61	1.61	294.26	596.16	1.01	294.26	1.74
5	25%	4.09	1.62	1.62	294.26	601.39	1.01	294.26	1.92
6	30%	4.79	1.62	1.61	294.24	599.68	1.01	294.24	2.13
7	35%	5.65	1.62	1.62	294.18	599.49	1.01	294.18	2.47
8	40%	6.37	1.62	1.62	294.16	601.04	1.02	294.16	2.74
9	45%	7.17	1.62	1.62	294.18	598.80	1.02	294.18	3.10
10	50%	7.99	1.62	1.61	294.07	598.47	1.02	294.07	3.54
11	55%	9.02	1.62	1.63	294.06	598.21	1.02	294.06	4.17
12	60%	9.72	1.63	1.61	294.04	601.03	1.02	294.04	4.74
13	65%	10.85	1.63	1.62	293.99	602.72	1.02	293.99	5.70
14	70%	11.52	1.63	1.62	293.98	600.53	1.02	293.98	6.30
15	75%	12.47	1.64	1.62	293.97	600.53	1.02	293.97	7.46
16	80%	13.54	1.64	1.62	293.78	605.06	1.02	293.78	8.61
17	85%	14.40	1.64	1.63	293.78	606.30	1.02	293.78	10.51
18	90%	15.32	1.65	1.62	293.76	603.99	1.02	293.76	12.20
19	95%	16.46	1.65	1.63	293.80	604.77	1.02	293.80	14.13
20	100%	17.18	1.64	1.61	293.80	590.82	1.02	293.80	16.04
21	95%	16.42	1.64	1.61	293.85	592.71	1.02	293.85	14.09
22	90%	15.52	1.64	1.61	293.85	595.20	1.02	293.85	11.80
23	85%	14.53	1.64	1.62	293.88	598.08	1.02	293.88	10.13
24	80%	13.43	1.64	1.62	293.78	605.06	1.02	293.78	8.61
25	75%	12.93	1.64	1.62	293.74	602.99	1.02	293.74	7.84
26	70%	11.52	1.63	1.62	293.70	605.12	1.02	293.70	6.38
27	65%	10.99	1.64	1.63	293.69	607.26	1.02	293.69	5.68
28	60%	9.70	1.63	1.62	293.74	604.84	1.02	293.74	4.73
29	55%	9.17	1.62	1.61	293.73	596.34	1.02	293.73	4.15
30	50%	8.34	1.63	1.62	293.73	602.11	1.02	293.73	3.56
31	45%	7.47	1.62	1.62	293.73	602.66	1.02	293.73	3.08
32	40%	6.56	1.62	1.62	293.68	601.45	1.02	293.68	2.70
33	35%	5.55	1.63	1.63	293.73	605.40	1.02	293.73	2.42
34	30%	5.11	1.62	1.61	293.70	599.36	1.01	293.70	2.21
35	25%	4.05	1.62	1.61	293.73	596.81	1.01	293.73	1.95
36	20%	3.32	1.62	1.61	293.72	596.89	1.01	293.72	1.74
37	15%	2.87	1.62	1.62	293.73	600.55	1.01	293.73	1.53
38	10%	2.16	1.62	1.62	293.70	602.39	1.01	293.70	1.38
39	5%	1.43	1.62	1.62	293.74	602.56	1.01	293.74	1.30

Table D.4: A3 Valve Plug Test Data with Corrected Pressure Offsets

A3 - Measured Data with Corrected Pressure Offsets									
Trial #	Stroke [ξ]	Stroke [ξ]	P100	P101	T101	DPT101	P102	T102	DPT102
	[%]	[mm]	[Bar]	[Bar]	[K]	[mBar]	[Bar]	[K]	[mBar]
1	6%	1.16	1.61	1.61	294.16	598.92	1.01	294.16	0.28
2	10%	1.88	1.61	1.61	294.18	598.96	1.01	294.18	0.31
3	15%	2.79	1.61	1.62	294.14	600.05	1.01	294.14	0.36
4	20%	3.29	1.61	1.61	294.10	598.00	1.01	294.10	0.42
5	25%	4.22	1.62	1.62	294.08	602.30	1.01	294.08	0.52
6	30%	4.87	1.61	1.61	294.08	598.79	1.01	294.08	0.64
7	35%	5.74	1.61	1.62	294.01	599.07	1.01	294.01	0.84
8	40%	6.38	1.62	1.62	294.06	601.61	1.01	294.06	1.02
9	45%	7.13	1.62	1.62	293.98	602.38	1.01	293.98	1.26
10	50%	8.18	1.62	1.61	293.98	597.88	1.01	293.98	1.69
11	55%	8.86	1.62	1.62	293.95	599.04	1.01	293.95	2.05
12	60%	9.90	1.62	1.62	293.97	599.47	1.02	293.97	2.76
13	65%	10.62	1.62	1.61	293.91	596.40	1.02	293.91	3.29
14	70%	11.56	1.61	1.63	293.91	598.31	1.02	293.91	4.29
15	75%	12.48	1.63	1.64	293.90	602.06	1.02	293.90	5.36
16	80%	13.44	1.63	1.64	293.89	596.18	1.02	293.89	6.79
17	85%	14.38	1.63	1.64	293.83	597.72	1.02	293.83	8.58
18	90%	15.37	1.64	1.64	293.81	596.14	1.02	293.81	10.85
19	95%	16.39	1.65	1.65	293.83	598.88	1.02	293.83	13.88
20	100%	17.17	1.66	1.67	293.78	605.46	1.02	293.78	16.84
21	95%	16.38	1.64	1.65	293.70	598.24	1.02	293.70	13.55
22	90%	15.35	1.64	1.65	293.73	599.41	1.02	293.73	10.70
23	85%	14.61	1.63	1.64	293.70	598.14	1.02	293.70	9.10
24	80%	13.74	1.63	1.64	293.70	600.69	1.02	293.70	7.35
25	75%	12.83	1.63	1.64	293.68	602.33	1.02	293.68	5.92
26	70%	11.47	1.62	1.63	293.70	598.52	1.02	293.70	4.17
27	65%	10.63	1.62	1.63	293.66	599.36	1.02	293.66	3.27
28	60%	10.04	1.62	1.63	293.71	599.08	1.02	293.71	2.90
29	55%	9.00	1.62	1.63	293.68	597.79	1.02	293.68	2.12
30	50%	8.33	1.62	1.63	293.68	601.80	1.02	293.68	1.61
31	45%	7.11	1.62	1.63	293.68	602.36	1.01	293.68	1.28
32	40%	6.66	1.62	1.62	293.69	599.29	1.01	293.69	1.10
33	35%	5.55	1.61	1.62	293.66	595.53	1.01	293.66	0.78
34	30%	5.13	1.61	1.62	293.72	597.61	1.01	293.72	0.64
35	25%	4.34	1.61	1.62	293.70	598.69	1.01	293.70	0.52
36	20%	3.34	1.61	1.62	293.70	599.84	1.01	293.70	0.43
37	15%	2.61	1.61	1.62	293.65	598.08	1.01	293.65	0.38
38	10%	2.17	1.61	1.62	293.73	599.57	1.01	293.73	0.31
39	6%	1.51	1.62	1.62	293.70	601.10	1.01	293.70	0.29

Table D.5: A4 Valve Plug Test Data with Corrected Pressure Offsets

A4 - Measured Data with Corrected Pressure Offsets									
Trial #	Stroke [ξ]	Stroke [ξ]	P100	P101	T101	DPT101	P102	T102	DPT102
	[%]	[mm]	[Bar]	[Bar]	[K]	[mBar]	[Bar]	[K]	[mBar]
1	5%	1.29	1.61	1.61	294.71	593.80	1.01	294.71	1.30
2	10%	1.99	1.62	1.62	294.69	600.63	1.01	294.69	1.43
3	15%	2.66	1.62	1.62	294.62	599.65	1.01	294.62	1.63
4	20%	3.36	1.62	1.62	294.57	599.50	1.01	294.57	1.77
5	25%	4.09	1.62	1.61	294.49	599.24	1.01	294.49	1.93
6	30%	4.98	1.61	1.61	294.49	595.05	1.01	294.49	2.18
7	35%	5.55	1.62	1.61	294.41	598.76	1.02	294.41	2.43
8	40%	6.47	1.62	1.61	294.36	598.60	1.02	294.36	2.84
9	45%	7.35	1.62	1.61	294.34	596.36	1.02	294.34	3.25
10	50%	7.98	1.62	1.61	294.31	594.28	1.02	294.31	3.57
11	55%	8.84	1.62	1.61	294.29	593.40	1.02	294.29	4.05
12	60%	9.72	1.62	1.61	294.25	595.81	1.02	294.25	4.69
13	65%	10.57	1.63	1.62	294.13	603.21	1.02	294.13	5.56
14	70%	11.49	1.63	1.62	294.11	598.56	1.02	294.11	6.34
15	75%	12.41	1.63	1.62	294.08	601.33	1.02	294.08	7.35
16	80%	13.59	1.64	1.62	294.10	605.27	1.02	294.10	8.99
17	85%	14.51	1.63	1.61	294.05	594.54	1.02	294.05	10.53
18	90%	15.37	1.64	1.62	293.93	596.03	1.02	293.93	12.28
19	95%	16.29	1.65	1.62	293.98	599.50	1.02	293.98	14.43
20	100%	17.15	1.65	1.62	293.92	599.64	1.02	293.92	16.83
21	95%	16.34	1.65	1.62	293.82	600.41	1.02	293.82	14.41
22	90%	15.40	1.65	1.63	293.86	604.93	1.02	293.86	12.35
23	85%	14.54	1.64	1.62	293.86	601.10	1.02	293.86	10.88
24	80%	13.60	1.64	1.63	293.84	605.70	1.02	293.84	9.23
25	75%	12.41	1.64	1.62	293.85	604.41	1.02	293.85	7.65
26	70%	11.51	1.63	1.62	293.83	602.47	1.02	293.83	6.65
27	65%	10.54	1.63	1.62	293.78	603.05	1.02	293.78	5.71
28	60%	10.08	1.63	1.62	293.85	602.11	1.02	293.85	5.25
29	55%	8.71	1.63	1.62	293.80	602.96	1.02	293.80	4.24
30	50%	7.92	1.63	1.62	293.84	605.28	1.02	293.84	3.74
31	45%	7.13	1.62	1.62	293.85	601.68	1.02	293.85	3.27
32	40%	6.31	1.63	1.62	293.80	603.02	1.02	293.80	2.86
33	35%	5.62	1.62	1.62	293.78	600.76	1.02	293.78	2.56
34	30%	4.93	1.62	1.62	293.83	601.11	1.02	293.83	2.29
35	25%	4.23	1.62	1.61	293.83	597.76	1.02	293.83	2.04
36	20%	3.40	1.62	1.62	293.85	601.19	1.01	293.85	1.80
37	15%	2.17	1.62	1.62	293.83	601.85	1.01	293.83	1.63
38	10%	1.44	1.62	1.62	293.86	601.75	1.01	293.86	1.52
39	5%	1.44	1.62	1.62	293.80	602.40	1.01	293.80	1.34

Table D.6: B1 Valve Plug Test Data with Corrected Pressure Offsets

B1 - Measured Data with Corrected Pressure Offsets									
Trial #	Stroke [ξ]	Stroke [ξ]	P100	P101	T101	DPT101	P102	T102	DPT102
	[%]	[mm]	[Bar]	[Bar]	[K]	[mBar]	[Bar]	[K]	[mBar]
1	5%	1.14	1.62	1.62	294.16	600.84	1.02	294.16	2.01
2	10%	2.09	1.62	1.62	294.04	601.42	1.02	294.04	2.22
3	15%	2.63	1.62	1.62	294.03	599.49	1.02	294.03	2.30
4	20%	3.5	1.62	1.61	293.98	598.84	1.02	293.98	2.50
5	25%	4.08	1.62	1.62	293.90	599.50	1.02	293.90	2.65
6	30%	4.82	1.62	1.61	293.87	598.30	1.02	293.87	2.92
7	35%	5.62	1.62	1.62	293.84	600.50	1.02	293.84	3.30
8	40%	6.33	1.62	1.62	293.84	599.44	1.02	293.84	3.64
9	45%	7.15	1.62	1.61	293.79	597.09	1.02	293.79	4.25
10	50%	8.01	1.63	1.62	293.73	598.44	1.02	293.73	5.19
11	55%	8.9	1.63	1.62	293.71	601.07	1.02	293.71	6.69
12	60%	9.83	1.64	1.62	293.65	599.42	1.02	293.65	9.28
13	65%	10.63	1.65	1.62	293.58	603.09	1.02	293.58	12.45
14	70%	11.56	1.65	1.62	293.48	600.80	1.02	293.48	17.21
15	75%	12.49	1.66	1.62	293.47	596.91	1.03	293.47	23.11
16	80%	13.56	1.70	1.64	293.42	607.37	1.03	293.42	34.41
17	85%	14.48	1.72	1.64	293.35	604.58	1.04	293.35	46.43
18	90%	15.42	1.72	1.62	293.37	579.14	1.04	293.37	59.15
19	95%	16.39	1.60	1.50	293.30	458.82	1.04	293.30	57.18
20	100%	17.13	1.53	1.42	293.26	375.62	1.04	293.26	57.96
21	95%	16.45	1.60	1.50	293.12	458.09	1.04	293.12	55.57
22	90%	15.44	1.74	1.64	293.17	600.47	1.04	293.17	59.97
23	85%	14.56	1.71	1.64	293.19	600.92	1.04	293.19	44.97
24	80%	13.53	1.68	1.63	293.26	597.85	1.03	293.26	31.19
25	75%	12.74	1.67	1.63	293.18	601.69	1.03	293.18	25.22
26	70%	11.55	1.65	1.62	293.18	598.92	1.02	293.18	16.04
27	65%	10.61	1.65	1.62	293.19	603.06	1.02	293.19	11.73
28	60%	9.71	1.63	1.61	293.22	594.39	1.02	293.22	8.77
29	55%	8.89	1.63	1.62	293.24	601.83	1.02	293.24	6.45
30	50%	8.31	1.63	1.62	293.24	599.39	1.02	293.24	5.58
31	45%	7.18	1.62	1.61	293.31	596.90	1.02	293.31	4.13
32	40%	6.66	1.62	1.62	293.30	599.92	1.02	293.30	3.69
33	35%	5.62	1.63	1.62	293.26	603.06	1.02	293.26	3.32
34	30%	5.12	1.62	1.61	293.26	597.64	1.02	293.26	2.94
35	25%	4.17	1.62	1.61	293.28	597.36	1.02	293.28	2.68
36	20%	3.43	1.62	1.62	293.31	600.79	1.02	293.31	2.43
37	15%	2.78	1.62	1.62	293.31	601.96	1.02	293.31	2.25
38	10%	2.19	1.62	1.62	293.31	602.73	1.02	293.31	2.13
39	5%	1.6	1.62	1.62	293.31	603.27	1.02	293.31	1.95

Table D.7: B2 Valve Plug Test Data with Corrected Pressure Offsets

B2 - Measured Data with Corrected Pressure Offsets									
Trial #	Stroke [ξ]	Stroke [ξ]	P100	P101	T101	DPT101	P102	T102	DPT102
	[%]	[mm]	[Bar]	[Bar]	[K]	[mBar]	[Bar]	[K]	[mBar]
1	5%	1.20	1.62	1.61	294.21	597.74	1.01	294.21	1.59
2	10%	1.96	1.61	1.61	294.16	594.75	1.01	294.16	1.78
3	15%	2.56	1.62	1.62	294.11	601.84	1.01	294.11	1.95
4	20%	3.46	1.62	1.62	294.04	602.02	1.01	294.04	2.17
5	25%	4.06	1.62	1.62	294.00	601.71	1.01	294.00	2.44
6	30%	4.79	1.62	1.61	293.98	599.01	1.02	293.98	2.77
7	35%	5.54	1.62	1.61	293.97	598.63	1.02	293.97	3.16
8	40%	6.32	1.62	1.62	293.95	600.25	1.02	293.95	3.66
9	45%	7.16	1.62	1.62	293.92	599.47	1.02	293.92	4.19
10	50%	8.08	1.62	1.61	293.81	597.59	1.02	293.81	5.10
11	55%	8.87	1.63	1.62	293.85	599.58	1.02	293.85	5.94
12	60%	9.81	1.63	1.62	293.80	599.38	1.02	293.80	7.24
13	65%	10.64	1.64	1.62	293.76	601.30	1.02	293.76	9.31
14	70%	11.57	1.65	1.62	293.70	600.45	1.02	293.70	13.12
15	75%	12.51	1.66	1.62	293.60	600.43	1.02	293.60	18.82
16	80%	13.42	1.68	1.63	293.55	598.28	1.03	293.55	30.27
17	85%	14.40	1.70	1.63	293.46	596.53	1.03	293.46	40.95
18	90%	15.46	1.71	1.61	293.46	568.43	1.04	293.46	58.23
19	95%	16.37	1.61	1.52	293.27	479.55	1.04	293.27	53.20
20	100%	17.05	1.55	1.44	293.32	400.06	1.04	293.32	59.23
21	95%	16.44	1.65	1.55	293.25	507.34	1.04	293.25	57.01
22	90%	15.49	1.73	1.64	293.25	603.20	1.04	293.25	54.97
23	85%	14.50	1.70	1.63	293.24	598.14	1.03	293.24	40.74
24	80%	13.45	1.68	1.63	293.26	602.53	1.03	293.26	29.31
25	75%	12.71	1.67	1.63	293.26	606.45	1.02	293.26	21.33
26	70%	11.79	1.65	1.63	293.26	602.82	1.02	293.26	14.83
27	65%	10.94	1.64	1.62	293.28	601.32	1.02	293.28	10.54
28	60%	9.66	1.63	1.62	293.27	601.91	1.02	293.27	6.79
29	55%	9.11	1.62	1.61	293.28	595.37	1.02	293.28	6.03
30	50%	8.27	1.63	1.62	293.27	601.33	1.02	293.27	5.20
31	45%	7.42	1.63	1.62	292.27	600.21	1.02	292.27	4.54
32	40%	6.33	1.63	1.62	293.30	604.54	1.02	293.30	3.84
33	35%	5.59	1.62	1.62	293.32	600.11	1.02	293.32	3.27
34	30%	4.85	1.62	1.62	293.30	601.60	1.02	293.30	2.83
35	25%	4.30	1.62	1.62	293.26	599.34	1.01	293.26	2.60
36	20%	3.38	1.62	1.62	293.32	603.76	1.01	293.32	2.24
37	15%	2.69	1.62	1.61	293.34	600.02	1.01	293.34	1.95
38	10%	1.98	1.62	1.61	293.31	598.02	1.01	293.31	1.81
39	6%	1.25	1.85	1.62	293.35	598.37	1.01	293.35	1.57
40	5%	1.25	1.85	1.62	293.33	598.30	1.01	293.33	1.57

Table D.8: B3 Valve Plug Test Data with Corrected Pressure Offsets

B3 - Measured Data with Corrected Pressure Offsets									
Trial #	Stroke [ξ]	Stroke [ξ]	P100	P101	T101	DPT101	P102	T102	DPT102
	[%]	[mm]	[Bar]	[Bar]	[K]	[mBar]	[Bar]	[K]	[mBar]
1	5%	1.14	1.62	1.62	293.64	601.18	1.02	293.64	0.31
2	10%	2.12	1.61	1.61	293.62	593.99	1.01	293.62	0.36
3	15%	2.76	1.62	1.61	293.63	600.18	1.01	293.63	0.45
4	20%	3.34	1.61	1.62	293.62	597.76	1.01	293.62	0.53
5	25%	4.27	1.61	1.61	293.62	597.32	1.01	293.62	0.72
6	30%	4.83	1.62	1.62	293.58	601.05	1.01	293.58	0.89
7	35%	5.55	1.62	1.61	293.60	597.53	1.01	293.60	1.31
8	40%	6.36	1.62	1.61	293.62	597.23	1.01	293.62	1.61
9	45%	7.15	1.62	1.61	293.56	595.84	1.01	293.56	2.28
10	50%	8.00	1.62	1.61	293.62	594.83	1.02	293.62	3.08
11	55%	8.85	1.62	1.62	293.59	598.08	1.02	293.59	4.23
12	60%	9.88	1.63	1.62	293.58	601.56	598.69	293.58	6.17
13	65%	10.61	1.63	1.62	293.48	601.93	1.02	293.48	7.96
14	70%	11.53	1.63	1.61	293.56	594.38	1.02	293.56	10.60
15	75%	12.45	1.65	1.62	293.52	598.26	1.02	293.52	14.20
16	80%	13.42	1.66	1.62	293.53	598.68	1.02	293.53	19.74
17	85%	14.38	1.67	1.62	293.47	596.20	1.03	293.47	28.18
18	90%	15.56	1.71	1.64	293.45	598.85	1.03	293.45	45.98
19	95%	16.42	1.69	1.59	293.40	544.68	1.04	293.40	58.18
20	100%	17.13	1.58	1.47	293.42	429.21	1.04	293.42	59.28
21	95%	16.41	1.69	1.58	293.37	543.22	1.04	293.37	59.05
22	90%	15.44	1.71	1.64	293.32	600.45	1.03	293.32	43.97
23	85%	14.56	1.69	1.63	293.41	605.05	1.03	293.41	29.85
24	80%	13.60	1.66	1.62	293.42	598.23	1.02	293.42	19.47
25	75%	12.76	1.65	1.62	293.35	595.96	1.02	293.35	15.10
26	70%	11.90	1.64	1.62	293.42	602.22	1.02	293.42	10.33
27	65%	10.55	1.64	1.62	293.42	602.67	1.02	293.42	7.90
28	60%	9.64	1.63	1.62	293.42	600.05	1.02	293.42	6.58
29	55%	9.18	1.63	1.62	293.42	603.93	1.02	293.42	4.40
30	50%	7.92	1.62	1.61	293.44	599.71	1.02	293.44	3.11
31	45%	7.16	1.62	1.62	293.45	602.90	1.01	293.45	2.21
32	40%	6.64	1.62	1.62	293.47	603.97	1.01	293.47	1.83
33	35%	5.71	1.62	1.62	293.51	602.24	1.01	293.51	1.26
34	30%	5.08	1.62	1.62	293.53	602.77	1.01	293.53	0.95
35	25%	4.35	1.62	1.61	293.53	599.40	1.01	293.53	0.76
36	20%	3.61	1.62	1.61	293.55	600.33	1.01	293.55	0.57
37	15%	2.66	1.62	1.61	293.52	600.68	1.01	293.52	0.42
38	10%	1.95	1.61	1.61	293.52	598.68	1.01	293.52	0.38
39	5%	1.24	1.62	1.62	293.56	602.12	1.01	293.56	0.31